Frederico Brízido Caldas de Oliveira

Thermo-Hydro-Mechanical analysis of CO_2 injection into deep aquifers

Dissertation to obtain the degree of Master in Civil Engineering

Supervisor: Professor Dr. Lyesse Laloui, École Polytechnique Fédérale de Lausanne

Co-Supervisor: Professor Dr. Armando Antão, Universidade Nova de Lisboa

Chair:	Professor Dr. António Pinho Ramos
Examiner:	Professor Dr. Rafaela Pinheiro Cardoso
Examiner:	Professor Dr. Luis Miguel Chagas Gil
Supervisor:	Professor Dr. Lyesse Laloui

FACULDADE DE CIÊNCIAS E TECNOLOGIA
UNIVERSIDADE NOVA DE LISBOA

July 2014

Frederico Brízido Caldas de Oliveira

Thermo-Hydro-Mechanical analysis of CO_2 injection into deep aquifers

Supervisor: Professor Dr. Lyesse Laloui, École

Polytechnique Fédérale de Lausanne

Co-Supervisor: Professor Dr. Armando Antão, Universidade Nova de Lisboa

July 2014

Thermo-Hydro-Mechanical analysis of CO_2 injection into deep aquifers

ACKNOWLEDGEMENTS

First, I would like to express my deepest gratitude to my supervisor Professor Lyesse Laloui for giving me the opportunity to work in his group. Furthermore, I would like to express my sincere gratitude to Li Chao for his supervision and guidance during my period at LMS-EPFL. It has been a privilege and a pleasure to work under their guidance.

I would like to express my gratitude to all my colleagues at LMS-EPFL more in particular to, Alice, Alessandro, Athanasia, Francesco, Nicolas and Timur for helping me during my stay and for all their advices.

I would also like to express my utmost gratitude to all my family, especially to my brother, father and mother, who always supported me during my life and for making this challenge possible.

I would also like to express my greatest gratitude to my co-supervisor, Prof. Armando Antão that despite being distant from the development of this study has always showed his support. I also would like to thanks for his guidance and advices during my academic journey. In addition, I greatly appreciate my Professor Nuno Guerra, who helped me during the whole process of developing my master dissertation abroad and for transmitting his wisdom during my academic journey. I take this opportunity, to demonstrate my acknowledgement to all my Professors from the Civil Engineering department of the Faculdade de Ciências e Tecnologias of Universidade Nova de Lisboa, for facilitating this entire apprenticeship and for helping me to improve as a person and as a professional.

I would like to thank all my friends, David Costa, David Henriques, Dione Guimarães, Diogo Pinto, Francisco Franco, Gonçalo Faustino, Joana Chaves, Joana Teixeira, Luís Viotty, Pedro Salvado, Rita Vieira, Sofia Pereira and Tomás Rantanen for all the good moments. I would also like to thank my friends António Mesquista and Magno Matos.

ABSTRACT

One of the biggest challenges for humanity is global warming and consequently, climate changes. Even though there has been increasing public awareness and investments from numerous countries concerning renewable energies, fossil fuels are and will continue to be in the near future, the main source of energy. Carbon capture and storage (CCS) is believed to be a serious measure to mitigate CO_2 concentration. CCS briefly consists of capturing CO_2 from the atmosphere or stationary emission sources and transporting and storing it via mineral carbonation, in oceans or geological media. The latter is referred to as carbon capture and geological storage (CCGS) and is considered to be the most promising of all solutions. Generally it consists of a storage (e.g. depleted oil reservoirs and deep saline aquifers) and sealing (commonly termed caprock in the oil industry) formations. The present study concerns the injection of CO_2 into deep aquifers and regardless injection conditions, temperature gradients between carbon dioxide and the storage formation are likely to occur. Should the CO_2 temperature be lower than the storage formation, a contractive behaviour of the reservoir and caprock is expected. The latter can result in the opening of new paths or re-opening of fractures, favouring leakage and compromising the CCGS project. During CO_2 injection, coupled thermo-hydro-mechanical phenomena occur, which due to their complexity, hamper the assessment of each relative influence. For this purpose, several analyses were carried out in order to evaluate their influences but focusing on the thermal contractive behaviour. It was finally concluded that depending on mechanical and thermal properties of the pair aquifer-seal, the sealing caprock can undergo significant decreases in effective stress.

Keywords: CCS, CO_2 storage, non-isothermal analysis, deep aquifers, liquid CO_2

RESUMO

Um dos maiores desafios para a humanidade é o aquecimento global e consequentemente as mudanças climáticas. Apesar da preocupação pública e dos investimentos por parte de inúmeros países terem vindo a aumentar, relativamente a energias renováveis, os combustíveis fósseis são e continuarão a ser, num futuro próximo, a principal fonte de energia. Acredita-se que a captação e armazenamento de CO_2 (CAC) seja uma séria medida para mitigar a concentração de CO_2. Resumidamente, o CAC, consiste na captação de CO_2 da atmosfera ou de fontes emissoras estacionárias, transporte e armazenamento via carbonatação mineral, em oceanos ou em formações geológicas. Este último é referido como captação e armazenamento geológico de carbono (CAGC) e é considerado a solução mais promissora. Em geral, consiste numa formação de armazenamento (e.g. reservatórios de petróleo já explorados e aquíferos salinos profundos) e uma formação de selagem (frequentemente denominada de *caprock* na indústria do petróleo). O estudo em questão diz respeito à injecção de CO_2 em aquíferos profundos e independentemente das condições em que o CO_2 é injectado, diferenças de temperatura entre o dióxido de carbono e a formação de armazenamento podem facilmente ocorrer. No caso em que a temperatura de injecção é menor que a da formação de armazenamento, um comportamento contráctivo é esperado. Isto pode resultar na abertura de novas passagens ou re-abertura de fracturas, comprometendo o projecto de CAGC. Durante a injecção de CO_2, fenómenos interligados térmo-hidro-mecânicos ocorrem, os quais devido à sua complexidade dificultam a sua avaliação. Para este fim, várias análises foram realizadas de modo a avaliar as suas influências mas tendo como principal foco o comportamento contráctil térmico. Finalmente concluiu-se que a dependendo das propriedades mecânicas e térmicas do par aquífero-selagem, a rocha de selagem pode sofrer decréscimos significativos de tensão efectiva.

Palavras-chave: CAC, armazenamento de CO_2, analise não isotérmica, aquíferos profundos, CO_2 líquido

TABLE OF CONTENTS

LIST OF TABLES

LIST OF FIGURES

LIST OF ABBREVIATIONS, ACRONYMS AND SYMBOLS

Abbreviations

d – days
CO_2 –carbon dioxide
CCGS – carbon dioxide capture and geological storage
CCS – carbon dioxide capture and storage
ECBM – enhancing coal bed methane
EOS – equation of state
EOR – enhancing oil recovery
Gt – gigaton
H – hydraulic
HM – hydro-mechanical
IR – injection rate
Mt – megaton
REV – representative elementary volume
SC – supercritical
TH – thermo-hydraulic
THM – thermo-hydro-mechanical
WRC – water retention curve

Acronyms

FEM - finite element method

Symbols

Roman letters

b	Biot's coefficient
c	specific heat capacity
c'	coesion
$\mathrm{CKC1}$	material parameters
$\mathrm{CKW1}$	material parameters
D_c	diffusion coefficient
E	Young modulus
H	enthalpy
I	identity matrix
$K_{eq,g-l}^{CO2}$	Henry's coefficient

K_{int}	intrinsic permeability
k_{rc}	carbon dioxide relative permeability
k_{rw}	water relative permeability
K_s	bulk modulus of solid material
K_o	inicial stress factor
m	Van Genuchten parameter
M	molar mass
M	slope of the critical state line
n	porosity
p_c	carbon dioxide pressure
$\mathrm{p_f}$	fluid pressure
P_r	Van Genuchten parameter
p_w	water pressure
p'	confinement pressure
q	deviatoric stress
R	gas constant
s	suction
s_E	air entry value
S	saturation
S_{res}	residual saturation
S_w	water phase saturation
T	temperature
V	volume
V_v	volume of voids
V_w	volume of water
$\mathrm{X_{dc}}$	mass fraction of dissolved carbon dioxide in water
Z	compressability parameter

Greek letters

α_t	linear thermal expansion coefficient
β_s	volumetric thermal expansion coefficient for solid material
β_w	volumetric thermal expansion coefficient for water
δ	Kronecker delta
ε	strain
θ_{ct}	critical angle
λ_α	thermal conductivity
μ	solid displacement
μ_c	carbon dioxide viscosity
μ_{JT}	Joule-Thomson coefficient

μ_w	water viscosity
ρ	density
σ	total stress
σ'	effective stress
τ	tortuosity
ν	poisson coefficient
Φ	fugacity coefficient

Subscript

c	dry carbon dioxide
dc	dissolved carbon dioxide
s	solid
w	water

Nota Bene: The standard sign convention of soil mechanics is used in this manuscript, i.e. compression is positive and extension is negative

1. INTRODUCTION

1.1. GENERAL CONTEXT

One of the biggest challenges for Humanity is global warming and, consequently the climate changes. Even though there has been increasing public awareness and investments from numerous countries concerning renewable energies, fossil fuels are and will continue to be in the near future the main source of energy due to their low cost, abundance and global distribution. However, energy from fossil fuels has its downsides due to the emission of greenhouse gases, of which carbon dioxide is included. Even though a direct relationship, has not yet been established, the Intergovernmental Panel on Climate Change (IPCC) states that the scientific community strongly believes that greenhouse gases contribute towards global warming (IPCC, 2007). Hence, the challenge is to lower CO_2 emissions or CO_2 atmosphere concentrations. However, in order to keep up with population growth and its living standards, lowering CO_2 emissions is not, as yet, a sustainable solution (Bachu, 2008).

Thus, a world convention was created, whose main objective is to establish plans and measures to mitigate CO_2 atmosphere concentrations, of which carbon capture and storage is included. Carbon capture and storage (CCS) is believed to be a serious measure and briefly consists of capturing CO_2 either directly from the atmosphere or from stationary sources (e.g. power plants, cement factory) and transporting and storing it via mineral carbonation, in oceans or in geological media. The latter, is referred to as carbon capture and geological storage (CCGS) and is considered to be the most promising of all solutions. It consists of injecting CO_2 into a storage formation (e.g. depleted oil and gas reservoirs and deep aquifers), being that confined by a sealing formation (commonly termed as “caprock” in the oil industry). However, despite the potential, this technology has not yet gained public acceptance, which was the motivation for carrying out the present study.

The major risk of a CCGS project is the possibility of leakage due to its potential consequences. Thus, the success of a CCGS project is directly related to the sealing efficiency, i.e. the caprock integrity. The present study addresses the injection of CO_2 into deep aquifers, focusing mainly on the mechanical behaviour of the caprock during the injection operation. The conditions in which CO_2 is injected depend on several factors. However, regardless of its conditions, temperature differences between injected fluid and storage formation are likely to occur. In cases where the fluid is injected with a lower temperature than the storage formation a contractive behaviour of the aquifer and sealing rock is expected. This contractive behaviour could result in the opening of pre-existing fractures or faults activation, compromising the success of the project. The latter brought the particular motivation for a non-isothermal analysis. Thus, in this manuscript the thermal effects are studied through a comparative analysis between injecting CO_2 in liquid conditions (non-isothermal) and in “supercritical” conditions (isothermal), similar to the work of Vilarrasa (2012).

Due to the high computational cost and the high coupled thermo-hydro-mechanical behaviour, the assessment of each influence is complex. For this purpose, a staged approach was adopted, firstly carrying out hydraulic analyses, followed by hydro-mechanical, thermo-hydro and finally thermo-hydro-mechanical analyses. The thermo-hydro-mechanical analysis is encompassed within a framework that takes into account the following processes: multiphase fluid flow occurring under pressure and temperature; interaction between fluids, which addresses the relative permeability evolution of water and CO_2 and the exchange terms due to CO_2 dissolution and degassing phenomena; heat flow through convection and conduction; stress-strain relationship; effective stress changes due to fluid pressure and temperature; fluid flows governed by advective and non-advective (diffusion) flows.

1.2. OBJECTIVES

The general objective of this study is to analyse the thermo-hydro-mechanical behaviour of the storage and especially the sealing formation during the injection operation. Should CO_2 be injected with a lower temperature than the storage and sealing formations, a contractive behaviour is expected which affects the mechanical regime. Thus, the main objective of the present study is to assess the influence of temperature on the mechanical behaviour of the aquifer and especially of the caprock.

1.3. OUTLINE OF THE WORK

Chapter 2 introduces the concept of CCS technology addressing its role, stages of the system and its current status. Of the various CCS technology solution, carbon capture and geological storage (CCGS) is described in more detail, addressing aspects such as: trapping mechanisms, suitable geological media, risks and monitoring.

Since deep aquifers are the geological media considered for this study, chapter 3 describes the general coupled thermo-hydro-mechanical behaviour occurring during CO_2 injection and some general knowledge of unsaturated geomaterials. Furthermore, the theoretical framework is presented, addressing the governing equations, i.e. mass balance conservation, momentum conservation, energy conservation and constitutive equations are presented.

Chapter 4 describes the characteristics of the FEM model: geometry, boundary conditions, material properties and simulation characteristics. These are the characteristics of what is considered to be the reference model from which several simulations are carried out in Chapter 5.

Chapter 5 presents the results of hydraulic, hydro-mechanical, thermo-hydro and thermo-hydro-mechanical analyses. This chapter focuses on the difference between “supercritical” (isothermal) and

liquid (non-isothermal) CO_2 injection. In addition, a comparison between the present study and Vilarrasa (2012) is addressed.

Chapter 6 presents the conclusions and future developments. .

2. GENERAL CONCEPTS OF CARBON DIOXIDE CAPTURE AND STORAGE (CCS)

2.1. ROLE OF CCS

When analysing the temperature over the last centuries, an increase in the average temperature becomes evident and predictions show a tendency for this to continue (IPCC, 2001c). Although a direct relationship has not yet been established, it is generally accepted that this temperature increase is due to the increase in concentrations of greenhouse gases in the atmosphere (IPCC, 2007 and American Geophysical Union, AGU, 2003). Thus, in order to mitigate climate changes, an important challenge is to reduce the greenhouse gases concentrations, of which CO_2 is included. Currently, this is one of humanity's biggest concerns, which has led to the creation of an international convention whose primary objective is to establish plans and measures for the stabilization of greenhouse gases concentrations (United Nations Framework Convention on Climate Change-UNFCCC). This prompted a portfolio being drawn up, comprising measures and actions to reduce CO_2 emissions, among which, carbon dioxide capture and storage. Alternative measures refer to the use of energies with lower gas emission, nuclear power, renewable energies, reducing the demand for energy by increasing efficiency during energy conversion, reducing greenhouse gases other than CO_2. In addition, this convention suggests that fossil fuels will still remain the main source of energy until the middle of the next century. Bachu (2008), also states that due to industry's major dependence on non-renewable energy and in order to maintain the population's quality of life, and also due to its low cost, versatility, easy storage and global distribution is not foreseen that the energy from the burning of fossil fuels will be replaced in the near future. A CCS system briefly consists of the separation and capture of carbon dioxide at a large stationary source, transporting and storing it and isolating the CO_2 from the atmosphere for long periods of time.

2.2. PROCESS OF CARBON DIOXIDE CAPTURE AND STORAGE

The process of a CCS system starts at the stationary emission sources of CO_2. The IPCC (2005) report mentions three main sources:

- Burning of fossil fuels: responsible for the highest percentage, this process results from the oxidation of carbon and is related to power plants, oil refineries, etc;
- Industrial processes: commercial production of metals from ores and the cement industry;
- Natural gas process: here the emissions are related to the fact that CO_2 is considered to be an impurity in the natural gas because it reduces the specific heat, thus its removal is necessary.

Once the emission sources have been identified, the three main stages comprising a CCS project (Figure 2.1), can be carried out: Capture, Transport and Storage.

2.2.1. CAPTURE

The capture phase represents a substantial portion of the investment needed for the implementation of a CCS technology and it is technically possible and economically viable for large-scale stationary sources of with high degrees of purity of CO_2. Generally, the capture systems can be divided into three categories: capture of exhaust gas (Post-Combustion), before combustion (Pre-Combustion and combustion with a high oxygen content (Oxyfuel Combustion). The application of each type of capture depends on the emission source. For more detailed information regarding the capture processes the reader should refer to IPCC (2005). Nowadays, it is possible to capture approximately 85 to 95% of the CO_2 produced. However, the implementation of a capture technology requires approximately 10 to 40% more energy than an equivalent plant without capture. Hence, the net amount of CO_2 captured is approximately 80 to 90%. With regard to the costs, a capture system implies an increase in electricity of about 20 to 85%, depending on the type of plant. Nevertheless, it is expected that with proper research and development and commercial deployment, the costs could be reduced by about 20 to 30% (IPCC, 2005).

2.2.2. TRANSPORT

Except in cases where the emission sources are located directly above the storage place, the captured CO_2 has to be transported. Of all stages that comprise a CCS system, this is the one that causes less complications on a technical level, as it has already been developed and deployed by the oil industry. The only concern to bear in mind is due to the fact that the state of CO_2 varies with temperature and pressure, which therefore requires monitoring during the transportation route in order to assure CO_2 transport conditions. Currently, there are two efficient methods for carrying out the transport stage. The most common is through pipelines where typically CO_2 is compressed and transported in liquid phase (higher density), as it is easier and less costly to perform the transportation. If transport overseas is necessary, transport can be carried out by ships, in which CO_2 is also transported in liquid state. However, the latter does not permit a continuous flow of CO_2 from the source to the storage site, meaning that an intermediate storage facility is required.

Regardless of the method of transport, the costs are directly related to the distance and to the quantity of CO_2. In the particular case of pipelines, costs are associated with location (Offshore, Onshore), type of area (inhabited or not), existence of obstacles (mountains, valleys), etc. With regard to ships, the costs are associated with the tank volume and the loading and unloading processes (IPCC, 2005).

2.2.3. STORAGE

In the context of a CCS project, the captured CO_2 needs to be stored in appropriate places. The question as to where it should be stored, leads us to the definition of three types of CCS technology that are currently being considered: Ocean storage, Mineral Carbonation and Geological Storage. In addition to

these three, the trapping of CO_2 through industrial products is also an option. However, it is not considered as a CCS solution. Regardless of the storage site, there are several aspects of the storage stage that must be considered:

- Long storage period: millions to millennia of years;
- The cost of storage (injection and monitoring) should be minimized;
- The applied methods can not infringe any national or international legislation;
- Environmental impacts need to be carefully studied and minimized;
- The probability of an accident occurring should be practically nil.

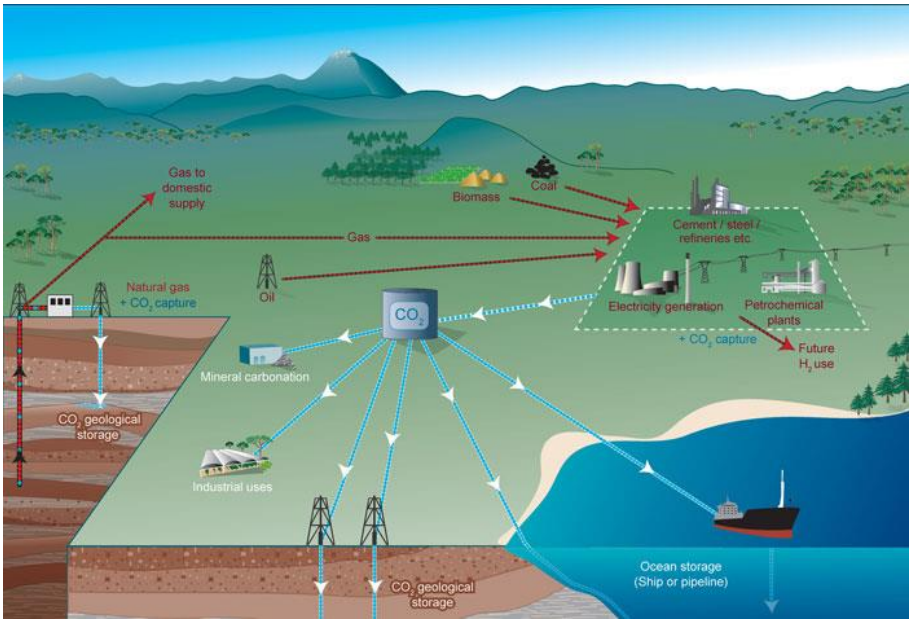

Figure 2.1 - Carbon dioxide capture and storage system (CO_2CRC, 2014)

Ocean Storage

Oceans are, in their nature large storage sites of CO_2. Carbon dioxide is soluble in water and gas exchange between the ocean surface and atmosphere occurs naturally. Therefore, the vast majority of CO_2 captured by oceans concentrates in the upper fraction, where an increase in the acidity of the water has already been detected, which is reflected in the decrease of the water's *p*H. However, at greater depths the *p*H remains stable (Brewer et al., 2000). Thus, the use of oceans as CO_2 storage sites, only hasten this slow but natural process.

This solution implies the injection of CO_2 in oceans where, depending on the depth, CO_2 dissolves in water or sinks and accumulates on the seabed (phenomenon known as "deep lake") (Aya et al., 2004). Despite this inherent advantage, which is the large storage capacity, it is expected that large scale injection can cause a change in the *p*H of the ocean that could bring consequences to the marine life. Due to the latter and due to several other physical and chemical phenomena that are still not well understood, ocean storage is not yet considered an economically and politically viable option (Chen et al., 2005).

Mineral Carbonation

Mineral carbonation involves converting CO_2 into inorganic solid carbonates by resorting to chemical reactions to accelerate this natural process. This process requires the existence of certain minerals found in silicate rocks, thus demanding their mining resulting in environmental impacts and high energy costs. Furthermore, following the conversion of CO_2 into solid carbonates, it is then necessary to proceed to the transport and disposal of the solid carbonates. Although this type of storage is the safest and also the one that requires less monitoring due to the high costs and environmental impacts this option is currently being excluded from large scale implementation (Bachu, 2008).

Geological Storage

In contrast to the two previous options, carbon dioxide and geological storage (CCGS) is currently and probably the best and only option in the short-medium term for significantly reducing CO_2 concentrations. This is due to the fact that besides storage in geological formations much resembling the natural accumulation of oil, gas and even CO_2, which provides confidence in long-term storage (Bradshaw and Dance, 2005), this technology has the advantage of rapid implementation due to extensive experience developed over the years by the oil and gas industries.

The geological formations currently considered for CCGS projects are: depleted oil and gas reservoir, coal beds and deep saline aquifers. These types of geological traps are relatively well distributed throughout the globe and can be found in sedimentary basins, either offshore or onshore. In addition, to these three main formations, structures such as salt caves and abandoned mines are also considered. Although, the storage capacity of these structures is not significant, those could act as intermediate reservoirs (IPCC, 2005). Regarding the storage capacity of the three main formations, there are not yet any studies that clearly define the overall capacity, mainly due to inexistent detailed knowledge concerning the saline aquifers. However, addressing the storage capacity in another way, i.e. by looking at a bigger picture and simply determining whether there is enough capacity for the amounts of CO_2 produced, present studies safely state that there is a capacity of 200Gt and a high probability of 2000Gt, which is the estimated amount of CO_2 to be produced over the XXII century (IPCC, 2005).

The storage of the injected CO_2 into geological formations, occurs through a combination of several physical and geochemical trapping mechanisms. Site selection is imperative for the success of CCGS projects, meaning that there are a series of criteria to set prior to selection. The criteria and trapping mechanisms are presented in more detail in section 2.4.

Industrial use

This solution consists of the industrial use of CO_2 in chemical and biological processes such as the production of urea and methanol and also in a variety of technological applications (refrigeration, welding and fire extinguishers). However, this option can not be considered a mitigation measure since neither capacity nor storage time are significant.

2.3. CURRENT STATUS AND ALTERNATIVE APPROACHES

From the three CCS technologies presented in the previous section, only CCGS is seriously taken into consideration. With regard to ocean storage, the technology is quite complex and still requires many studies on both a technical and environmental level. Since the environmental impacts that could result are not yet well understood ocean storage is so far, not seen as a serious mitigation solution. Furthermore, due to the high costs and also the strong environmental impacts that it may cause, mineral carbonation is excluded as an option to be pursued. However, despite the obvious disadvantages of these solutions compared to CCGS, both are object of investment and development by some countries but not expected to be applied on a large scale in the short-medium term (IPCC, 2005).

Thus, the current state of CCGS is promising compared to the others, as it is the one which is the easiest to implement due to its high maturity as a technology implemented by the oil and gas industries. The capture and separation stages are already carried out by the oil and chemical industries. The transport of CO_2 on a large scale is also implemented. In addition, the geophysical exploration for the selection of suitable storage sites has long been practiced along with the injection process which has been in under development by "Enhancing Oil Recovery" (EOR) projects for 30 years (IPCC, 2005). Regarding the storage stage, evidence from oil and gas reservoirs indicate storage times of about 5-100 million years (Bradshaw and Dance, 2005).

Nevertheless, despite all three stages already being implemented separately, their integration into a CCGS project is not a simple task. This is because of the high cost of capture, the transport being limited to the pipeline network and the high probability of the capture site being far from the storage site, which involves long-distance transport, resulting in a considerable increase in costs. Injection and storage operations require further investigation in order to ensure that no leakage of CO_2 occurs and because of the lack of experience in implementing a monitoring project. These aspects result in the fact that CCGS projects are only viable for very particular cases. IPCC (2005), mentions the conditions which make a project viable. However, being realistic and transparent, currently, this technology is only economically feasible if one of the following premises is verified: implementing this technology in an EOR or ECBM (enhancing coal bed methane) project; significant increase in the market cost of CO_2 emission licenses; added value for underground CO_2.

Enhancing fuel recovery in the particular case of EOR, is performed through an injection well where CO_2 is injected, pushing the oil to the capture well. Moreover the dissolution of CO_2 in oil decreases its viscosity, thereby facilitating its flow. In the case of ECBM, injected CO_2 causes the release of methane gas, which is naturally found adsorbed into the organic coal matter, due to greater affinity of the carbon dioxide compared to the methane. Thus, the profits obtained from the additional extraction of fuel can cover the costs of the technology. In the present context, CO_2 has economic value if found in the atmosphere (through the payment of CO_2 emission licenses). However, the current market cost is still too low to enable the deployment of such technology and moreover, the latter does not apply to underground CO_2. Therefore, should there be a significant monetary incentive for subsurface CO_2, the implementation would be facilitated. According to IPCC (2005) report, in the near future, it is not likely

that the last two premises will change, restricting the application of this technology only to enhancing fuel recovery projects, which greatly reduces the overall storage capacity (360Mt/year). Although only applicable to specific situations, it is expected that this solution could significantly contribute towards mitigating CO_2 concentrations.

Currently, even though none of them have the main objective of storing CO_2, there are three projects on a commercial scale that have implemented CCGS technology. The Sleipner project in Norway (Figure 2.2), is an offshore platform located in the North Sea, from where CO_2 obtained from an ECBM operation is injected into a nearby saline formation about 800 meters below the seabed. This project is injecting about 1 Mt/year and is expected to store a total of 20 Mt by the end of the operations. The main objective of the *In Salah* project in Algeria is also the stimulation of natural gas extraction. CO_2 is separated from natural gas and afterwards injected at a ratio of 1.2Mt/year into a saline formation 1800 meters deep. The EOR project in Weyburn, Canada aims to store almost all the CO_2 (20Mt) produced and used in the oil recovery operations.

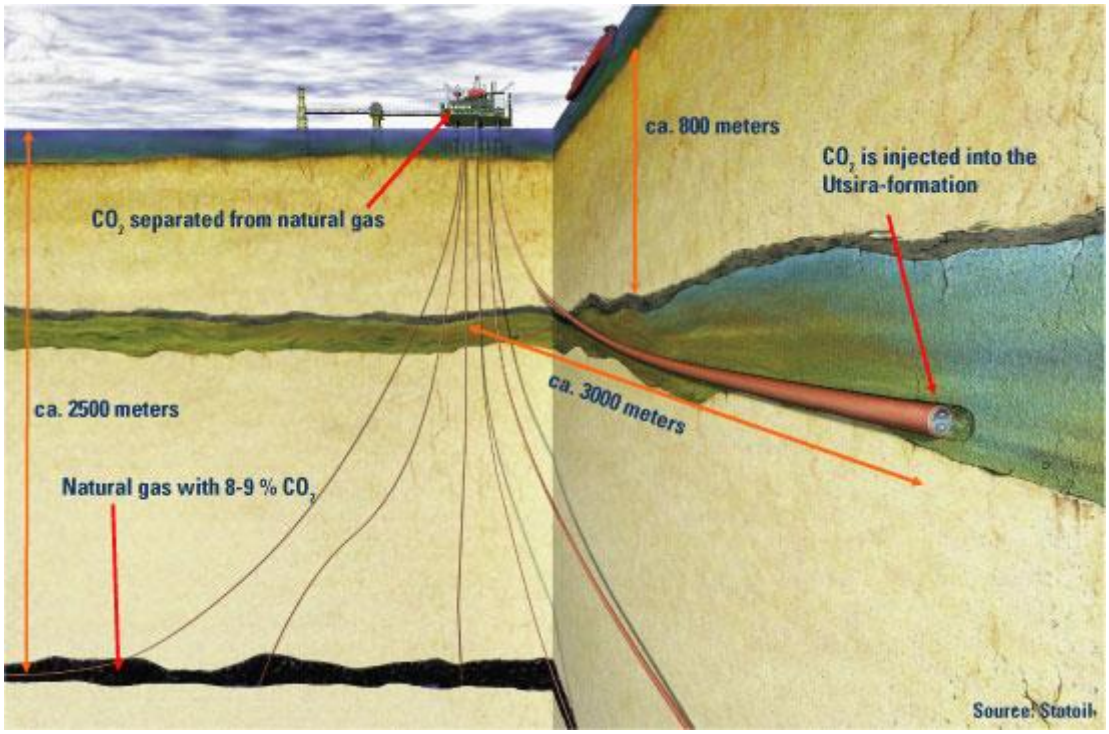

Figure 2.2 – Sleipner Project (Statoil, 2014)

2.4. CCGS TRAPPING MECHANISMS AND SUITABLE GEOLOGICAL MEDIA

Bearing in mind the current status described above and the context of the present work, this section, presents only the trapping mechanisms referring to CCGS technology.

The sequestration of CO_2 in geological formations occurs through a combination of various trapping mechanisms. These entrapment phenomena can be of a chemical or physical nature and depend

obviously on the storage site in question. In oil reservoirs and saline aquifers the operating mechanisms are very similar, where the main phenomenon being the static trapping where CO_2 is prevented from flowing due to a physical barrier (less permeable rock), meaning that if there is an available pathway, CO_2 will flow. Apart from this, other secondary mechanisms act, such as residual trapping, solubility trapping and mineral trapping. The first relates to the fact that CO_2 is trapped in the geomaterial pores due to capillary forces formed between CO_2 and resident fluid and even if a pathway exists, it will not flow. Solubility trapping is a chemical phenomenon in which CO_2 dissolves in the resident fluid. This process is optimized for cases where underground flows exist, so that the resident fluid saturated with CO_2 is replaced by unsaturated fluid. These geological traps are found in sedimentary basins that often contain minerals such as olivine and serpentine, which chemically react with CO_2 forming other mineral solids such as calcite and magnesium.

As far as coal beds are concerned, the trapping mechanism relates to the adsorption of CO_2 into the organic coal matter, more specifically, it is trapped in the micropore walls of the coal. It is important to highlight the fact that storing CO_2 in coal beds implies that these become impracticable for exploitation, since once atmospheric pressure is observed, CO_2 desorbs.

Due to their different natures (chemical or physical), the mechanisms have different functions and time windows. Firstly, the injected CO_2 is trapped by primary mechanisms, static in the case of oil reservoirs and aquifers, and by adsorption in coal beds, whose main role is storage capacity. Afterwards, secondary mechanisms such as residual, solubility and mineral mechanisms start to act, not contributing significantly to the overall capacity but indisputably increasing safety storage, since CO_2 is no longer found as a free phase (Bachu, 2008). Figure 2.3, shows the time window of the different trapping mechanisms acting in a geological formation such as depleted oil reservoirs and deep aquifers.

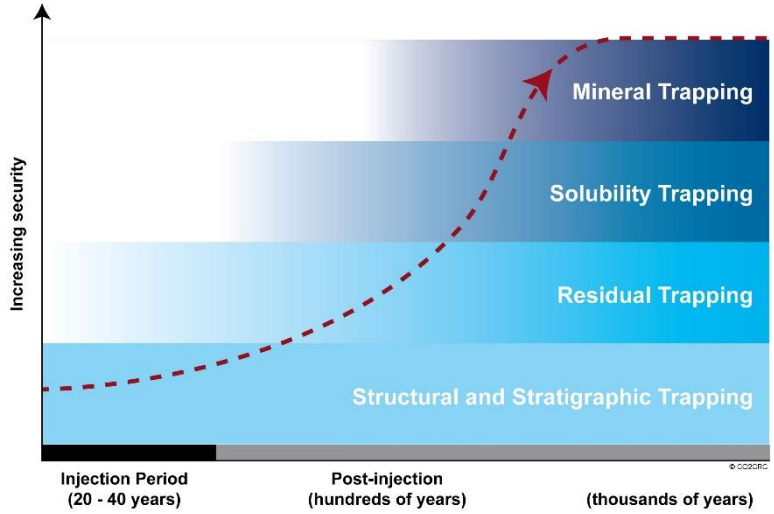

Figure 2.3 - Time frame of the primary and secondary trapping mechanisms acting in depleted oil reservoir or deep aquifers (CO_2CRC, 2014)

Although it is known that formations such as oil reservoirs, saline aquifers and coal beds are potential CO_2 storage sites, selection and suitability is somewhat complex and it is necessary to carry out an analysis in order to determine a series of aspects. Excluding coal beds, in brief the geological formations must consist of a reservoir-seal pair. As already mentioned, such geological media are found in

sedimentary basins, because only sandstone and carbonate rocks have the porosity and permeability required for high storage capacity and injection rates, while being confined by a very low permeable shale. This low permeability barrier is often termed “caprock” in the oil industry. The existence of a sealing formation above the storage formation is of extreme importance, since due to a lower density of carbon dioxide compared to the one of the resident fluid (oil or water), buoyancy forces act all the time, imposing a vertical flow with upwards direction.

According to Bachu (2008) the requirements for a potential geological storage site are:

- Accessibility: the location is economical available and the enterprise responsible for the storage has all the legal rights to do so;
- Capacity: the geological formation has the sufficient porosity, i.e. storage capacity for the target volume of injected source;
- Injectivity: the aquifer has the desired permeability in order to allow the injection at the same rate as the CO_2 is captured at the source;
- Storage Security: the caprock is impermeable enough to avoid vertical migration (leakage); well defined trapping mechanisms; the geologic environment is stable enough to guarantee storage site integrity (no seismic actions); fault system well defined to assure that no vertical and/or horizontal migration is possible.

Once a potential geological formation has been detected, it is necessary to make a geological, hydrogeological, geochemical and geotechnical characterization of the storage site and its surroundings. Hence, and according to Bachu (2008) and Chevalier et al. (2010), the following criteria should be addressed:

- Depth: due to CO_2 properties, variation with pressure and temperature, depth affects CO_2 mobility through porous media, ergo affects storage capacity and security. Hence, depth should be such that it ensures high density and viscosity of CO_2 in order to diminish buoyancy forces, increase storage capacity and security but at the same time not so deep that drilling costs and energy requirements for carbon dioxide compression would be too high;
- Thickness of the storage formation: considering homogeneous porosity and permeability throughout the aquifer, then its thickness is directly proportional to storage capacity;
- Geothermal gradient: the *in situ* temperature at the storage formation is a relevant criterion to be evaluated since it affects the CO_2 and resident fluid density and viscosity, influencing the CO_2 plume mobility. Furthermore, if the fluid is injected with a lower temperature than the storage formation, thermal contraction will occur;
- Hydrogeology: despite its complex evaluation, the groundwater flow should be studied with regard to the charging and discharging areas, in order to identify the magnitude and direction of the water flow;

- Seismicity: having a record of the seismicity history of the surrounding area is crucial. A low seismicity is convenient, otherwise seismic actions may open pre-existing fractures or fault activation, causing CO_2 leakage;
- Fault systems: faults can be either favourable, creating structural traps or unfavourable, providing pathways for fluid circulation leading to a possible leakage. Chevalier et al. (2010), mentions three classes of faulted zones. One featuring high fault density and/or with faults that cut through the entire sequence of lithology, hence favouring leakage. Another, featuring faults that do not cross the caprock, which are considered to be favourable to storage due to their structural traps and finally an area that presents very little evidence of faulting. Thus, it is crucial to carry out a detailed study of the fault system, especially any that encounter the caprock;
- Structural traps: despite not being a pre-requisite for CO_2 storage a detailed evaluation of the structural traps can be economically advantageous, since some effective structure traps can constrain the injected carbon dioxide into a limited area thereby resulting in a reduction of the site investigation required to establish an appropriate injection site;
- Stress regime: the existing state of stress (K_0) needs to be carefully judged and investigated during the CCGS design stage. According to Rutqvist et al. (2008) thrust regimes ($K_0 < 1$) are less favourable for CO_2 storage.

2.5. RISKS AND MONITORING

Like any human activity, this technology involves some risks that need to be properly assessed and studied in order to provide public confidence in this technology as a serious solution to mitigate CO_2 concentrations. The risks arise mainly from the storage stage that includes the injection operation and the storage itself. With regard to the transport stage, excluding the possibility of a pipeline rupture, no major risks are projected. In fact, since the oil industry has been set up, only a few cases like the latter have been reported (Damen et al., 2006). As far as the storage stage is concerned, there are a number of risks that must be evaluated, such as:

- CO_2 leakage through the injection well;
- Leakage through abandoned wells;
- Leakage through undetected faults or fractures;
- Activation of existing faults or opening of pre-existing fractures;
- Rupture of the reservoir;
- Surface settlements;
- Increasing pore pressure caused by CO_2 injection which can trigger seismic events.

Nevertheless, leakage represents the main risk due to its potential consequences. This risk is provided by the buoyant forces that act on CO_2 at any time, meaning that leakage can occur either during or after

the injection stage. However, greater attention is needed during injection stage due to the increasing pore pressure in the reservoir, which can affect the mechanical stability of the seal which may result in the opening of fractures or fault activation. Thus, and according to IPCC (2005), the risk of leakage can be classified as global or local. It is considered global if the release of CO_2 is of such an order that it could contribute significantly to climate change and affect populations, ecosystems or potable water aquifers. Except in a catastrophe situation, a leakage at a global level is not likely to occur since current CCGS projects have evidence of retention fractions close to 99%. Local risks can occur though abandoned wells, undetected faults or fractures.

Many of the above risks can be avoided in advance through a correct selection of the storage site and can still be detected after their occurrence through monitoring methods. Although no methodology has yet been formulated, IPCC (2005) mentions some aspects that should be monitored:

- Control the quantity of injected and stored CO_2;
- System to detect possible leakages;
- System to detect micro-seismicity;
- Surface changes;
- Pressure at the injection well;
- Routine seismic analysis;
- Analysis of the geomaterials between the storage formation and surface.

The risk can be evaluated through risk assessment, i.e. by means of probabilistic analysis (He et al., 2011) or through a technical analysis that can create a solid knowledge about a certain phenomenon enabling the definition of safety factors (Rutqvist and Tsang, 2002). In the present study, the objective is to better assess the mechanical behaviour of the seal during the injection process through a finite element analysis.

2.6. CHALLENGES AND BARRIERS FOR DEPLOYMENT OF CCGS

Through projects such as Sleipner and In Salah, CCGS has been proven to be technologically possible. However, the relevant issue to address is whether this technology is indeed economically viable. Bachu (2008) states that many entities argue that this is the biggest barrier and in fact it is, should none of the following premises be detected: added value to the stored CO_2, implementation of the technology in EOR or ECBM operations; increase of the market value of CO_2 emission licenses. The question arises as to whether this technology is economically viable due to the high implementation costs, more in particular, with the capture system, this being a challenge rather than a barrier. Other issues such as detailed assessment of costs, experience in integrating the three stages, studies to establish the relation between emission sources and geological storage site represent other challenges.

However, there are issues that really constitute barriers such as public acceptance, where studies have shown that the public does not consider CCGS to be a mitigation technology, even being considered

one of the last, only surpassed by nuclear power and ocean storage (Shackley et al., 2004 and Itaoka et al., 2005). The latter was the motivation for studying geological sequestration. Nevertheless, acceptance increases when explanations are provided (Bachu, 2008). Finally and, probably, the biggest barrier is the lack/absence of legislations and regulations for CCGS implementation. Storage is a long-term operation in which CO_2 is expected to be retained for no less than a few centuries. The latter, hampers the stipulation of entities responsible for future problems and a monitoring programme (International Energy Agency Green House Gas, IEA GHG, 2004b and 2004c). Therefore, whilst there are issues such as one entity being defined as responsible, when the three stages (capture, transport and storage) are carried out by different entities, and/or legislation in force defines that injection shall be carried out in one country and leakage is detected in other, CCGS will not be implemented on a commercial scale.

3. CO_2 STORAGE IN DEEP AQUIFERS

3.1. COUPLED THERMO-HYDRO-MECHANICAL BEHAVIOUR

The focus of the present study is to analyse the injection of CO_2 in deep aquifers. CCGS projects that have deep aquifers as geological formations result in complex, thermo-hydro-mechanical coupled processes. Injecting carbon dioxide requires that the injection pressure is greater than the one established in the formation. In addition, the injection of CO_2 results in a desaturation process of the aquifer by displacing the resident water. The latter implies pressure build-up within the aquifer, which affects the effective stress regime resulting in deformations of the aquifer and caprock (Vilarrasa, 2012). The increasing pressure and spatial distribution depends on several aspects such as the injection rate, reservoir permeability and thickness, CO_2 conditions, injection temperature, etc.

Suitable media for CCGS projects should ideally be placed at depths of around 800 meters (Bachu, 2008), in order to ensure injection of CO_2 either in "supercritical" or liquid conditions, i.e. higher densities. It should be emphasized that there is no "supercritical" state and this is just a figure of expression in order to facilitate the designation of CO_2 at a certain temperature and pressure in which CO_2 behaves as a gas and a liquid. Taking this into consideration, the expression "supercritical state" is employed in order to facilitate description, whilst its true definitions should never be forgotten. In addition, regardless its conditions carbon dioxide will always be lighter than the resident water. Consequently, buoyancy forces rise and CO_2 tends to float. Figure 3.1, shows the CO_2 saturation profile, being observed the tendency of the CO_2 to accumulate at the top of the aquifer due to the buoyancy forces. This means that a sealing rock is required and should be characterized by a very low permeability, in order to prevent vertical migration.

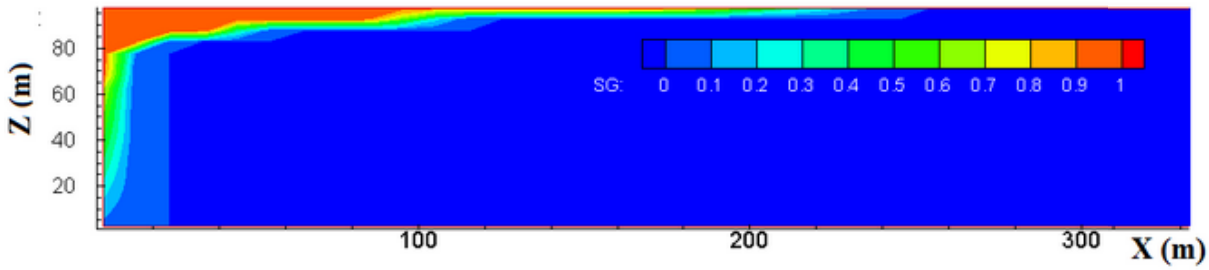

Figure 3.1 – CO_2 saturation profile (Zhang, 2014)

Thermal effects emerge if the injected CO_2 has a different temperature from the storage formation. In the context of this study the isothermal analysis refers to injecting CO_2 in supercritical conditions and the non-isothermal, to CO_2 in liquid conditions (lower temperature than the reservoir). Liquid injection brings several advantages when compared to supercritical. Liquid CO_2 is characterized by a higher density than in supercritical conditions. Therefore, for a given mass of CO_2, a smaller volume of resident

water of the formation has to be displaced, leading to a lower overpressure in the reservoir. Furthermore, should CO_2 is injected in liquid conditions, buoyancy forces are lower and viscosity higher, implying safer storage conditions. In addition, Vilarrasa (2012) states that injecting liquid CO_2 is energetically more efficient than in supercritical conditions, since injection is carried out in the same state as that in which CO_2 is transported. However, liquid CO_2 implies lower temperature, inducing thermal stresses i.e. contractive behaviour that could affect caprock integrity. The latter brought the motivation for carrying out a non-isothermal study. Figure 3.2 represents in a schematic and simple way, through Mohr circles, the mechanical behaviour during CO_2 injection where the effective stress of the geomaterial is first reduced due to overpressure during the desaturation process followed by an additional reduction due to thermal contraction.

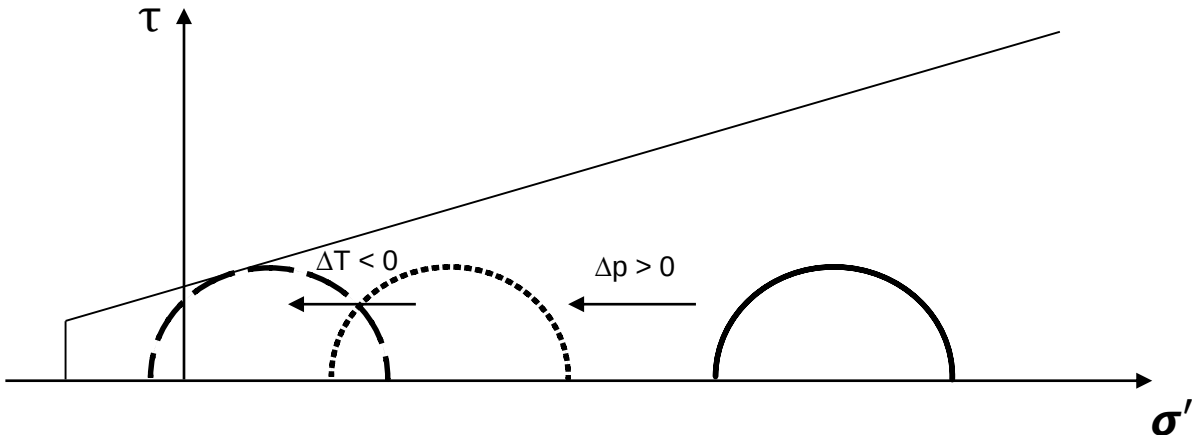

Figure 3.2 – Scheme of Mohr-Coulomb circles stress path during CO_2 injection

Once injected in deep aquifers, several physical and chemical phenomena take place such as:

- Fluid flow due to pressure gradients imposed by injection;
- Fluid flow due to natural hydraulic gradients;
- Buoyancy forces due to differences between resident water and CO_2;
- CO_2 dissolution in water;
- Mineral carbonation;
- Diffusion.

3.2. UNSATURATED GEOMATERIAL

Due to the desaturation process, some concepts of unsaturated geomaterials will be presented below. The matrix of a geomaterial is comprised by three phases. The grains of the geomaterial comprise the solid matrix, whereas the remaining phases are enclosed within what are called voids. The voids can be either filled with liquid, gas or both. Unsaturated conditions imply that the pores are filled simultaneously with water and CO_2. Each one has its own mass, volume and pressure. The degree of

saturation is the parameter used to describe the state of a geomaterial and is defined as the ratio between the volume of water and the volume of voids (Equation 3.1). Figure 3.3 illustrates the geomaterial matrix concept.

$$S = \frac{V_w}{V_v} \tag{3.1}$$

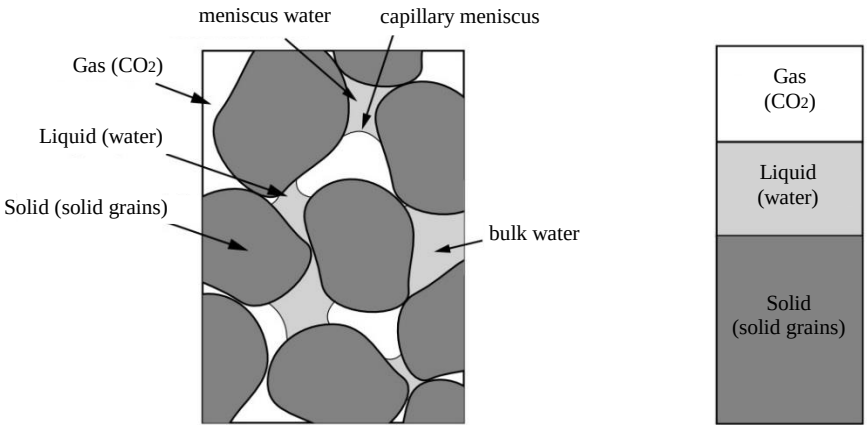

Figure 3.3 – Geomaterial matrix concept (adapted from Eichenberger, 2013)

Capillary Mechanisms

Capillary phenomena can be described as the motion of water in porous media that counters the gravity force. This physical mechanism depends on the type of liquid (surface tension) and on the surface (contact angle). Figure 3.4a, shows that in the bulk fluid the forces acting on a molecule are equal in all directions, so the molecule feels no net force. However, there are regions where unbalanced attractive forces with a downward direction are generated. In these conditions the liquid phase along with the gaseous phase form an interphase which when in contact with the solid particles, it curves and a meniscus is formed (Figure 3.4b) (Laloui, 2010).

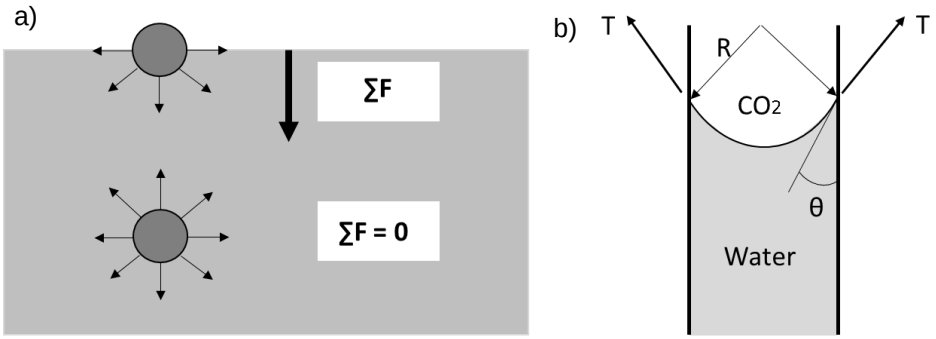

Figure 3.4 – a) Equilibrium of water molecules; b) Capillary meniscus (adapted from Laloui, 2010)

Geomaterial Suction

In the context of soil/rock mechanics the capillary meniscus results in the appearance of suction forces, which are defined as:

$$s = (p_c - p_w) \tag{3.2}$$

where, p_c is CO_2 pressure and p_w water pressure.

Water Retention Behaviour

Assuming that a saturated geomaterial is exposed to desaturation, it starts to lose water on the interface. With the continuous water loss, capillary menisci are generated, while the geomaterial remains in almost saturated conditions. The appearance of this capillary mechanism is followed by an increase in negative pore water pressure, i.e. suction. With the continuous evolution of the desaturation process, the meniscus curvature will increase until it reaches a critical angle (θ_{cr}). As soon as this critical value is reached the meniscus is displaced and CO_2 enters the geomaterial matrix. The suction value above which the degree of saturation becomes lower than one, is called 'air entry value' (s_E). At this stage the geomaterial is in a partially saturated condition. The mechanism described occurs from the larger pores to the smaller ones until it reaches a state of residual saturationS_{res}. The relation between suction and degree of saturation enables us to describe the water retention behaviour of a geomaterial and it is represented by the water retention curve (WRC) presented in Figure 3.5.

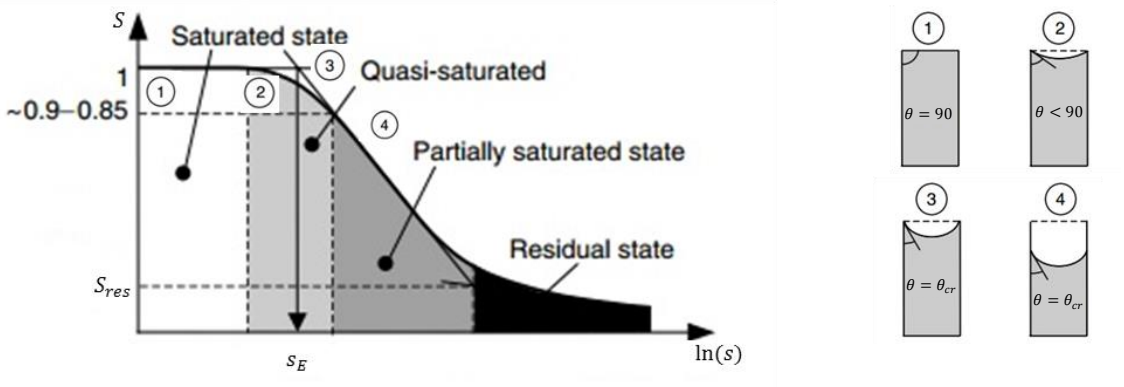

Figure 3.5 – Water retention curve (adapted from Eichenberger, 2013)

3.3. THEORETICAL FRAMEWORK AND FIELD EQUATIONS

The theoretical framework treats a partially saturated medium as a multiphase system, in which the voids are filled with liquid water and carbon dioxide. Therefore, the system is broken down into three phases (water, CO_2 and solid), of which the water phase consists of liquid water and dissolved carbon dioxide, the CO_2 phase of dry CO_2 and the solid consists of the solid grains. Finally, the system can be described, resorting to the representative elementary volume (REV) with the following components:

- Solid material, i.e. the solid phase, denoted here by the subscript *s;*
- The CO_2 phase, consisting of the injected CO_2 denoted here by the subscript *c*;
- The water phase, consisting of the water formation (*w*) and the dissolved carbon dioxide in water (*dc*).

The framework presented below takes into account the following processes: multiphase fluid flow occurring under pressure and temperature governed by advective and non-advective (diffusion) flows; interaction between fluids, addressing relative permeability evolution of water and CO_2 and the exchange terms due to CO_2 dissolution and degassing phenomena; heat flow through convection and conduction; stress-strain relationship; effective stress changes due to fluid pressure and temperature variations. Figure 3.6 shows the components of the mixture.

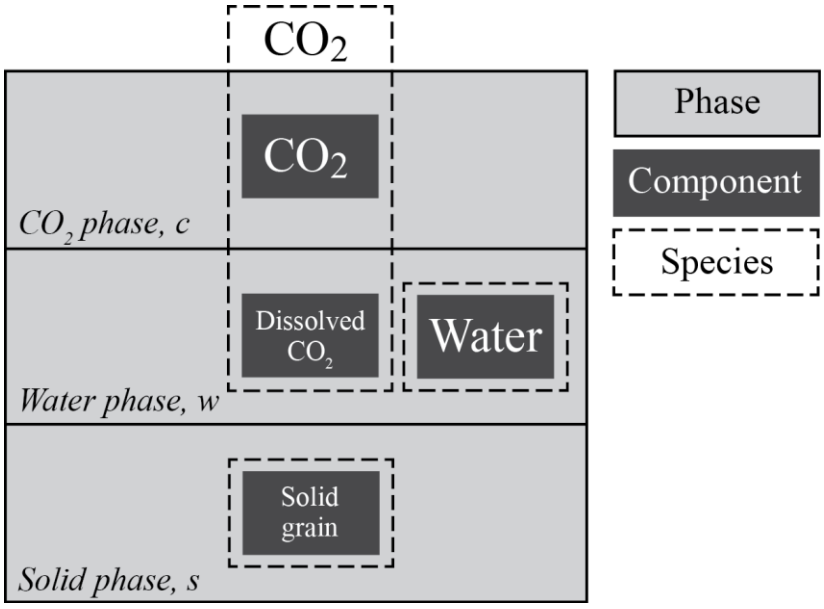

Figure 3.6 - Phases and species of the system (Li C., 2013)

The equations are written following the macroscopic approach because on a microscopic level the status of a phase is described in such a scale that discontinuities, which are smaller than the macroscopic magnitudes, can be examined. Such a level of detail is not necessary and for a more practical description and to enable the assessment of quantities that can be measured through laboratory tests, a macroscopic approach is more advantageous. On a macroscopic level, the porous medium domain is equivalent to a material where all the phases are thought to be continuously distributed throughout space, i.e. at any point all phases are present implying that the latter discontinuities can no longer be

detected. Thus, only three mass balance equations are required (one for each species) along with momentum, energy and constitutive equations to fully describe the thermo-hydro-mechanical behaviour (Bear, 1988).

3.3.1. MASS CONSERVATION EQUATIONS

Following the compositional approach (Panday and Corapcioglu, 1989), the mass balance equations are written for the species rather than the phases. This has the advantage of the exchange terms between phases being cancelled out. Furthermore, the equations follow the Lagrangian updated formulation (Charlier, 1987), which considers that the surface of the volume element is moving along with the fluid. This implies that fluid flow cannot cross this surface, hence the total mass within the volume element is automatically conserved and large deformations and displacements are considered. Water phase pressure p_w, CO2 phase pressure p_c, temperature T and solid displacement field $\boldsymbol{u}$ are considered as the primary state variables to describe the state of the material.

3.3.1.1. SOLID

Considering a compressible solid phase and for a certain volume V of the REV the mass conservation equation for the solid species can be written as:

$$\frac{\partial}{\partial t}\left((1-n)\rho_s\right) + div\left[(1-n)\rho_s\left(\frac{\partial \boldsymbol{u}}{\partial t}\right)\right] = 0 \tag{3.3}$$

where n is porosity, ρ_s solid density, t is time and $\frac{\partial u}{\partial t} = \boldsymbol{v_s}$ is the volumetric deformation rate. Expanding the equation (3.3) we obtain:

$$-\frac{\partial n}{\partial t}\rho_s + (1-n)\frac{\partial \rho_s}{\partial t} - (1-n)\boldsymbol{grad}(\rho_s)\boldsymbol{v_s} + \rho_s div\left((1-n)\boldsymbol{v_s}\right) = 0 \tag{3.4}$$

dividing equation 3.4 by ρ_s,the latter, can also be written as follows:

$$\frac{\partial n}{\partial t} = (1-n)\frac{1}{\rho_s}\frac{d^s\rho_s}{dt} + div[(1-n)(\boldsymbol{v_s})] \tag{3.5}$$

Resorting to Lewis and Schrefler (1987) the expression for the solid density variation is expressed as:

$$\frac{1}{\rho_s}\frac{d^s\rho_s}{dt} = \frac{1}{1-n}\left[(b-n)\frac{1}{K_s}\frac{d}{dt}(S_w p_w + (1-S_w)p_c) - \beta_s(b-n)\frac{\partial T}{\partial t} - (1-b)div(\boldsymbol{v_s})\right] \tag{3.6}$$

where, K_s is the bulk modulus of the solid material, S_w water phase saturation, $(1-S_w)$ is CO2 phase saturation, p_w water phase pressure, p_c CO2 phase pressure, β_s volumetric thermal expansion coefficient for the solid material, T temperature and $(1-b) = {}^{K_T}/_{K_s}$ is the Biot's constant which represents the relation between the compressibility of the solid skeleton with the solid grains. Neglecting the saturation temperature dependency, saturation is a function of the capillary pressure (suction), expressed by s in further expressions and which can be expressed as the difference between the carbon

dioxide phase pressure and the water phase pressure. Finally, by introducing (3.6) in (3.5) we can express the porosity variation through the primary state variables:

$$\frac{\partial n}{\partial t} = (b-n)\left[\frac{1}{K_s}\frac{d}{dt}(S_w p_w + (1-S_w)p_c) - \beta_s \frac{\partial T}{\partial t} + div(\boldsymbol{v_s})\right] \tag{3.7}$$

3.3.1.2. WATER SPECIES

The mass balance for water species can be written as:

$$\frac{d^w(nS_w\rho_w)}{dt} + \rho_w n S_w div(\boldsymbol{v_w}) = 0 \tag{3.8}$$

where, the first term refers to the storage term and the second to the water phase advective flow, and ρ_w is the water phase density. The equation (3.8) can be expanded as follows:

$$S_w\rho_w\frac{\partial n}{\partial t} + n\rho_w\frac{\partial S_w}{\partial t} + nS_w\frac{\partial \rho_w}{\partial t} + \boldsymbol{grad}(\rho_w n S_w)\boldsymbol{v_{ws}} + \rho_w n S_w div(\boldsymbol{v_w}) = 0 \tag{3.9}$$

where $v_{ws} = v_w - v_s$. Using a Lagrangian description of continuum deformation, the motion of the species is expressed with respect to the motion of the solid phase. Thus introducing the equation (3.7) in (3.9) and resorting to Darcy's law to describe the advective flow, the mass balance equation for the water species results in:

$$\begin{aligned}
&\left[n\rho_w\frac{\partial S_w}{\partial s} + \frac{(b-n)}{K_s}S_w\rho_w\left(1 - S_w - \frac{\partial S_w}{\partial s}s\right)\right]\frac{\partial p_c}{\partial t} \\
&\left[-n\rho_w\frac{\partial S_w}{\partial s} + S_w n\frac{\partial \rho_w}{\partial p_w} + \frac{(b-n)}{K_s}S_w\rho_w\left(S_w + \frac{\partial S_w}{\partial s}s\right)\right]\frac{\partial p_w}{\partial t} \\
&-[nS_w\rho_w\beta_w + (\mathrm{b}-\mathrm{n})S_w\rho_w\beta_s]\frac{\partial \mathrm{T}}{\partial t} \\
&+b\,\rho_w S_w\, div(\boldsymbol{v_s}) \\
&+div\left(\rho_w\frac{k_{rw}\boldsymbol{k}_{int}}{\mu_w}\left(-\boldsymbol{grad}(p_w) + \rho_w\boldsymbol{g}\right)\right) = 0
\end{aligned} \tag{3.10}$$

where, β_w is the volumetric thermal expansion coefficient of water, k_{rw} is the water relative permeability, related to the state of saturation and k_{int} the intrinsic permeability and μ_w the water viscosity. The concepts of intrinsic and relative permeabilities are addressed in more detail in section 3.3.4.2.

3.3.1.3. CO_2 SPECIES

Hereinafter, firstly the mass balance equations will be presented separately for the components, CO_2 and dissolved CO_2 and following that, the mass balance equation for the species will be expressed.

CO2 Component

The mass balance equation for the CO2 component in the gas phase can be expressed as:

$$\frac{d^c(nS_c\rho_c)}{dt} + \rho_c n S_c div(\boldsymbol{v_c}) = f_{CO2-w} \tag{3.11}$$

where, S_c is the carbon dioxide saturation which is defined as $S_c = (1 - S_w)$, ρ_c the carbon dioxide density and f_{CO2-w} refers to the exchange term, i.e the process of dissolution of carbon dioxide in water. Following the same logic used for the water species the mass balance equation can be written as:

$$\begin{aligned}
&\left[-n\rho_c \frac{\partial S_w}{\partial s} + (1 - S_w) n\, \rho_c \frac{\partial \rho_c}{\partial p_c} + \frac{(b-n)}{K_s}\,(1 - S_w)\,\rho_c \left(1 - S_w - \frac{\partial S_w}{\partial s} s\right)\right] \frac{\partial p_c}{\partial t} \\
&+ \left[n\rho_c \frac{\partial S_w}{\partial s} + \frac{(b-n)}{K_s}\,(1 - S_w)\,\rho_c \left(S_w + \frac{\partial S_w}{\partial s} s\right)\right] \frac{\partial p_w}{\partial t} \\
&+ \left[-(b-n)\,(1 - S_w)\,\rho_c \beta_s + (1 - S_w) n\, \rho_c \frac{\partial \rho_c}{\partial T}\right] \frac{\partial T}{\partial t} \\
&+ b\,\rho_c\,(1 - S_w)\, div(\boldsymbol{v_s}) \\
&+ div\left(\rho_c \frac{k_{rc}\boldsymbol{k}_{int}}{\mu_c}\,(-\boldsymbol{grad}(p_c) + \rho_c \boldsymbol{g})\right) = f_{co2-w}
\end{aligned} \tag{3.12}$$

where, k_{rc} is the carbon dioxide relative permeability, k_{int} the intrinsic permeability of the medium and μ_c the carbon dioxide viscosity. The terms $\partial\rho_c/\partial p_c$ and $\partial\rho_c/\partial T$ represent the carbon dioxide density variation with pressure and temperature, respectively. Carbon dioxide being a real gas requires a parameter which describes the non-ideal behaviour of the gas. For this purpose, and resorting to Peng and Robinson (1976) state equation a Z parameter is introduced. Hence the relation between density and pressure can be written as follows:

$$\rho_c = \frac{1}{Z}\frac{M}{R}\frac{p_c}{T} \tag{3.13}$$

where, Z is the compressibility parameter, M is the CO2 molar mass and R is the gas constant. It is important to note that Z is pressure and temperature-dependent. Hence the density variation with respect to time is expressed as:

$$\frac{d\rho_c}{dt} = \frac{\partial \rho_c}{\partial p_c}\frac{\partial p_c}{\partial t} + \frac{\partial \rho_c}{\partial T}\frac{\partial T}{\partial t} \tag{3.14}$$

where,

$$\frac{\partial \rho_c}{\partial p_c} = \frac{M}{ZRT}\left(1 - \frac{p_c}{Z}\frac{dZ}{dp_c}\right) \; and \; \frac{\partial \rho_c}{\partial T} = -\frac{p_c M}{ZRT}\left(\frac{1}{T} + \frac{1}{Z}\frac{dZ}{dT}\right) \tag{3.15}$$

Dissolved CO_2 component

The mass conservation for the dissolved CO_2 component is written as:

$$\frac{d^{dc}(nS_w\rho_{dc})}{dt} + div(\boldsymbol{i}_{dc}) + \rho_{dc} n S_w div(\boldsymbol{v_w}) = f_{w-CO2} \tag{3.16}$$

where, ρ_{dc} is the mass of dissolved CO_2 per unit volume of water, the second term refers to the non-advective flow (diffusion), which is governed by Fick's law and the term on the right hand side is the rate at which the dissolved CO_2 transfers from the water phase to the CO_2 phase (degassing phenomenon). Developing equation 3.16, it is obtained:

$$\begin{aligned}
&\left[n\rho_{dc}\frac{\partial S_w}{\partial s} + n\,S_w\frac{\partial \rho_{dc}}{\partial p_c} + \frac{(b-n)}{K_s}\;S_w\,\rho_{dc}\left(1 - S_w - \frac{\partial S_w}{\partial s}s\right)\right]\frac{\partial p_c}{\partial t}\\
&\left[-n\rho_{dc}\frac{\partial S_w}{\partial s} + \frac{(b-n)}{K_s}\;S_w\,\rho_{dc}\,(S_w + \frac{\partial S_w}{\partial s}s)\right]\frac{\partial p_w}{\partial t}\\
&\left[-(b-n)\;S_w\,\rho_{dc}\,\beta_s + nS_w\frac{\partial \rho_{dc}}{\partial T}\right]\frac{\partial T}{\partial t}\\
&+b\,\rho_{dc}\,S_w\;div(\boldsymbol{v_s})\\
&+div\left(\rho_{dc}\frac{k_{rw}\boldsymbol{k}_{int}}{\mu_w}\;(-\boldsymbol{grad}(p_w) + \rho_w\,\boldsymbol{g})\right)\\
&-div\left[n\;S_w\,\tau\;D_c\,\rho_w\,\boldsymbol{grad}\left(\frac{\rho_{dc}}{\rho_w}\right)\right] = f_{w-co2}
\end{aligned} \tag{3.17}$$

where, τ is the tortuosity of the porous media and D_c the diffusion coefficient of the dissolved carbon dioxide in water phase. Finally, and remembering the compositional approach, if we add the equation (3.12) with (3.17), the exchange terms will cancel out. In addition, by introducing the equation (3.14), the mass conservation for CO_2 species can be written as:

$$\begin{aligned}
&\left\{\begin{matrix} n(\rho_{dc}-\rho_c)\frac{\partial S_w}{\partial s} + n\,S_w\frac{\partial \rho_{dc}}{\partial p_c} + (1-S_w)n\,\rho_c\frac{\partial \rho_c}{\partial p_c} \\ +\frac{(b-n)}{K_s}\;[(1-\;S_w)\rho_c + \;S_w\,\rho_{dc}](1 - S_w - \frac{\partial S_w}{\partial s}s)\end{matrix}\right\}\frac{\partial p_c}{\partial t}\\
&+\left\{-n(\rho_{dc}-\rho_c)\frac{\partial S_w}{\partial s} + \frac{(b-n)}{K_s}\;[(1-\;S_w)\rho_c + \;S_w\,\rho_{dc}](S_w + \frac{\partial S_w}{\partial s}s)\right\}\frac{\partial p_w}{\partial t}\\
&-\left\{\begin{matrix}(b-n)\;\beta_s\;[(1-\;S_w)\rho_c + \;S_w\,\rho_{dc}] - nS_w\frac{\partial \rho_{dc}}{\partial T} \\ +(1-\;S_w)\,n\,\rho_c\frac{\partial \rho_c}{\partial T}\end{matrix}\right\}\frac{\partial T}{\partial t}\\
&+[(1-\;S_w)\rho_c + \;S_w\,\rho_{dc}]b\;div\,(\boldsymbol{v_s})\\
&+div\left[\rho_{dc}\frac{k_{rw}\boldsymbol{k}_{int}}{\mu_w}\;(-\boldsymbol{grad}(p_w) + \rho_w\,\boldsymbol{g})\right]\\
&+div\left[\rho_c\frac{k_{rc}\boldsymbol{k}_{int}}{\mu_c}\;(-\boldsymbol{grad}(p_c) + \rho_c\,\boldsymbol{g})\right]\\
&-div\left[n\;S_w\,\tau\;D_c\,\rho_w\,\boldsymbol{grad}\left(\frac{\rho_{dc}}{\rho_w}\right)\right] = 0
\end{aligned} \tag{3.18}$$

3.3.2. MOMENTUM CONSERVATION

If the inertial terms are neglected, the equilibrium of the multiphase media can be expressed as:

$$\boldsymbol{div}(\boldsymbol{\sigma}) + \rho \boldsymbol{g} = 0 \tag{3.19}$$

where, $\boldsymbol{\sigma}$ is the total stress tensor and ρ is the mixture density, which can be written as:

$$\rho = (1-n)\rho_s + nS_w\rho_w + n(1-S_w)\rho_c \tag{3.20}$$

Resorting to the generalized effective stress formulation (Laloui and Nuth, 2009) the effective stress is defined as:

$$\boldsymbol{\sigma}' = \boldsymbol{\sigma} - bp_c\boldsymbol{I} + bS_w(p_c - p_w)\boldsymbol{I} \tag{3.21}$$

where, $\boldsymbol{I}$ is the identity matrix and b is the Biot coefficient, which was considered to be equal to 1. This formulation describes most of the effects of suction in a single equation, which is particularly interesting when dealing with coupled hydro-mechanical processes by defining an average fluid pressure as follows:

$$p_f = S_w p_w + (1-S_w)p_c \tag{3.22}$$

the effective stress can be expressed as:

$$\boldsymbol{\sigma}' = \boldsymbol{\sigma} - bp_f\boldsymbol{I} \tag{3.23}$$

3.3.3. ENERGY CONSERVATION EQUATION

Prior to the equation it is important to emphasize the fact that this framework assumes local thermal equilibrium (LTE). Due to this assumption, a unique temperature can be defined for the medium ($T_s = T_w = T_c = T$) and a unique energy conservation equation is required. The basic form of the energy conservation equation can be defined as:

$$\frac{\partial H}{\partial t} + div[(-\lambda_{medium})\boldsymbol{grad}T] + div(\boldsymbol{q}) = 0 \tag{3.24}$$

where, λ_{medium} is the thermal conductivity of the medium, q is the convection flow and H is enthalpy. Neglecting the enthalpy pressure dependency (addressed in the next section), one can be written as:

$$H = \left[nS_w\rho_w c_{p,w} + n(1-S_w)\rho_c c_{p,c} + (1-n)\rho_s c_{p,s}\right](T - T_0) \tag{3.25}$$

Neglecting the contribution of the dissolved CO_2, the convection term of the solid part, the latent heat due to phase change and bearing in mind that the exchange terms cancelled out due to the compositional approach, the energy conservation equation can be expressed as (Lewis and Schrefler, 1988):

$$\begin{aligned}&\left[nS_w\rho_w c_{p,w} + n(1-S_w)\rho_c c_{p,c} + (1-n)\rho_s c_{p,s}\right]\frac{\partial T}{\partial t}\\&-div[(n\lambda_w + n\lambda_c + (1-n)\lambda_s)\boldsymbol{grad}T]\\&+\left[n\rho_w c_{p,w}\boldsymbol{q_w} + n\rho_c c_{p,c}\boldsymbol{q_c}\right]gradT = 0\end{aligned} \tag{3.26}$$

where, λ_α and $c_{p,\alpha}$ refer to the thermal conductivity and the specific heat capacity of the components, respectively. The first term refers to the storage term, the second to the conduction term which is governed by Fourier's law and the third term to the convection flow.

3.3.4. CONSTITUTIVE EQUATIONS

3.3.4.1. CO_2 PROPERTIES

It was pointed out in section 2.4 that one of the crucial criteria to evaluate during the design stage of a CO_2 injection project is the aquifer depth. The reason for this is due to the high oscillations of CO_2 properties with pressure and temperature. Therefore, it is necessary to make a detailed assessment of its properties. For this purpose the state equation (EOS), proposed by Peng and Robinson (1976) was employed to determine the CO_2 density and a compressibility factor Z was introduced to account for the deviation from a perfect gas behaviour.

The Peng-Robinson Equation of State is presented as follows (Peng and Robinson, 1976):

$$p = \frac{RT}{V_m - b} - \frac{a}{V_m^2 + 2 * b * V_m - b^2} \tag{3.27}$$

where,

$$a_c = 0.457235\frac{R^2T_{cri}^2}{p_{cri}}\ ;\ b = \frac{0.077796*R*T_{cri}}{p_{cri}};\ \alpha = (1+\kappa(1-T_r^{0.5}))^2\ ;\ a = a_c * \alpha \tag{3.28}$$

and,

$$p = \frac{RT}{V_m - b} - \frac{a}{V_m^2 + 2 * b * V_m - b^2} \tag{3.29}$$

where p is the absolute pressure [Pa], p_{cri} the critical pressure $\left(p_{cri,CO2} = 7377300\ [Pa]\right)$, T the absolute temperature, T_{cri} the critical temperature $\left(T_{cri,CO2} = 304.1282\ [K]\right)$, V_m the molar volume ($V_m = \frac{Volume}{number\ of\ moles}$), R the ideal gas constant $R = 8.314472\ \left[\frac{J}{mol*K}\right]$, ω is the acentric factor of the species ($\omega_{CO2} = 0.239\ [-]$), and T_r is the reduced temperature [-].

We can then plot the compressibility factor in the real gas law, to get the corrected volume:

$$V_{corrected} = Z.\frac{R.T}{P} \tag{3.30}$$

and finally the density can be expressed as follows:

$$\rho_{CO2} = \frac{MW}{V_{corrected}} = \frac{MW_{CO2}.P}{Z.R.T} \tag{3.31}$$

where ρ_{CO2} is the CO2 density and MW_{CO2} is the molar mass of CO2.

To describe the equilibrium between dissolved CO2 and gaseous CO2, Henry's Law is employed which defines the quantity of dissolved CO2 in water, using the following expression:

$$P_c = K_{eq,g-l}^{CO_2} X_{dc} \tag{3.32}$$

where, P_c is the pressure at which the carbon dioxide will dissolve, $K_{eq,g-l}^{CO_2}$ is Henry's coefficient which depends only on temperature and X_{dc} is the mass fraction of dissolved CO2 in water. Equation (3.32) is valid for low pressures. However it over predicts gas dissolution at higher pressures. For this reason, an extended Henry's law was employed, which accounts the CO2 dissolution in water at higher pressures through the fugacity coefficient (Pruess and Garcia, 2002) and is defined as:

$$\phi P_c = K_{eq,g-l}^{CO_2} X_{dc} \tag{3.33}$$

where, ϕ is the carbon dioxide fugacity coefficient and is determined according to Peng and Robinson (1976). The Peng and Robinson EOS was computed in the LAGAMINE source code (Charlier et al., 2001) by Li C. (2013) and Figure 3.7 shows the relation of the compressibility factor Z, density, fugacity and viscosity with temperature and pressure. The CO2 viscosity is determined according to Fenghour et al. (1998).

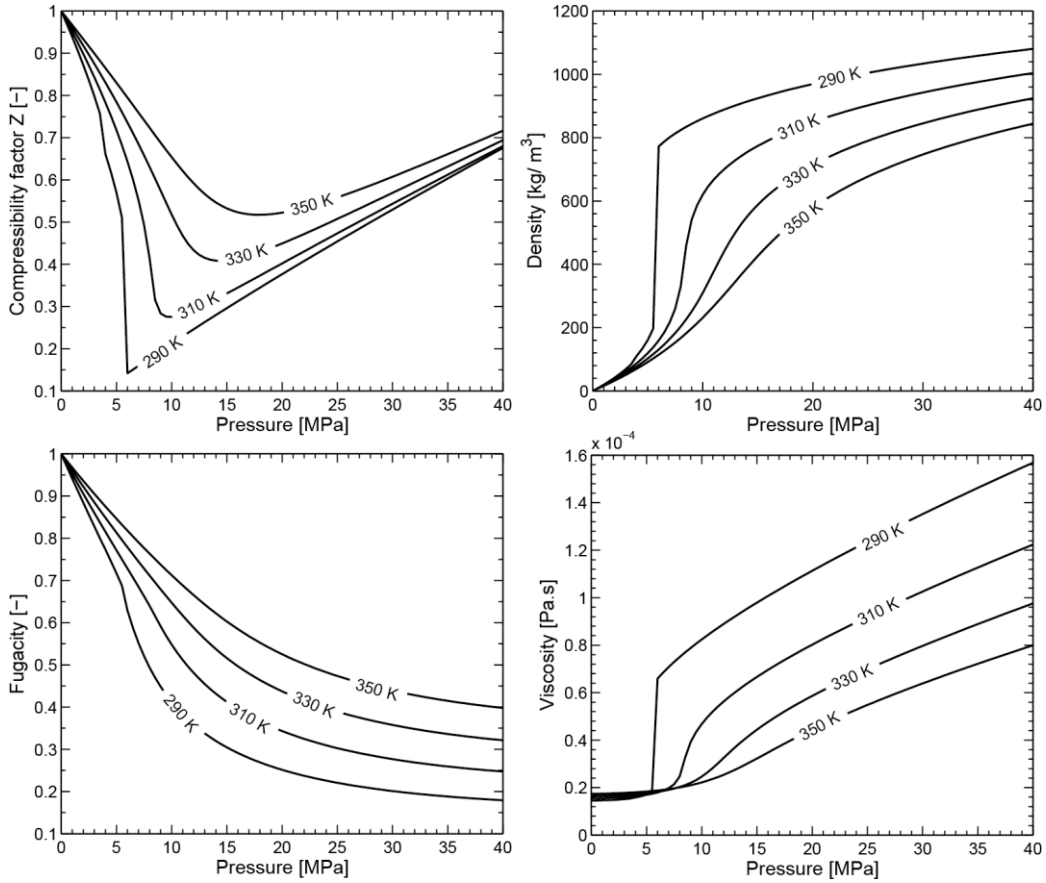

Figure 3.7 - Calculated compressibility factor Z, density, fugacity and viscosity (Li C., 2013)

In addition, as carbon dioxide is a real gas, the Joule-Thomson effect has to be addressed. This effect describes the temperature variation that occurs when a gas expands or contracts at constant enthalpy. Enthalpy measures the heat flow of a reversible work system at constant pressure and depends on temperature and pressure:

$$H = f(T, P) \tag{3.34}$$

The latter can be written in the infinitesimal form as follows:

$$dH = \left(\frac{\partial H}{\partial T}\right)_P dT + \left(\frac{\partial H}{\partial P}\right)_T dP \tag{3.35}$$

As stated before, for a reversible process at constant pressure, enthalpy is equal to the changes of heat and can be written as:

$$dH = \left(\frac{\partial H}{\partial T}\right)_p dT = c_p dT \tag{3.36}$$

Hence,

$$c_p = \left(\frac{\partial H}{\partial T}\right)_p \tag{3.37}$$

where, c_p is the specific heat capacity at constant pressure. To determine the second term, let us consider an adiabatic process (no heat changes, i.e. constant enthalpy):

$$c_p dT + \left(\frac{\partial H}{\partial P}\right)_T dP = 0 \tag{3.38}$$

$$\left(\frac{\partial H}{\partial P}\right)_T = -c_p \left(\frac{\partial T}{\partial P}\right)_H = -c_p \mu_{JT} \tag{3.39}$$

where, μ_{JT} is the Joule-Thomson coefficient, which relates the increasing temperature with increasing pressure (heating phenomenon) and the decreasing temperature with decreasing pressure (cooling phenomenon). The Joule-Thomson coefficient can be measured through an experiment that consists of a thermal isolated system, where on one side we have a gas with a pressure P1, volume V1 and temperature T1 and on the other we have the same gas at P2, V2 and T2 (Figure 3.8). It is important to state that these two sides are divided by a porous plug and that the system is not in equilibrium (P1>P2), implying that the gas will flow from side 1 to side 2. By carrying out several experiments at different ΔP

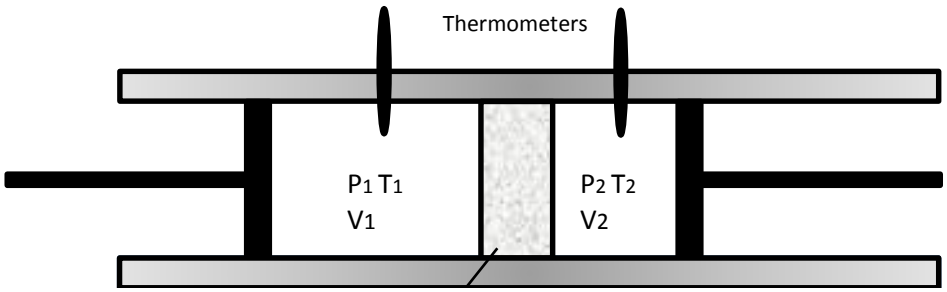

Figure 3.8 - The Joule-Thomson experiment

and measuring the ΔT on both sides a graph ΔT vs ΔP can be plotted and an almost linear function is obtained where the slope is the μ_{JT} (Bawendi and Keith, 2008).

Regarding CO_2 injection into deep aquifers, the major concern relative to the Joule-Thomson effect is the initial sharp increase in pressure during the desaturation process, which can result in a temperature increase. However, depending on the project conditions this effect can be neglected. Oldenburg (2008) carried out several studies concerning this effect in CCGS projects, concluding that it has a minor effect and that, when analysing the Joule-Thomson effect in porous media, it is diminished due to the effects of permeability and porosity. Even though, the latter study considers different conditions, what is at stake is the temperature variation with pressure. Resorting to the National Institute of Standards and Technology (NIST) online database, a pressure difference of 5 MPa results in an increase of 3.7K for a pressure range of 10 to 15 MPa (Figure 3.9).

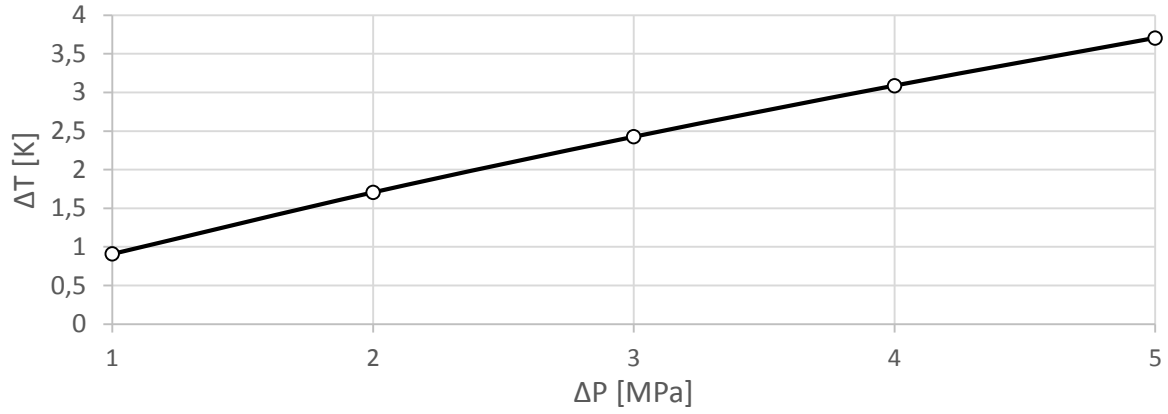

Figure 3.9 - Joule Thomson effect for a temperature reference of 300K (NIST web chemistry book)

3.3.4.2. HYDRAULIC PROPERTIES

The relation between suction $(s = p_c - p_w)$ and the degree of saturation enables us to describe the water retention behaviour which can be described by the water retention curve (WRC). The Van Genuchten (1980) function is widely employed to describe the WRC:

$$S = \left[1 + \left(\frac{s}{P_r}\right)^{\frac{1}{1-m}}\right]^{-m} \tag{3.40}$$

where, m and P_r are a material parameters. Here it should be enlightened that the latter formulation, was obtained by carrying out laboratory experiments considering partially saturated porous media with water and air, instead of CO_2. Hence, this formulation is employed, whilst the author is aware that the presence of CO_2 would eventually affect the contact angle between the geomaterial and fluid, thus affecting the shape of the WRC.

Looking at the geomaterial matrix composition, there are two flowing phases considered in the system: the liquid phase and the gas phase. And in order to analyse multi-phase flow in reservoirs, it is essential

to define and understand the relative permeability of each flowing phase, as it affects the flow characteristics of reservoir fluids.

Relative permeability is a unique parameter for every fluid. It is defined as the ratio of the effective permeability of a fluid at a given saturation, compared to a base permeability. It depends on multiple factors such as fluid saturation, geometry of the pore space and pore size distribution in the geomaterial matrix, wettability of the fluids, and the fluid saturation history. However, the present work considers the relative permeabilities of each fluid phase as a function of water saturation.

The relative permeabilities, $k_{r\alpha}$ can be defined as a function of the degree of saturation. The following equations for the relative permeability of water and carbon dioxide are commonly employed:

$$k_{rw} = S_w^{CKW1}$$
$$k_{rc} = (1 - S_w)^{CKC1} \tag{3.41}$$

where, $CKW1$ and $CKC1$ are material parameters and the values used in this work are presented in Table 4.2. Equation 3.41, implies that once water saturation increases, the gas relative permeability decreases and the water relative permeability increases. Furthermore, it should be very clear that the relative permeabilities are related to the fluid phases while the intrinsic permeability is a solid phase property.

3.3.4.3. THERMO ELASTIC GEOMECHANICAL MODEL

For the mechanical behaviour of the isotropic material, a linear elastic model is applied, through the generalized Hooke's Law:

$$\boldsymbol{\sigma} = \boldsymbol{E}\varepsilon \tag{3.42}$$

where, $\boldsymbol{\sigma}$ is the stress tensor, $\boldsymbol{E}$ is the linear elastic tensor and ε the strain tensor. However, to take into account the deformations due to temperature, the stress-strain relationship is extended to the form:

$$\boldsymbol{\sigma} = \boldsymbol{E}\varepsilon - \boldsymbol{\eta}\Delta T \tag{3.43}$$

where, $\boldsymbol{\eta}(T - T_0)$ is the strain contribution due to temperature, which for an isotropic material is defined as:

$$\boldsymbol{\eta} = \frac{E}{1 - 2\nu}\alpha_T \boldsymbol{I} \tag{3.44}$$

where, E is the Young modulus, υ the Poisson coefficient and α_T is the linear thermal expansion coefficient. Finally, the total elastic deformation is defined as the sum of the mechanical and the temperature strains:

$$\varepsilon = \frac{1}{\boldsymbol{E}}\boldsymbol{\sigma} + \alpha_T \Delta T \boldsymbol{I} \tag{3.45}$$

4. MODEL CHARACTERISTICS

4.1. GEOMETRY AND BOUNDARY CONDITIONS

The geometry consists of an axisymmetric three layer model: an aquifer confined by an upper and bottom seals, with 100, 50 and 20 meters thickness, respectively. The top of the upper seal (caprock) is located at a depth of 1000 meters and the length of the model is 1000 meters. A vertical injection well is placed on the left hand side of the model with a radius of 0.15 meters in order to simulate parallel injection along the thickness of the aquifer. The mesh consist of 16811 quadrilateral elements with 8 nodes each. The mesh is refined close to the injection well, increasing progressively away from the well.

With regard to the hydraulic boundaries, the aquifer is considered to be open, which in modelling terms means holding a constant head boundary in time for CO_2 and for water (hydrostatic pressure) at the right boundary. The latter is placed at a certain distance, ensuring that the boundary condition does not influence the results. The thermal boundaries are defined with constant temperature at the top and bottom. The thermal perturbation doesn't reach these boundaries, so the nature of the boundary does not affect the results. The horizontal displacements in the right and left boundary are constrained and the vertical ones are blocked at the bottom. A constant vertical stress is applied on the upper part of the sealing caprock, through which the weight from the upper layer is represented. The latter, was computed considering only one layer from the surface until 1000 meters, with a specific mass of 2400 kg/m^3. All layers are in saturated conditions at an initial temperature of 330K. The temperature was determined, considering a geothermal gradient of 33K/km and a surface temperature of 297K. Figure 4.1 illustrates the geometry, boundary conditions and the elements that will be constantly measured, whereas, Figure 4.2 shows the mesh.

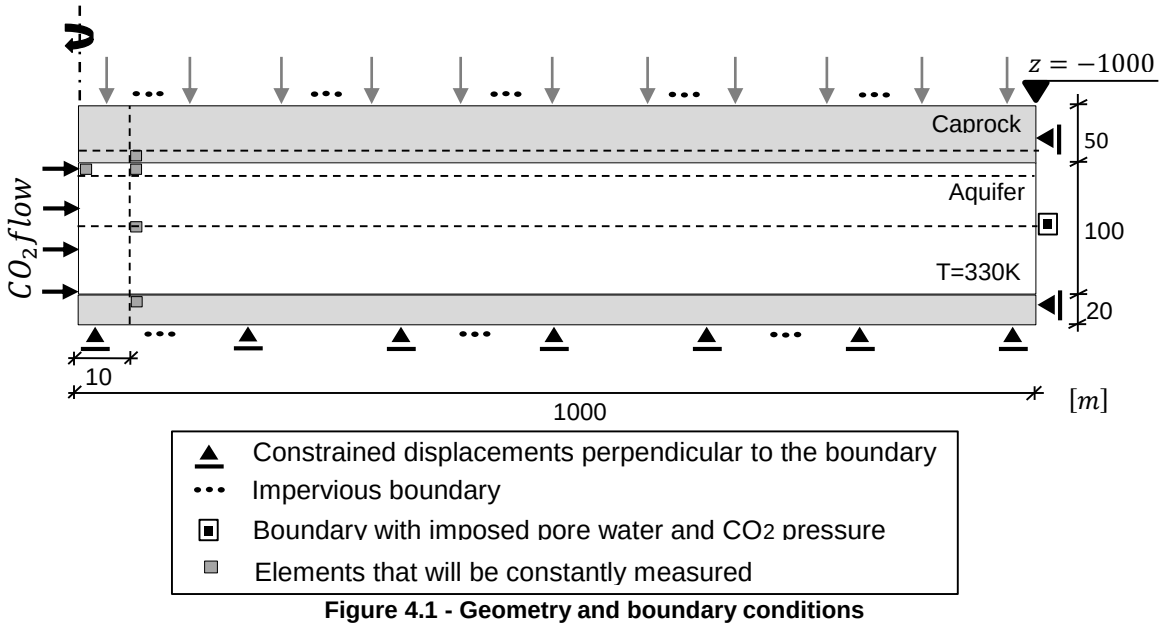

Figure 4.1 - Geometry and boundary conditions

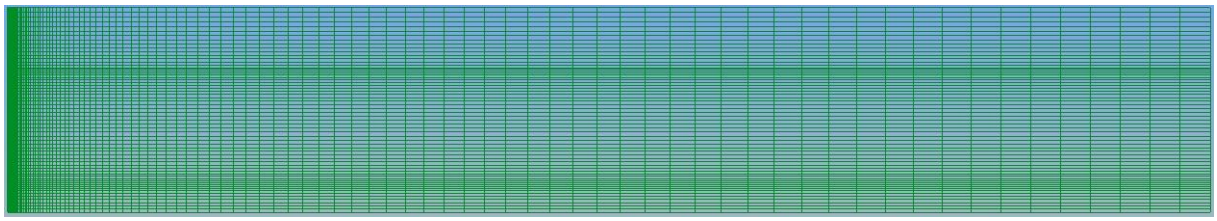

Figure 4.2 – Mesh of the model

4.2. MATERIAL CHARACTERISTICS

The material properties for the aquifer and caprock, correspond to reference values of sandstone and shale respectively. From Table 4.1 it can be observed that the mechanical and thermal properties of these materials have a wide range.

The properties adopted for the solid material and the two fluid are shown in Table 4.2. The main criteria for the chosen properties were the adopted values of Vilarrasa (2012) study and secondly the literature review. The evolution of the relative permeabilities of CO_2 and water for the aquifer and caprock are given in Figure 4.3.

Table 4.1 - Range of mechanical and thermal parameters of sandstone and shale from a literature review

Material	Reference	E $[GPa]$	υ $[-]$	λ $[W/mK]$	$\alpha_T \times 10^{-5}$ $[K^{-1}]$	c_p $[J/kgK]$	Comments
Shale	*Eseme et al. (2006)*	4.5-16	0.2-0.35	-	-	-	Experimental
	Rutqvist&Tsang (2002)	5	0.25	-	-	-	Numerical
	Vilarrasa (2012)	5	0.3	1	-	-	Numerical
	Bock (2009)	3.6-8.5	0.33	1.7	-	-	Experimental
	Robertson&Peck (1974)	-	-	-	1-3	770	Experimental
	Jobmann&Polster (2007)	4	0.33	1.5	0.75-1.55	1140-1380	Experimental
	Willeveau. (2005)	4-10	0.24-0.33	-	-	-	-
	Gens et al. (2007)	4-10	0.24-0.33	1.7	0.9-2.1	-	-
	Gilliam&Morgan (1987)	-	-	0.9-4.8	1.3	900-1465	Experimental
	Midttomme et al.(1998)	-	-	-	1.05-1.45	-	-
Sandstone	*Rutqvist&Tsang (2002)*	5	0.25	-	-	-	Numerical
	Vilarrasa (2012)	2.5	0.3	1	-	-	Numerical
	Somerton (1992)	5-30	0.33	1.3-2	1-10	-	Experimental
	Robertson&Peck (1974)	-	-	1	1.5-5.5	930	Experimental
	Gens et al. (2007)	4-10	0.24-0.33	1.7	0.9-2.1	-	-
	Abdulagatova et al. (2009)	-	-	-	2.8-3.62	-	Experimental
	Midttomme (1998)	-	-	-	2.5-4.2	-	-
	Wu et al. (2013)	5-40	0.05-0.5	-	-	-	Experimental
	Schärli&Rybach (2001)	-	-	-	-	750-1000	Experimental

Table 4.2 - Material properties of the simulation

Thermal parameters	Symbol	Unit	Caprock	Aquifer
Solid thermal conductivity	λ_s	W/(m.K)	1.50	2.50
Water thermal conductivity	λ_w	W/(m.K)	0.67	0.67
CO_2 thermal conductivity	λ_c	W/(m.K)	0.08	0.08
Solid specific heat capacity	$c_{p,s}$	J/(kg.K)	950	850
Water specific heat capacity	$c_{p,w}$	J/(kg.K)	4183	4183
CO_2 specific heat capacity	$c_{p,c}$	J/(kg.K)	2990	2990
Solid thermal expansion coefficient	β_s	K^{-1}	1.5×10^{-5}	1×10^{-5}
Water thermal expansion coefficient	β_w	K^{-1}	4.4×10^{-5}	4.4×10^{-5}
Flow parameters				
Intrinsic permeability	k_{int}	m^2	1×10^{-18}	1×10^{-13}
CO_2 relative permeability	k_{rc}	-	S_c^6	S_c^3
Water relative permeability	k_{rw}	-	S_w^6	S_w^3
Van Genuchten parameter	m	-	0.80	0.50
Van Genuchten parameter	P_r	MPa	0.60	0.02
Initial porosity	n_0	-	0.01	0.10
Other parameters				
Solid specific mass	ρ_s	kg/m^3	2700	2400
Water specific mass	ρ_w	kg/m^3	1000	1000
CO_2 specific mass	ρ_c	kg/m^3	801	801
Mechanical parameters				
Young modulus	E	GPa	5.0	2.5
Poisson ratio	υ	-	0.30	0.30
Initial stress factor	K_0	-	0.60	0.60

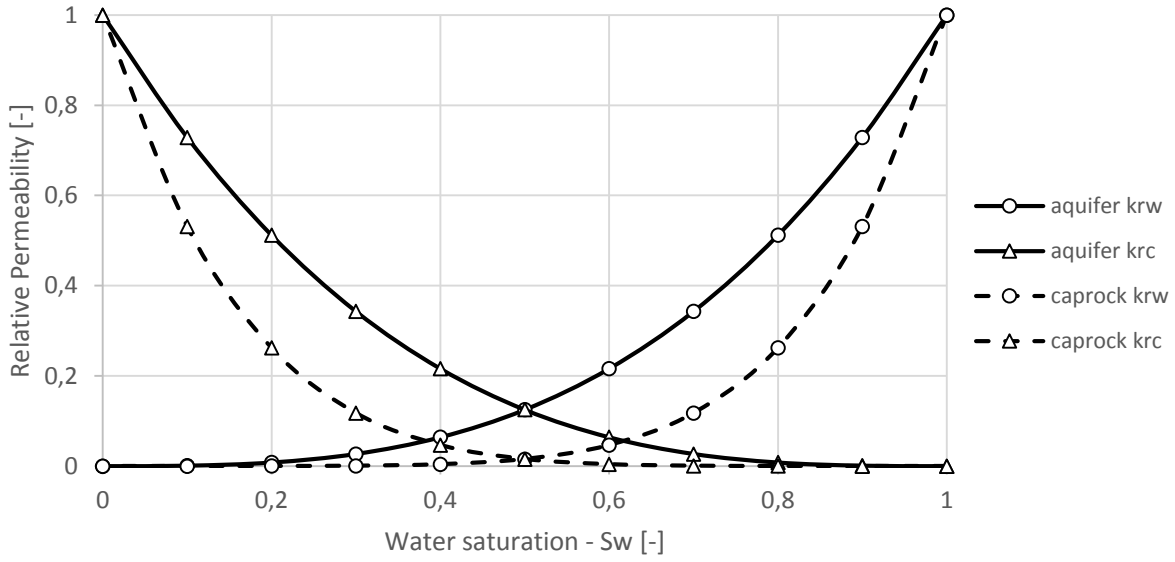

Figure 4.3 - Evolution of the water and CO_2 relative permeabilities for the aquifer and caprock

4.3. SIMULATION CHARACTERISTICS

An injection rate of 1 Mt per year is being considered over a period of 6 months (180 days), as described in Figure 4.4. The initial stresses are governed by the initial stress factor defined in equation 4.1. Rutqvist et al. (2008) found that values of $K_0 < 1$ are less favourable. Thus, a value of $K_0 = 0.6$ is considered. The model was designed on the finite element code LAGAMINE, developed by University of Liege (Charlier et al., 2001).

$$K_0 = \frac{\sigma_h}{\sigma_v} \tag{4.1}$$

Table 4.3 – Characteristics of the reference model simulation

Reference model	
Thermal conductivity formulation	$\lambda_m = nS_w\lambda_w + nS_c\lambda_c + (1-n)\lambda_s$
Heat flow	Conduction + Convection
Retention behaviour	$S = \left[1 + \left(\frac{s}{P_r}\right)^{\frac{1}{1-m}}\right]^{-m}$
Mechanical behaviour	Thermal elastic model

where, λ_m, λ_w, λ_c and λ_s refer to the thermal conductivities of the medium, water, CO_2 and solid, respectively. The thermal conductivities of the components are considered to be constant.

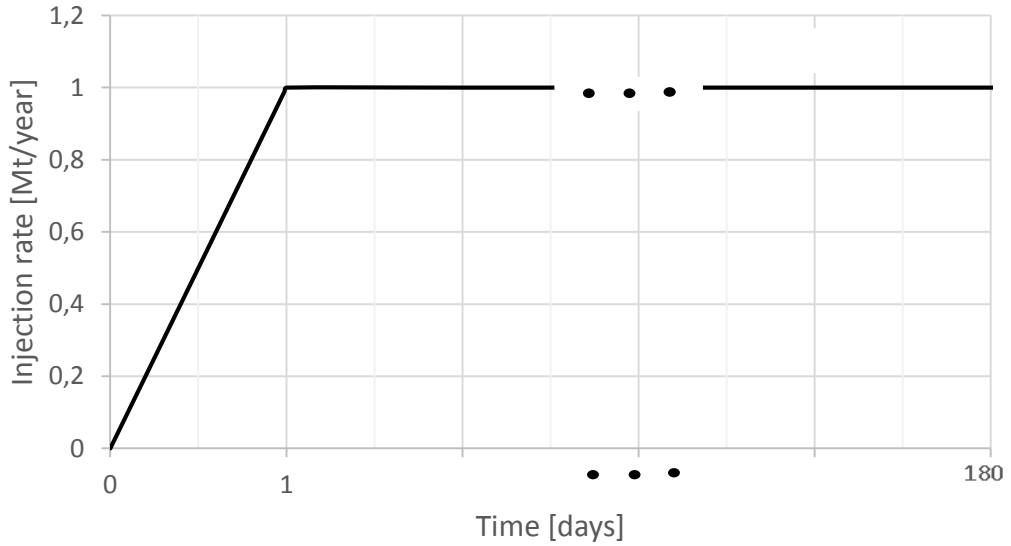

Figure 4.4 - Injection rate evolution

5. SIMULATION RESULTS

The thermo-hydro-mechanical coupling effects are studied through a staged analysis allowing a better perception of each process on the general behaviour. Thus, through a hydraulic analysis, a preliminary study involving the Van Genuchten (1980) retention parameters is carried out. Then hydro-mechanical and thermo-hydraulic analyses are performed, in order to provide the reader with required knowledge for the final thermo-hydro-mechanical analysis.

Furthermore, thermal effects, in this kind of problems are not yet well understood by the scientific community. Only a few studies have been performed (e.g. Vilarrasa, 2012 and Gor et al., 2013) in order to evaluate them. Recalling Figure 3.7, which shows the variation of density and viscosity with respect to temperature and pressure. On the one hand, injecting liquid CO_2, i.e. lower temperature, means higher density, thus a lower volume of the resident water has to be displaced, resulting in lower fluid overpressure. On the other hand, lower temperatures imply higher viscosity, which influences the CO_2 plume evolution. Moreover, when considering a thermo-hydro-mechanical analysis, the low temperature close to the injection well, results in a contractive behaviour by the sealing caprocks and aquifer.

Before proceeding, it should be very clear that thermal effects take place regardless of CO_2 conditions. However in the context of this study, since the reservoir is found with a temperature of 330K, injecting CO_2 in supercritical conditions (330K) imply an isothermal analysis (hydro-mechanical) whereas liquid conditions (300K) implies a non-isothermal analysis (thermo-hydro-mechanical).

It should be emphasized that the simulations are carried out based on the reference model described in Chapter 4, from which several analyses are made. Moreover, due to the high computational cost involved, certain simulations have small differences in the geometry. Table 5.1, summarises all simulations, their characteristics and objectives.

Since this study is based on Vilarrasa (2012) work, Table 5.2 compares the respective properties of each model. The model of Vilarrasa (2012) is axisymmetric and the top of the aquifer is located 1500 meters deep and it extends laterally up to 20 kilometres. The aquifer is 100 meters thick and CO_2 injection is simulated along its thickness through a vertical injection well with a radius of 0.15 meters. Moreover, Vilarrasa (2012) carries out the HM and THM simulations with an injection rate of 1 Mt/year over a period of 8 months and resorting to the code, CODE_BRIGHT (Olivella et al., 1994, 1996). For the thermal analysis, he considers the reservoir at an initial temperature of 331K and the liquid CO2 is simulated with an injection temperature of 293K.

Table 5.1 – Simulations characteristics and objectives

Simulations						
Section	Type	IR $[Mt/year]$	Layers	CO_2 state	Study	Objective
5.1	H	0,3 and 1	1 (aquifer)	SC	Parametric study of “Pr” and “m”	Define a stability zone of good convergence
5.2	HM	1	2 (aquifer and upper seal)	SC	HM behaviour during SC CO_2 injection	How hydraulics affect mechanics
5.3.1	TH	1	2 (aquifer and upper seal)	Liquid	2 simulations comparing different formulations of thermal conductivities	Study the influence of the thermal conductivity formulations
5.3.2	TH	1	2 (aquifer and upper seal)	Liquid	2 simulations considering convection OFF and ON	Analyse the influence of the convection term during CO_2 injection
5.3.3	H vs TH	1	2 (aquifer and upper seal)	SC vs Liquid	2 simulations comparing different injection temperatures: Liquid (300K) vs SC (330K)	How temperature affects the hydraulics
5.4	HM vs THM	1	3 (aquifer, upper and bottom seals)	SC vs Liquid	3 simulations: 1 injecting SC and 2 injection Liquid CO_2	How temperature affects the mechanics

Tabel 5.2 – Properties of the Vilarrasa (2012) and the present study model

Properties	Present study		Vilarrasa (2012)	
Thermal parameters	Caprock	Aquifer	Caprock	Aquifer
Solid thermal conductivity, λ_s $[\mathrm{W/m.K}]$	1.50	2.50	1.50	1.50
Solid specific heat capacity, $c_{p,s}$ $[\mathrm{J/kg.K}]$	950	850	874	874
Solid thermal expansion coefficient, α_s $[\mathrm{K^{-1}}]$	1.5×10^{-5}	1×10^{-5}	1×10^{-5}	1×10^{-5}
Flow parameters				
Intrinsic permeability, k_{int} $[\mathrm{m^2}]$	1×10^{-18}	1×10^{-13}	1×10^{-18}	1×10^{-13}
CO_2 relative permeability, k_{rc} $[-]$	S_c^6	S_c^3	S_c^6	S_c^3
Water relative permeability, k_{rw} $[-]$	S_w^6	S_w^3	S_w^6	S_w^3
Van Genuchten parameter, m $[-]$	0.80	0.50	0.80	0.50
Van Genuchten parameter,P_r $[\mathrm{MPa}]$	0.60	0.02	0.60	0.02
Initial porosity, n_0 $[-]$	0.01	0.10	0.01	0.10
Mechanical parameters				
Young modulus, E $[\mathrm{GPa}]$	5.0	2.5	5.0	2.5
Poisson ratio, υ $[-]$	0.30	0.30	0.30	0.30
Initial stress factor K_0 $[-]$	0.6	0.6	0.5	0.5

5.1. HYDRAULIC ANALYSIS: INFLUENCE OF THE RETENTION PARAMETERS

The following analysis was carried out based on Garcia et al. (2011) study. The latter, addresses the effects of the retention parameters at the onset of instability of an unsaturated soil subjected to water infiltration whereas the present study addresses the desaturation of a saturated geomaterial. Although the characteristics of the studies are not exactly the same, the hydraulic phenomena are similar. For this purpose, a hydraulic analysis which only considers the aquifer layer from the reference model was employed. Figure 5.1 shows the influence of each parameter on the shape of the water retention curve.

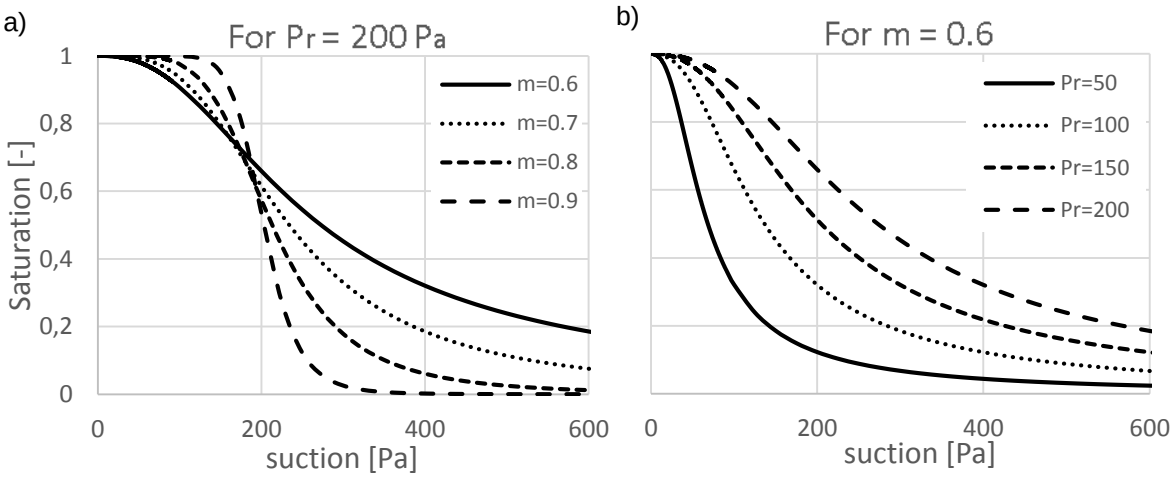

Figure 5.1 - Influence of the retention parameters: a)"m" and b)"Pr" on the water retention behaviour

From Figure 5.1a and Figure 5.1b it can be observed that m and P_r, control the slope of the WRC and that lower values of P_r and higher values of m, reflect steeper curves. This implies a more abrupt transition between saturated and unsaturated states, which is not suitable for calculation issues. Figure 5.2 presents several points. Each point refers to a simulation, of which the "crosses" mean an unstable behaviour, i.e. the simulation had no convergence and the "diamond" shape represents good convergence. Furthermore, it is emphasized the fact that the simulations conditions were all the same, except the values of m and P_r. In addition, two injection rates were considered: Figure 5.2a 0.3Mt per year and Figure 5.2b 1 Mt per year.

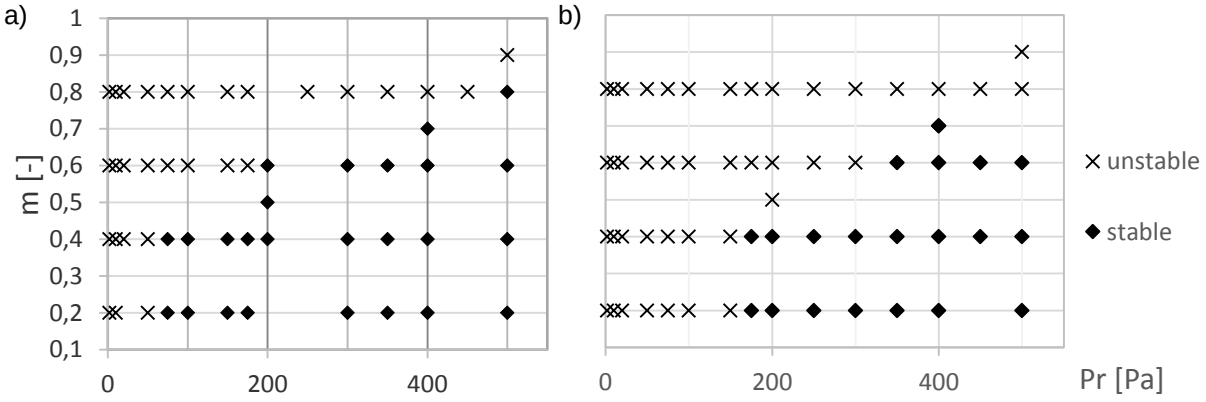

Figure 5.2 - Stability line defining the values of "m" and "Pr" for which good convergence is achieved. a) 0.3 Mt per year and b) 1 Mt per year

The results show that for steeper shapes of the water retention curve unstable behaviour is verified, resembling the ones obtained by Garcia et al. (2011). Instability is reached when an abrupt change from a saturated to unsaturated state occurs, resulting in an abrupt stop of the numerical simulation. Furthermore, it is noticeable that for a higher injection rate the stability line tends to shift to the right for the simple reason that for higher injection rates, the change between saturated and unsaturated states will occur more abruptly, therefore requiring an even smoother shape for the water retention curve. Knowing that a thermo-hydro-mechanical simulation requires a high computational cost, this prior study is of great relevance, enabling a potential stable region to be defined, where good convergence is obtained.

5.2. HYDRO-MECHANICAL ANALYSIS

As mentioned in section 3.1, injecting CO_2 results in a desaturation process of the aquifer. Analysing the porous media close to the injection well, the pores are completely filled with water. Hence, when CO_2 is injected, it has to displace a certain volume of resident water and due to its very low relative permeability, pressure close to the injection well builds up. Nevertheless, in the course of time, the pores close to the injection well are filled with CO_2, resulting in an increase of the CO_2 relative permeability (Figure 4.3) allowing an easier flow (Vilarrasa, 2012). As a consequence, the sharp increase reported in the first few days of injection will slowly decrease. This phenomenon affects the stress field of both aquifer and caprock, inducing deformations. These deformations could compromise the caprocks mechanical stability, which require every attention, in order to avoid eventual damage and opening of new flow paths.

From Figure 5.3a it can be observed that the pressure build-up takes place during the first 8 days of injection, after which a slow decrease is observed. Analysing Figure 5.3b it can be observed that during the first 8 days the mean effective stress decreases 1MPa and the deviatoric stress 0.5 MPa. This indicates less favourable conditions of mechanical stability. However, after reaching the maximum overpressure at 8 days, the confinement is recovered by an increase of mean effective stress with the same ratio, whereas the deviatoric stress remains almost constant, implying safer injection conditions. Both graphs refer to an element close to the injection well and at the top of the aquifer.

Analysing the stress path in a *q-p'* plane, it can be observed that during the first 8 days the stress path moves to the left, i.e. towards a possible failure envelope, after which turns back with a similar trend, implying safer injection conditions.

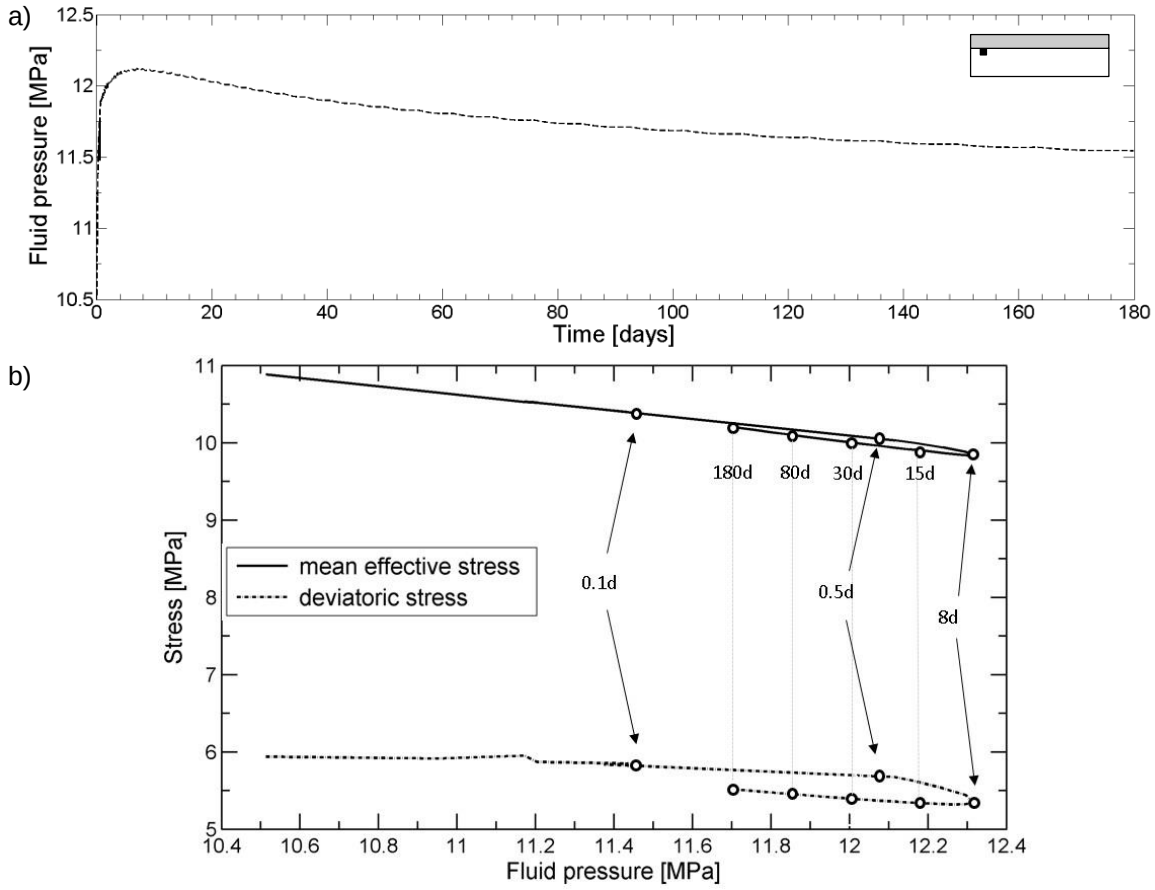

Figure 5.3 - a) Fluid pressure evolution for an element 10 meters away from the injection well and at the top of the aquifer; b) time evolution of the mean and deviatoric stresses at the same element with respect to fluid pressure

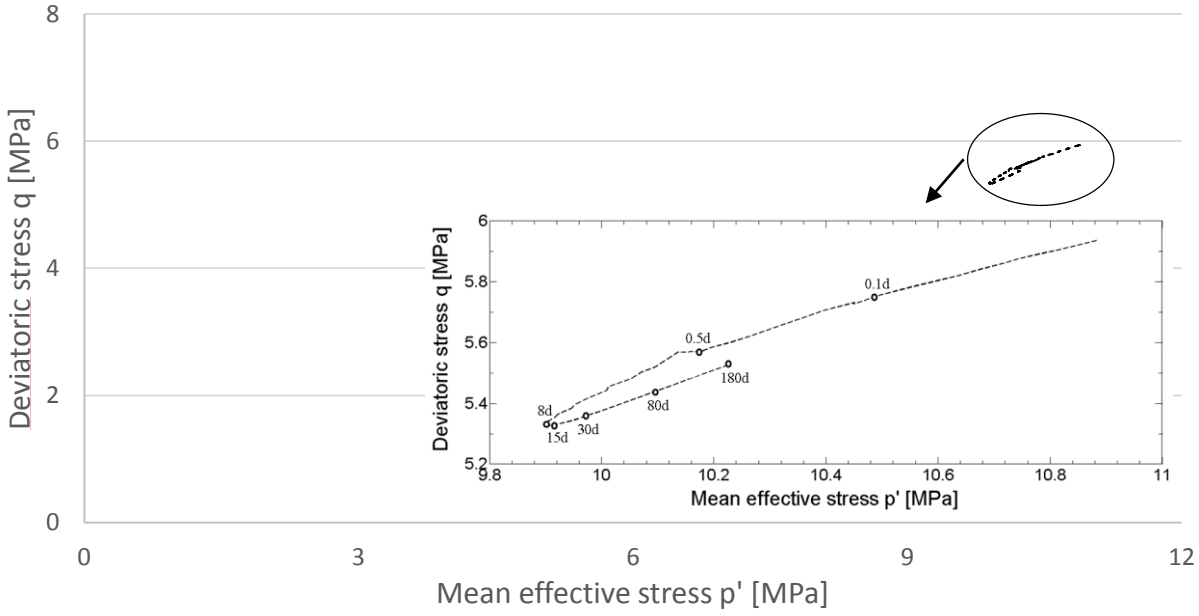

Figure 5.4 - Stress pass in a *q-p'* plane for an element 10 meters away from the injection well at the top of the aquifer

Moreover, the fluid pressure at the top of the aquifer dissipates as we move away from the injection well. Comparing the horizontal profiles of fluid pressure with water saturation, Figure 5.5a and Figure 5.5b respectively, it can be observed that a drop in fluid pressure is verified at the interface between CO_2 and water. The latter is due to the fact that at the interface CO_2-water, a capillary fringe exists, where the suction forces are responsible for that drop.

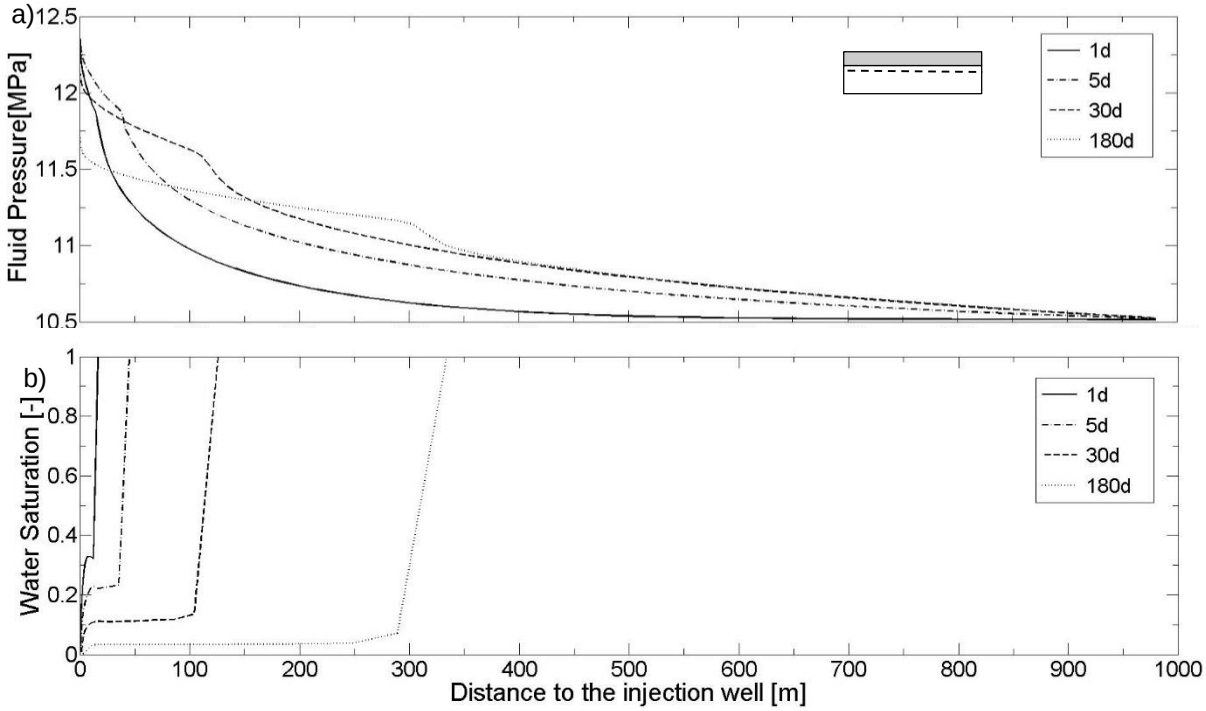

Figure 5.5 - Horizontal profile at the top of the aquifer comparing fluid pressure (a) and water saturation (b) for four different time steps

It has been observed that injection of CO_2 produces an increase in the fluid pressure. This results in a vertical and lateral expansion of the aquifer, pushing the caprock upwards and the aquifer away from the injection well. Figure 5.6 shows the vertical displacements for several time steps. As expected the vertical displacement at 180 days is lower than at 5 days due to the fluid pressure dissipation. Furthermore, the vertical displacement decreases with distance from the injection well, which is consistent with that observed on Figure 5.5a. It should be stated that the results presented so far are consistent with the ones of Vilarrasa (2012), providing confidence in the model.

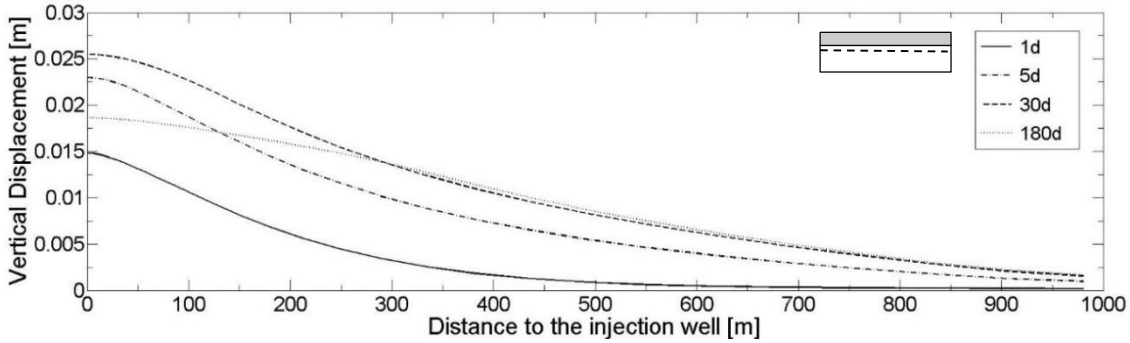

Figure 5.6 - Vertical displacement evolution with the distance from the injection well for an element at the top of the aquifer and for different time steps

5.3. THERMO-HYDRAULIC ANALYSIS

5.3.1. INFLUENCE OF THE THERMAL CONDUCTIVITY FORMULATION

The thermal conductivity of the medium depends on the thermal conductivities, saturation of the components and on the porosity. This section addresses this issue by comparing results from two simulations: one with the reference model formulation and another considering the thermal conductivity of the medium as constant.

$$\lambda_{m_{reference}} = nS_w\lambda_w + nS_c\lambda_c + (1-n)\lambda_s \tag{5.1}$$

$$\lambda_{m_{constant}} \tag{5.2}$$

where, λ_m is the medium thermal conductivity, λ_w is the water conductivity, λ_c the carbon dioxide conductivity and λ_s the solid conductivity. All the thermal conductivities of the phases, in equation 5.1, are being considered constant. Figure 5.7a, shows the temperature evolution for 5, 50 and 100 days with the distance from the injection well, whereas Figure 5.7b presents the evolution of the fluid pressure with respect to time for an element at the top of the aquifer and close to the injection well. From the latter we can conclude that a thermal conductivity formulation depending on porosity and saturation does not affect the overpressure significantly. However, since it is more realistic, it will be considered for the following simulations.

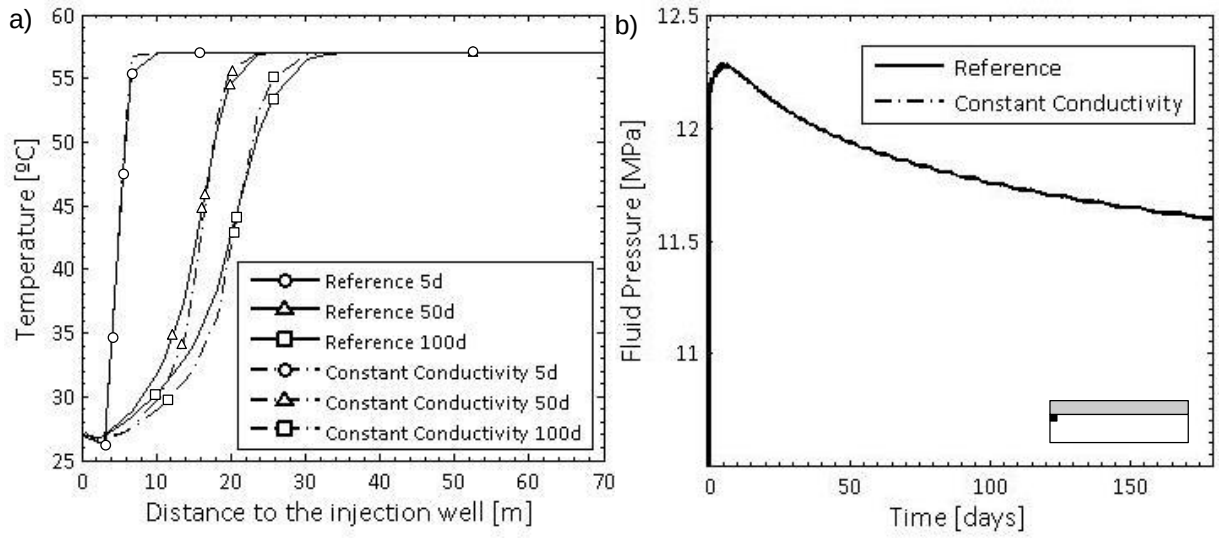

Figure 5.7 - a) Temperature evolution with respect to the distance to the injection well; b) Fluid pressure evolution with time for an element at the top of the aquifer

5.3.2. INFLUENCE OF THE CONVECTIVE TERM

Recalling Equation 3.26, the heat flow is governed by conduction and convection. The present code allows us to consider, or not, the convection term. In order to evaluate each influence, two simulations were carried out. The results in Figure 5.8 refer to the temperature profile for the reference formulation (a) and to the case that only considers conduction (b).

Through this study, we come to the following conclusions: the heat flow is governed by convection; due to the buoyant CO_2, which accumulates at the top of the aquifer, convection contributes to the transference of temperature to the caprock; a lower fluid pressure is observed considering convection (Figure 5.9). The latter, is due to the fact that a higher volume of CO_2 will be found in liquid state, i.e. higher densities, meaning less volume of resident water to be displaced. Nevertheless, despite its small influence the conduction term should not be ignored, since due to the very low permeability of the caprock, it is the only process that allows the caprock to experience temperature differences.

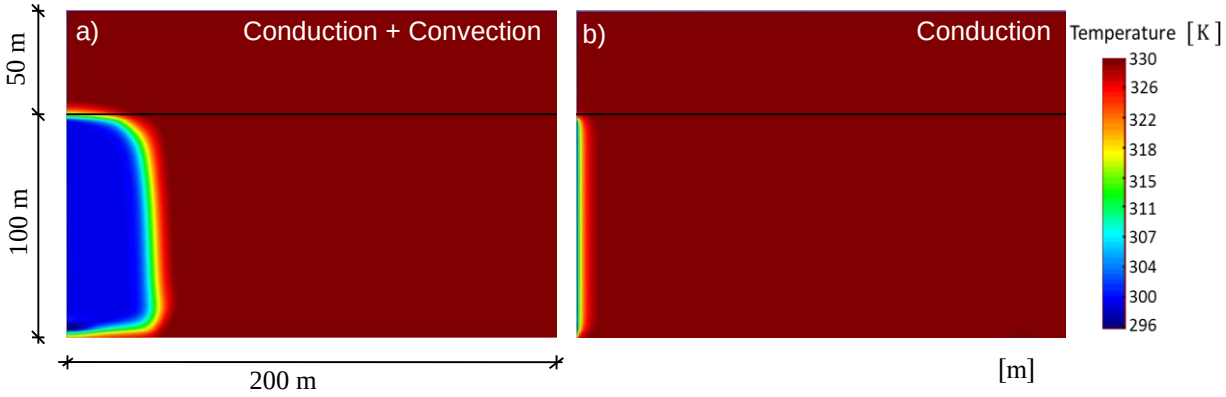

Figure 5.8 - Temperature profile considering a) convection and conduction and b) conduction

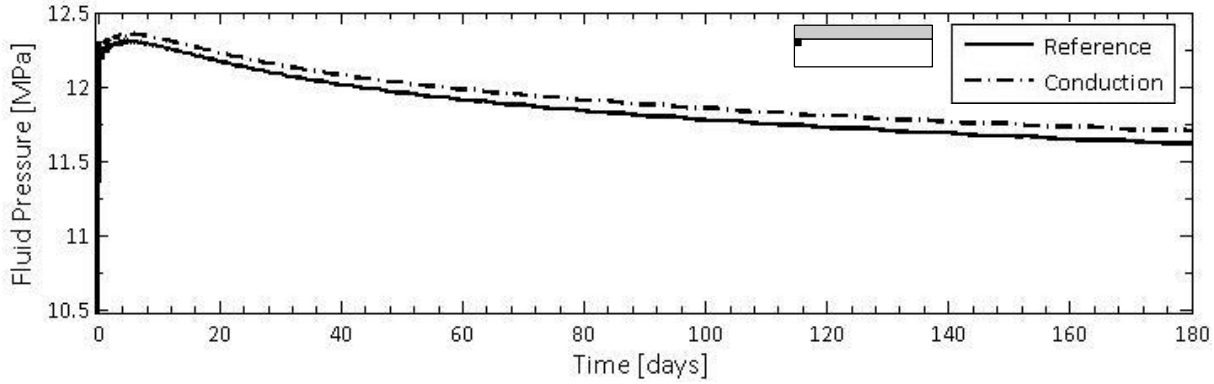

Figure 5.9 - Fluid pressure evolution for an element at the top of the aquifer and close to the injection well

5.3.3. INFLUENCE OF THE INJECTION TEMPERATURE

In this section, two thermo-hydraulic simulations are carried out: A – Liquid CO_2 (300K) and B – Supercritical CO_2 (330K). Figure 5.10, illustrates the CO_2 states for each simulation. As expected the results show a lower overpressure for liquid injection, due to the higher density. Figure 5.11 presents the fluid pressure evolution with time, for an element close to the injection well and at the top of the aquifer, showing a difference of about 0.1 MPa after 180 days.

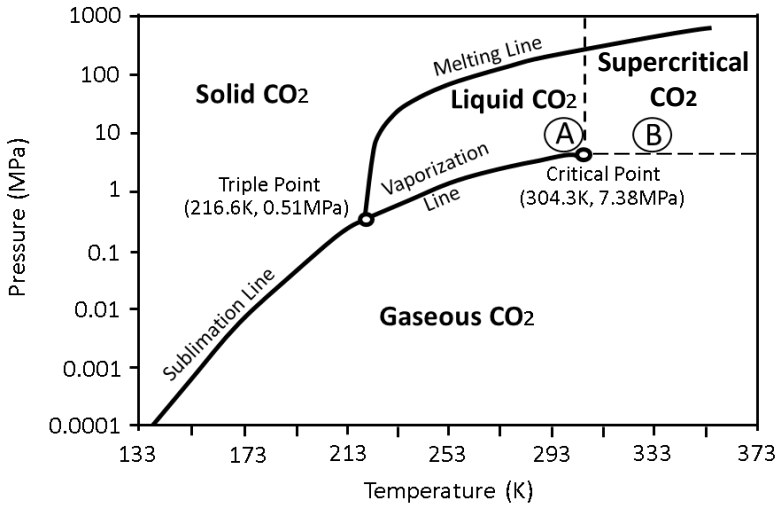

Figure 5.10 - CO_2 state for case A (liquid) and B (supercritical) (modified from Bachu, 2008)

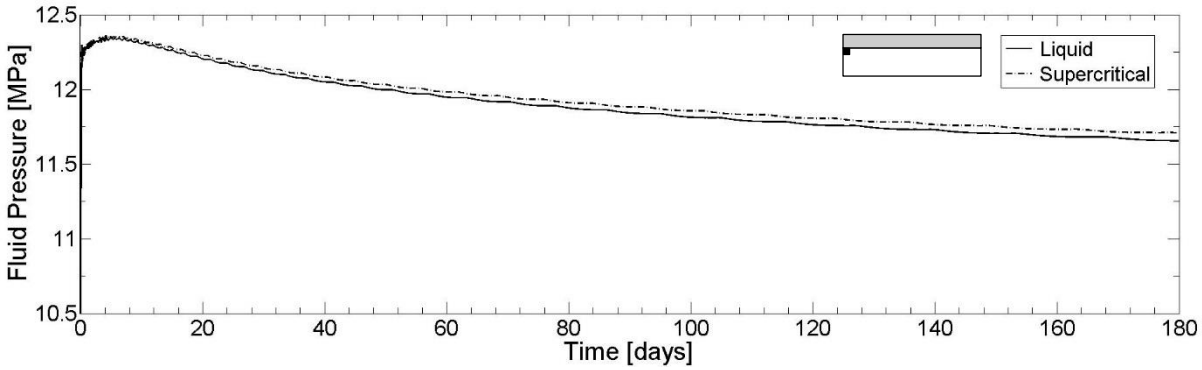

Figure 5.11 - Fluid pressure evolution with time for liquid and supercritical conditions for an element at the top of the aquifer and close to the injection well

Furthermore, as stated previously, CO_2 in liquid conditions is characterized by a higher viscosity than in supercritical. This can be observed in Figure 5.13, where the supercritical CO_2 plume reaches 56 meters further than the liquid one, after 1 year of injection. These simulations were carried out for 1 year because at 6 months, the differences were not significant. This higher viscosity of liquid CO_2 favours the containment period as well as a smaller area for future monitoring.

Moreover, the influence of temperature on the CO_2 plume profile, can also be detected in the area close to the injection well, where the lower temperatures due to the liquid injection are present, inducing higher densities and viscosities. However, as we move away from the injection well, CO_2 reaches thermal

equilibrium, evolving to a supercritical state. Figure 5.12 compares Figure 5.13a with the respective temperature profile, enlightening the phenomenon described before.

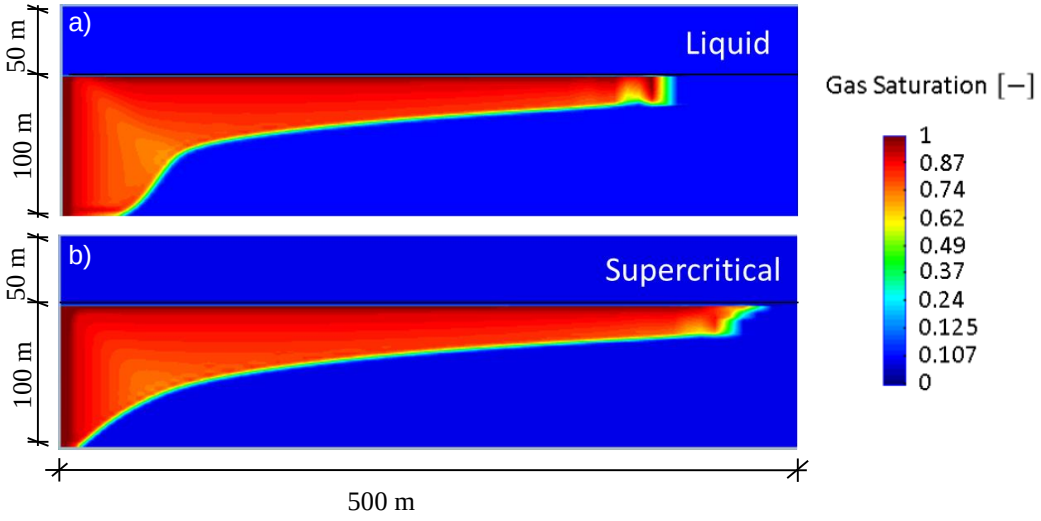

Figure 5.13 - CO2 plume after 1 year of injection for a) Liquid and b) Supercritical conditions

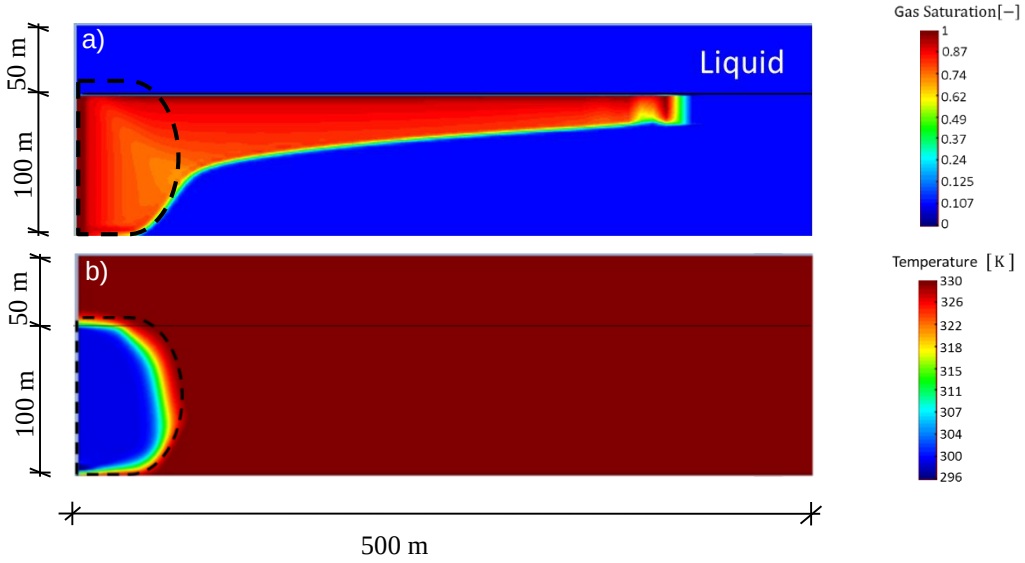

Figure 5.12 - Profiles after 1 year of injection. a) CO2 saturation and b) Temperature

Vilarrasa (2012), defines a gravity number N which relates the gravity forces with the viscous forces. The relationship is established through a ratio, where in the numerator we have the gravity forces and in the denominator we have the viscous forces, in the following manner:

$$N = \frac{\Delta\rho g}{\frac{Q_m \mu_c}{2\pi k r_c d \rho_c}} \tag{5.3}$$

where, $\Delta\rho$ is the difference between water and carbon dioxide densities, g gravity, Q_m the CO2 mass flow rate, μ_c carbon dioxide viscosity, k_{int} aquifer intrinsic permeability, r_c characteristic length, d aquifer thickness and ρ_c the CO2 density. The characteristic length has been chosen as the distance to the injection well. Through equation (5.3) is clear that for values of $N > 1$, buoyancy forces dominate and

for $N < 1$, viscous forces dominate. Figure 5.14, shows the gravity number N for supercritical and liquid injection. As expected, N increases as we keep away from the injection well for both cases. However, it can be observed that due to the temperature effect, the viscous forces dominate further away in the liquid injection. In supercritical conditions, the viscous forces dominate until 6 meters, whereas for liquid conditions they dominate until 15 meters.

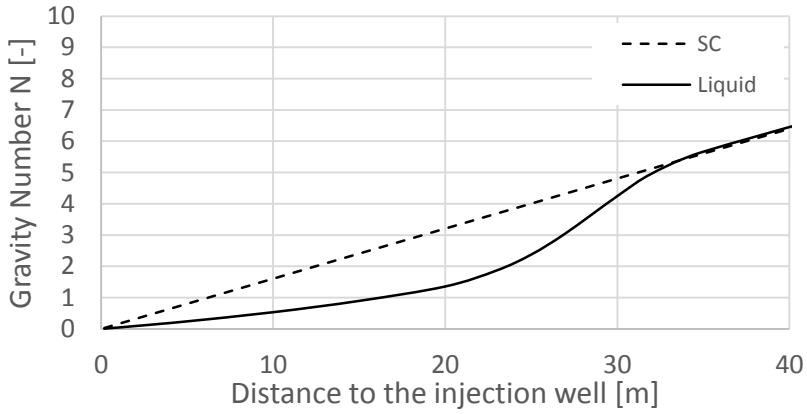

Figure 5.14 - Gravity number evolution along the top of the aquifer length for supercritical and liquid injections

Moreover, it is interesting to notice the influence that the buoyancy forces have on the temperature profile. Looking back at the energy conservation equation (Equation 3.26), it is noticeable, through the convection term that the heat flow tends to follow the hydraulic one. For this purpose, four simulations were carried out with an injection rate of 0.3 Mt per year, over a period of 180 days and for four different values of intrinsic permeabilities of the aquifer. In Figure 5.15, it can be observed a tendency for the temperature profile to reach greater distances at the top. This was expected, since increasing permeability implies stronger buoyancy forces.

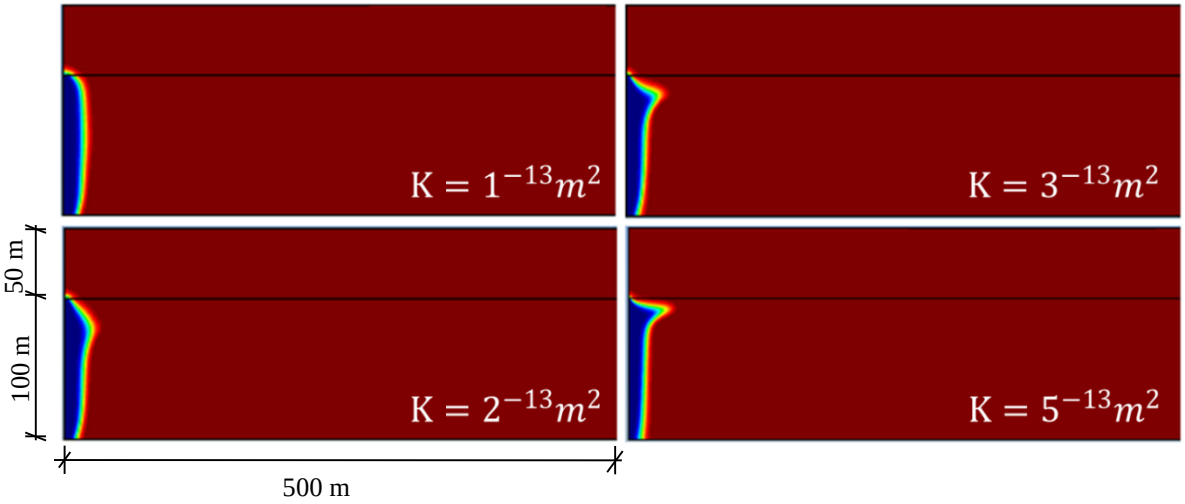

Figure 5.15 - Temperature profiles for four different intrinsic permeabilities after 180 days of injection

5.4. THERMO-HYDRO-MECHANICAL ANALYSIS

Regardless of the CO_2 conditions, its injection produces an increase in the fluid pressure, resulting in an expansion of the aquifer. In case injection in carried out in supercritical conditions, there is a lateral expansion away from the injection well and upwards vertical displacements of the sealing caprock, whereas in liquid conditions a contractive behaviour takes place close to the injection well. Figure 5.16, shows the vertical profile of the horizontal displacements for supercritical and liquid injection, 10 meters away from the injection well. The negative values mean displacements towards the injection well and two observations can be made. First, the contractive behaviour is more pronounced at the middle of the aquifer than at the top, reaching a maximum negative displacement of 2 millimeters, while at the interface with the caprock less than 1 millimeter is observed. Secondly, during the first moments, the horizontal displacements are governed by overpressure rather than thermal effects (analyse the curves for 0.2 days in Figure 5.16). With regard to the vertical displacements, Figure 5.17, compares the evolution of the vertical displacements (positive values mean upwards displacements) along the length of the aquifer after 6 months of injection at three different locations (middle aquifer, top aquifer and caprock). A straightforward observation is that the vertical displacements are greater at the top aquifer and caprock, due to the expansion of the aquifer. Finally, it can be observed that the vertical displacements close to the injection well for liquid injection are lower than the supercritical one which is in agreement with Goodarzi et al. (2010). However, this is only observed close to the injection well, where CO_2 is found in liquid conditions. As we move away from the injection well, CO_2 evolves to supercritical conditions due to thermal equilibrium with the aquifer, resulting in very similar displacements between supercritical and liquid injections. To better analyse the latter, Figure 5.18a and b), show the vertical displacements and temperature evolution along 100 meters from the injection well.

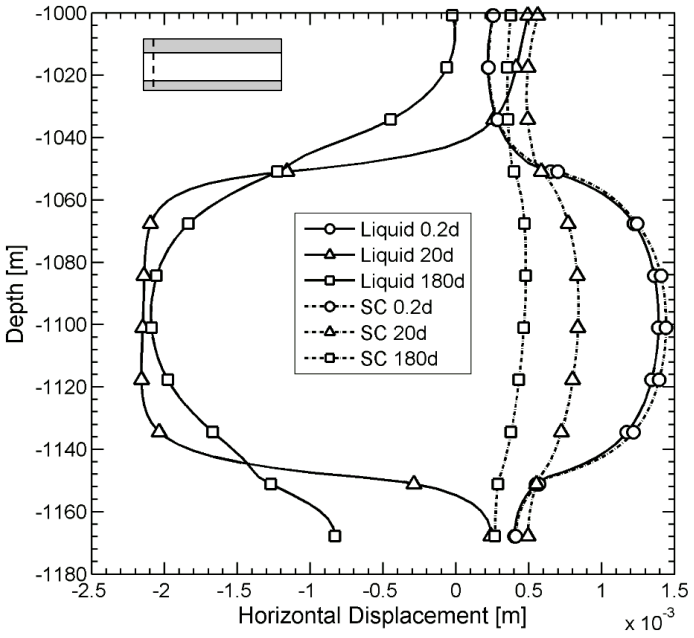

Figure 5.16 - Horizontal displacements for a vertical profile 10 meters away from the injection well for three different time steps

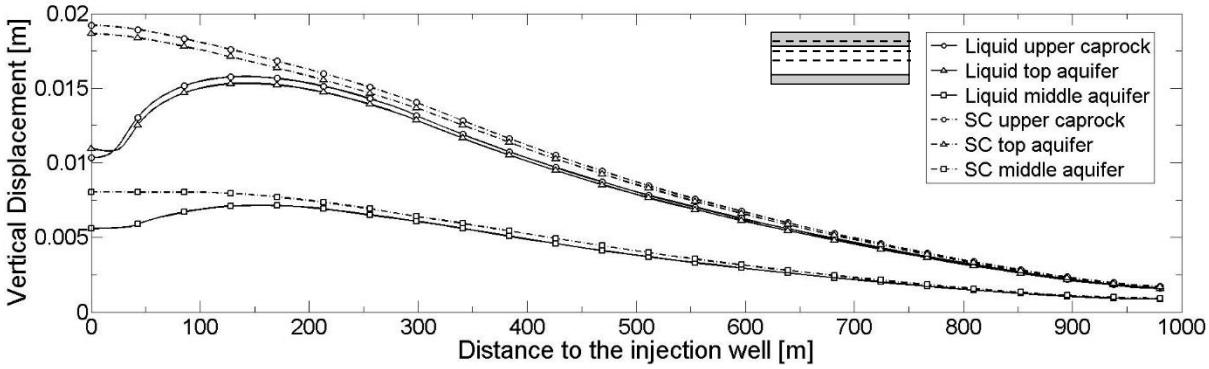

Figure 5.17 - Vertical displacements for three different elements along the length of the aquifer after 180 days of injection

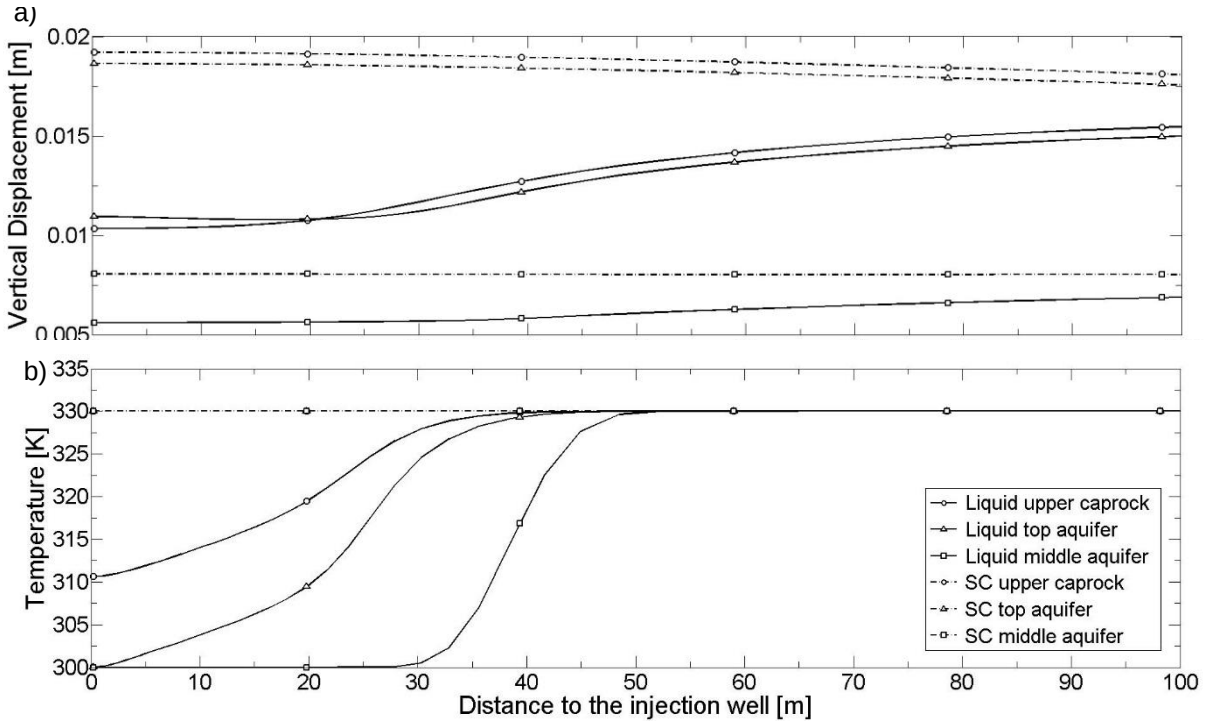

Figure 5.18 - a) Vertical displacements and b) Temperature profiles along the length of the aquifer at the caprock, top and middle aquifer after 180 days of injection

Once again, close to the injection well, the CO_2 is not in thermal equilibrium with the aquifer. Therefore it induces changes in the effective stress field which could compromise the mechanical stability. Figure 5.19, compares the time evolution of the vertical, horizontal effective stresses, fluid pressure and temperature for an element 10 meters from the injection well and at the top of the aquifer during 180 days of injection. A straightforward observation is that the decrease in effective stress is more pronounced for liquid injection than supercritical. Analysing the evolution profile of the fluid pressure, a 0.1MPa difference is found after 180 days of injection. However, after 180 days, a difference of about 0.7MPa and 0.9MPa is found for the vertical and horizontal effective stress, respectively. Thus, it can be concluded that the differences in the mechanical behaviour are due to thermal effects rather than fluid pressure.

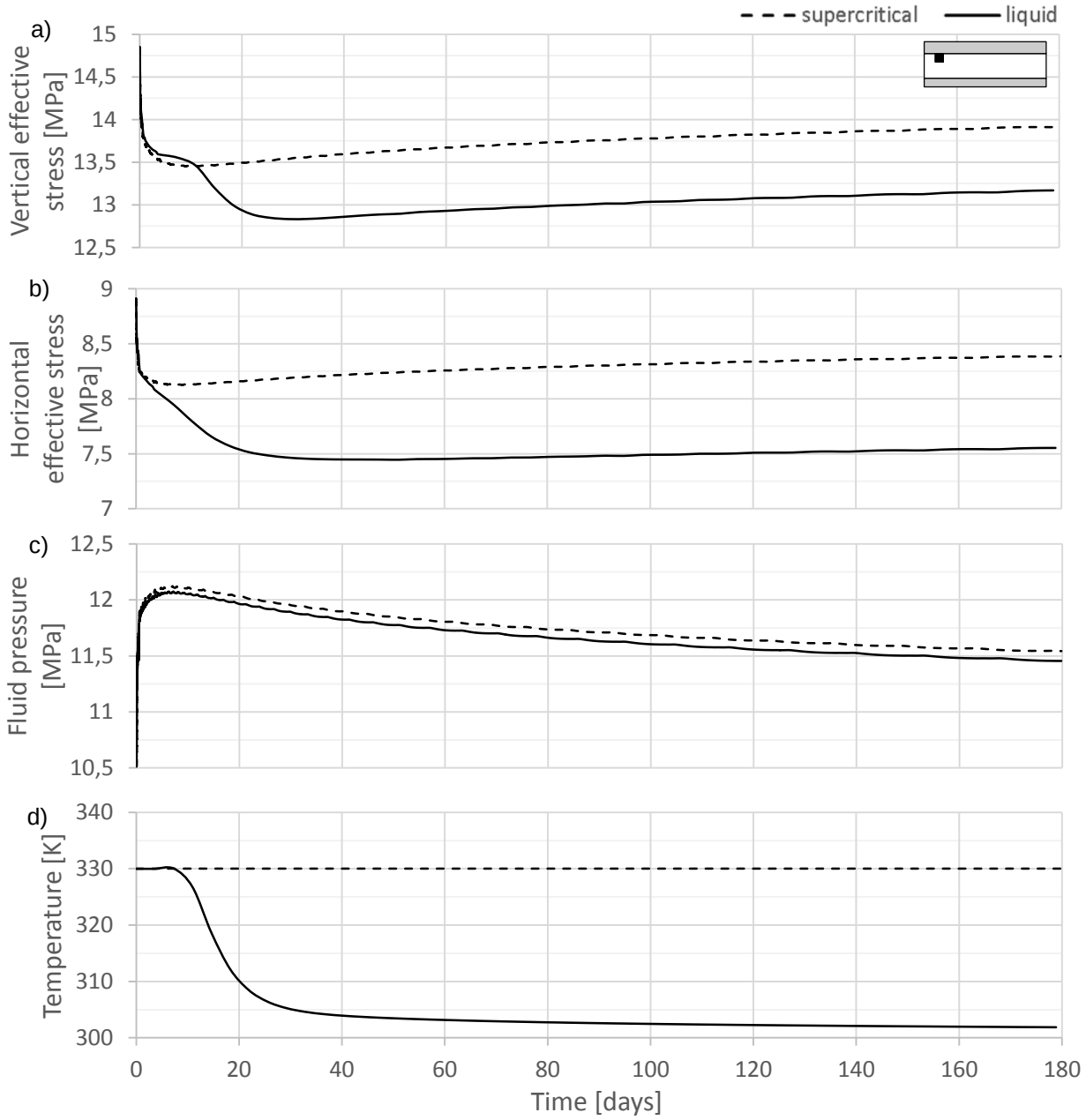

Figure 5.19 - Vertical (a), horizontal effective stress (b), fluid pressure (c) and temperature (d) time evolution for an element 10 meters away from the injection well and at the top of the aquifer

From a mean effective and deviatoric stress perspective, the liquid injection produces a higher decrease in the confinement pressure up to 20 days while the deviatoric stress follows the same stress path than in supercritical conditions. After 20 days both stresses increase in similarity with what was observed in section 5.2 for supercritical conditions. However, the thermal effects close to the injection cause a permanent decrease in the confinement pressure, as long as injection is carried out continuously with the same temperature (Figure 5.21). Analysing the latter in a *q-p'* plane it can be observed that only after 10 days the stress path start to diverge, which is exactly when the thermal effects start to take place. In addition, it can be observed that the stress path for liquid conditions moves further up and to the left, implying less stable conditions (Figure 5.20).

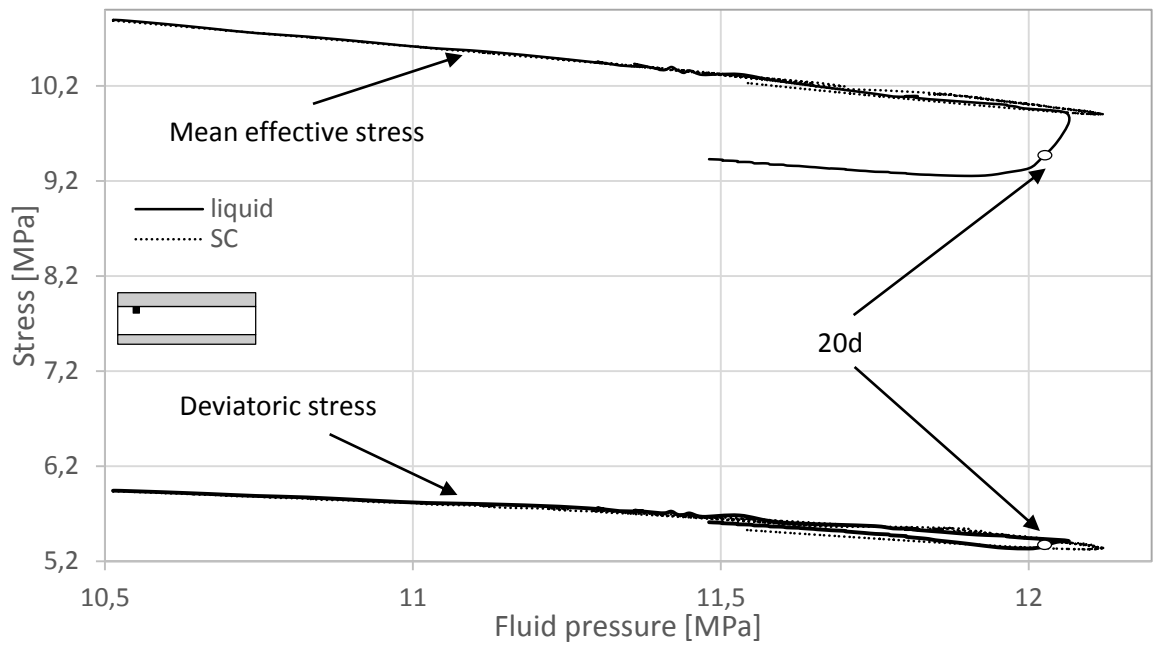

Figure 5.21 - Mean and deviatoric effective stress evolution with respect to fluid pressure

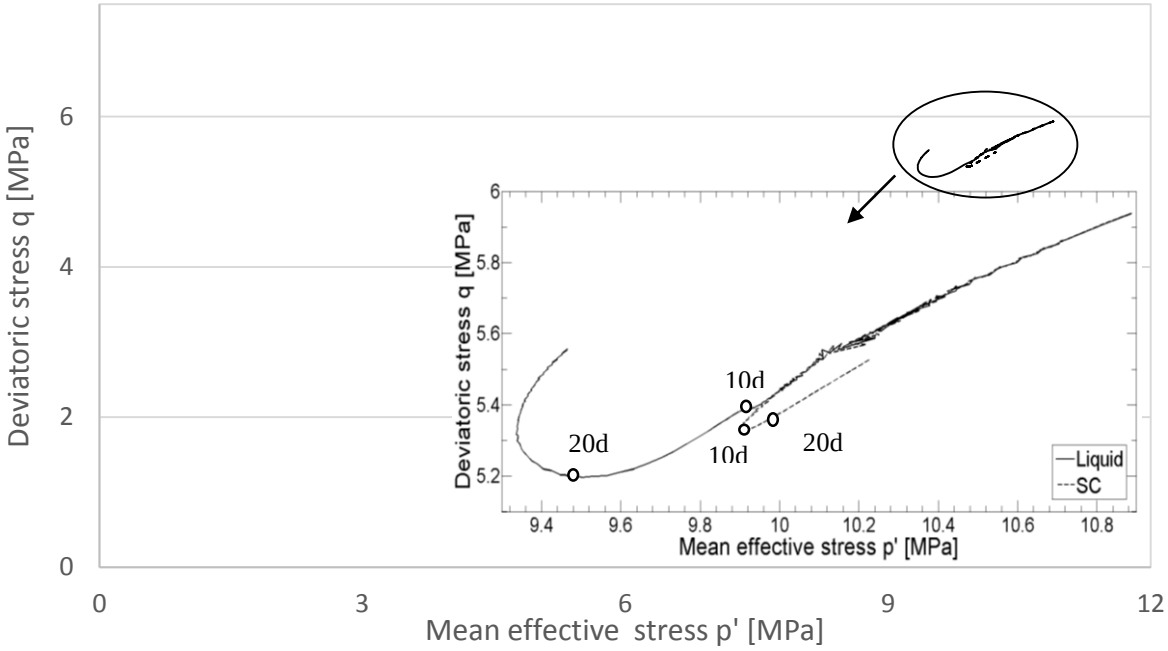

Figure 5.20 - Stress pass in a *q-p'* plane for an element 10 meters away from the injection well at the top of the aquifer for liquid and supercritical injection

When analysing the vertical profiles of the horizontal and vertical effective stress, 10 meters away from the injection well (Figure 5.22) it can be observed that the liquid injection produces a higher decrease of effective stress within the aquifer.

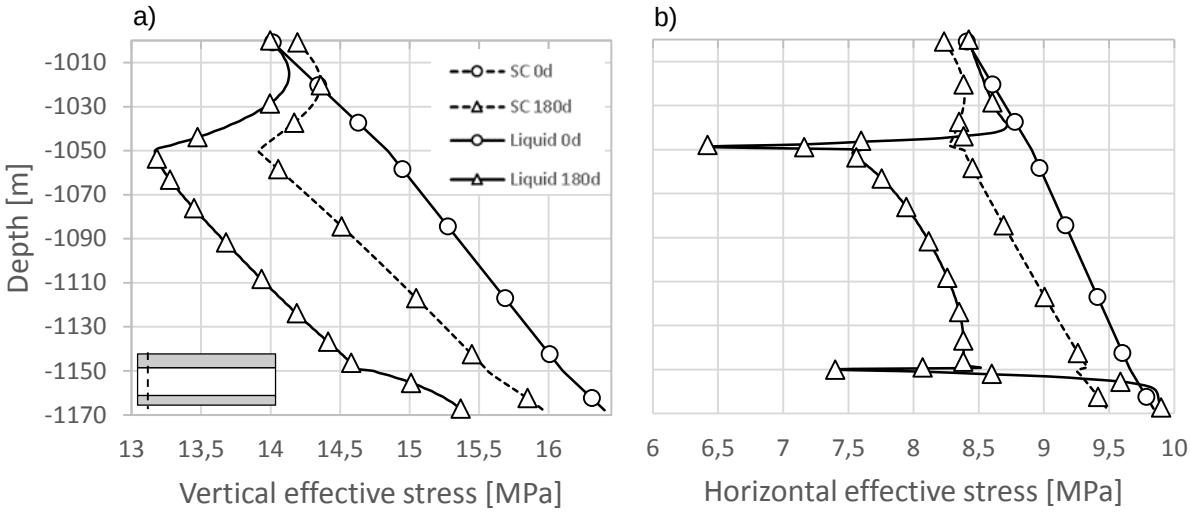

Figure 5.22 - Vertical profiles 10 meters away from the injection well: a) horizontal effective stress and b) vertical effective stress

From the literature review, the most recent study found, regarding non-isothermal analysis of CO_2 injection into deep aquifers was the one carried out by Vilarrasa (2012), in which this study is based. The results presented so far are consistent with his work except the sharp decrease in the horizontal effective stress detected at the upper and bottom seals (Figure 5.22b). While Vilarrasa (2012) states that the highest reduction of horizontal effective stress takes place close to the interface, although inside the aquifer, the results obtained through this study report it to be close to the interface but in the caprock. Figure 5.23, shows in a schematic way the differences between the results of Vilarrasa (2012) and those of the present study. Moreover, this sharp decreases were also detected in Simone et al. (2013) study where THM analyses are carried out, cold water injection into a fracture zone.

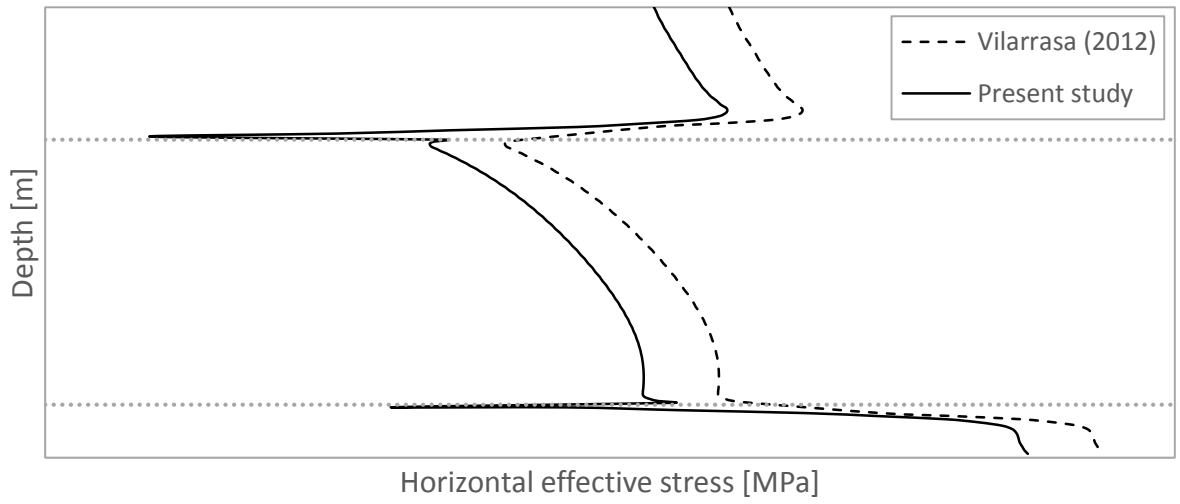

Figure 5.23 - Schematic comparison between the vertical profiles of the horizontal effective stress of Vilarrasa's and present study

In fact, when analysing the results of the present study more carefully, it can be noticed that there is a tendency for the horizontal effective stress to increase close to the interface in a similar way to Vilarrasa (2012). However that trend is superimposed by a sharp decrease as soon as we enter the caprock. The explanation for that lies with material properties. As seen in Table 5.2 the material properties were chosen to be as similar as those adopted by Vilarrasa (2012). Nonetheless, while Vilarrasa (2012) considers the same thermal expansion coefficient for caprock and aquifer ($\alpha = 1 * 10^{-5}\ K^{-1}$), here, a higher thermal expansion coefficient is considered for the caprock, implying a more sensitive behaviour upon temperature differences.

Even though temperature differences at the caprock are less pronounced (only conduction transference allowed), it can be demonstrated that due to the material properties assumed, the caprock undergoes a much higher decreases of effective stress for the same temperature difference.

$$Caprock: \Delta\sigma' = \frac{E}{(1-2\nu)}\alpha_T \Delta T = \frac{5\times10^3}{(1-2\times0.3)}1.5\times10^{-5}(-6) = -1.31\ MPa \quad (5.4)$$

$$Aquifer: \Delta\sigma' = \frac{E}{(1-2\nu)}\alpha_T \Delta T = \frac{2.5\times10^3}{(1-2\times0.3)}1\times10^{-5}(-6) = -0.37\ MPa \quad (5.5)$$

In order to facilitate the expression of the sharp decrease in the horizontal effective stress at the caprock, hereinafter, the latter will be termed as “peak”. Figure 5.25, shows the time evolution of the horizontal effective stress, temperature and fluid pressure for elements at the caprock and top aquifer, 10 meters away from the injection well. Once again the differences in the mechanical behaviour are mainly due to the thermal effects since the differences between fluid pressures are not significant, i.e. the 0.25MPa difference between fluid pressures after 180 days can not explain the 1.2MPa difference in the horizontal effective stress. During the first 18 days when the thermal effects are not significant at the caprock, the horizontal effective stress paths, follow the same trend for both elements. However, after 18 days, when the caprock starts experiencing lower temperatures due to conduction, a higher decrease in the horizontal effective stress is noticed. The latter can also be analysed through the vertical profile 10 meters away from the injection well. Figure 5.26a shows in detail the “peak” evolution for several time steps and, as expected, after 18 days of injection, the horizontal effective stress at the aquifer and caprock have the same magnitude. Moreover, the “peak” decreases as we keep moving away from the injection well, since CO_2 evolves from liquid to supercritical conditions due to the thermal equilibrium with the aquifer. Figure 5.26b presents the vertical profiles at 10, 30 and 50 meters after 180 days of injection.

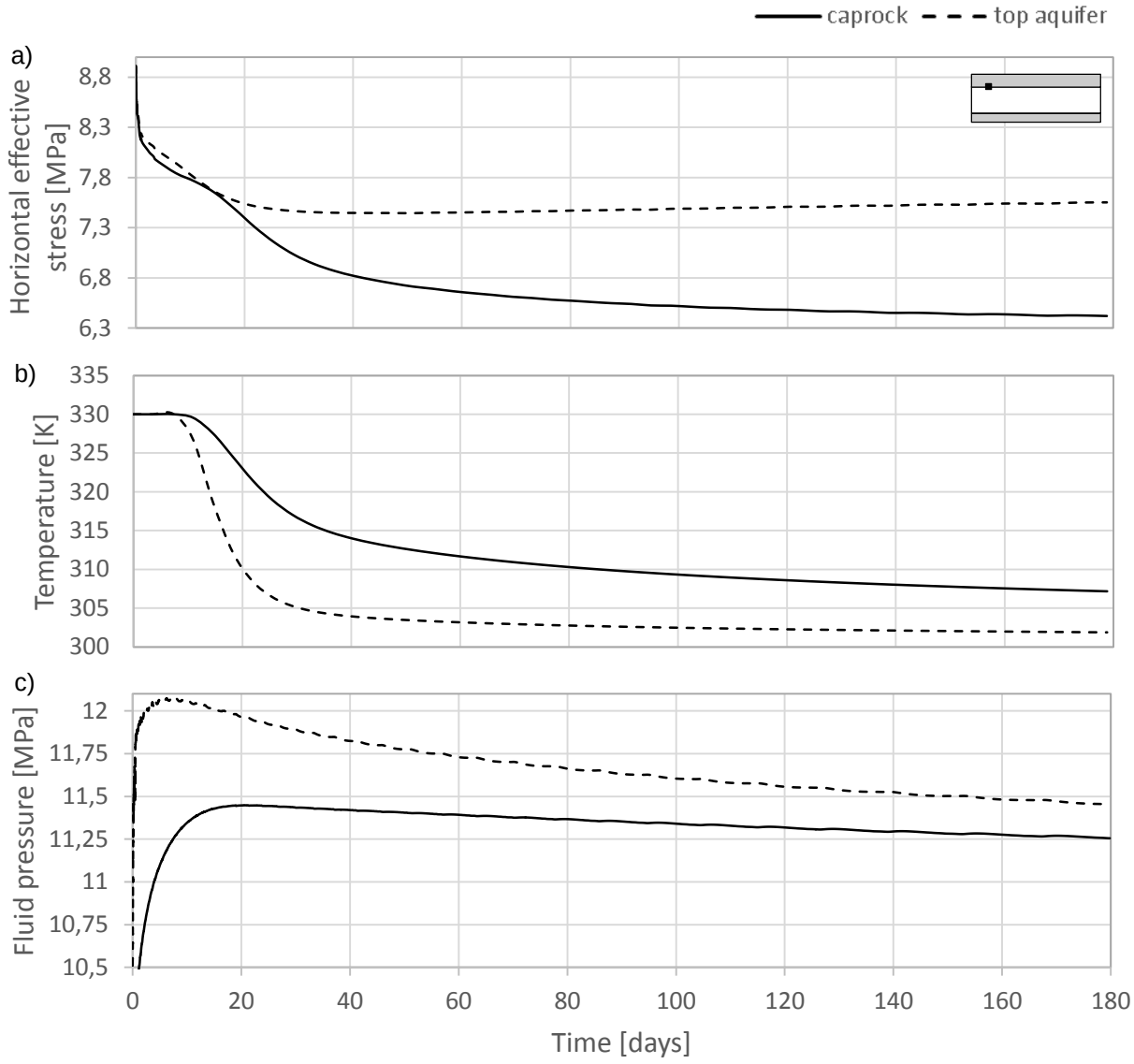

Figure 5.25 - Horizontal effective stress a) temperature; b) and fluid pressure; c) time evolution for two elements 10 meters away from the injection well (caprock and top aquifer)

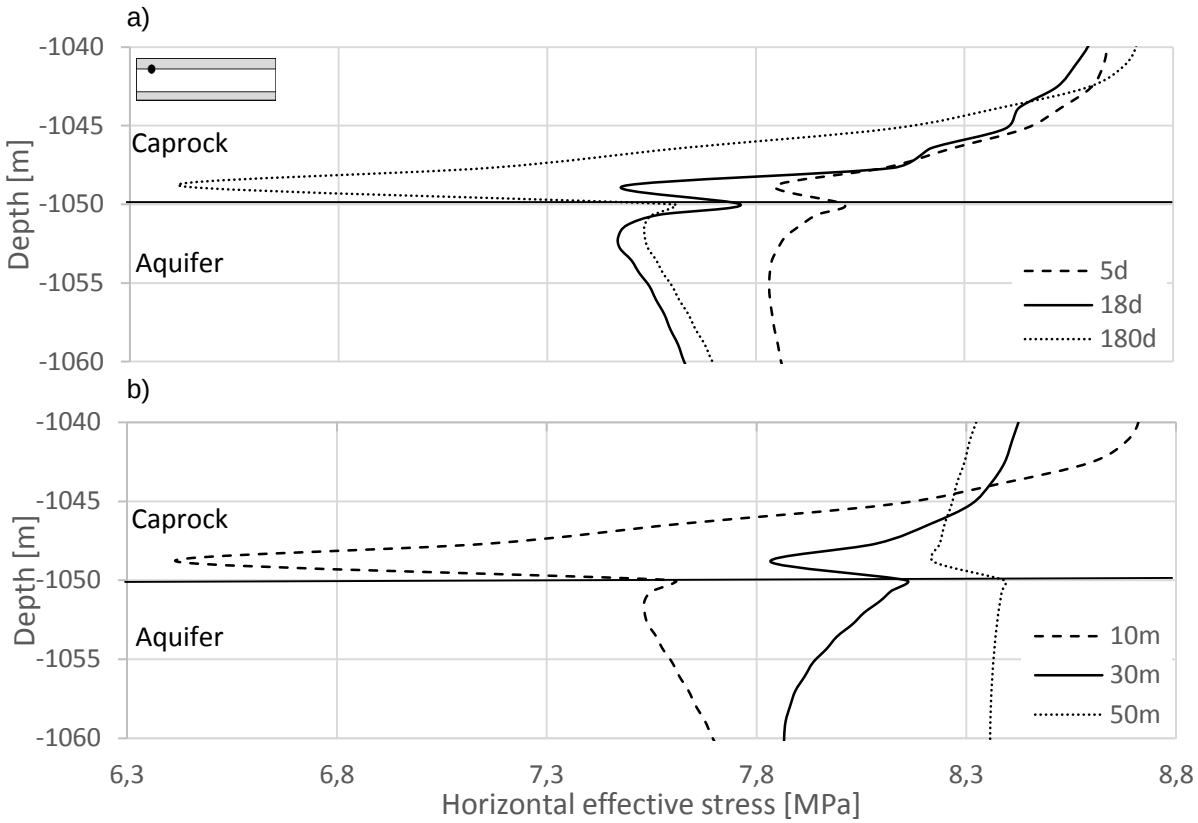

Figure 5.26 - Vertical profiles of the horizontal effective stress for: a) 10 meters away from the injection well and for 5, 18 and 180 days and b) 10, 30 and 50 meters away from the injection well after 180 days

The statements above can be compared with a simplified analytical solution presented by Vilarrasa (2012) for the problem conditions:

$$\Delta\sigma'_H = \frac{1-2\nu}{1-\nu}\Delta p + \frac{E}{1-2\nu}\alpha_T \Delta T - \Delta p \tag{5.6}$$

For this purpose, temperature and fluid pressure variation for both elements should be recalled (Figure 5.25b and Figure 5.25c). The values presented in Table 5.3, show the horizontal effective stress decrease due to fluid pressure and temperature variations. Although the values are not exactly the same as the ones of the simulation, they are consistent, providing confidence to the results.

Table 5.3 – Decrease in horizontal effective stress due to temperature and fluid pressure

Element	**ΔT $[K]$**		**Δp $[MPa]$**		**Decrease in Horizontal effective stress$[MPa]$**	
	18 days	180 days	18 days	180 days	18 days	180days
Caprock	5.5	22.8	1.24	1.06	0,499	3,82
Top Aquifer	18	28.1	1.75	1.21	0,375	1,23

Figure 5.27, compares the stress path in a *q-p'* plane for liquid and supercritical conditions for an element at the caprock, 10 meters away from the injection well. The liquid and supercritical injection follow a same trend until 10 days, after which they start diverging. Moreover, the stress path for liquid injection changes direction abruptly, after 20 days, moving towards to a possible failure envelope. Unlike, the stress path seen for the element in the aquifer, one brings more concern.

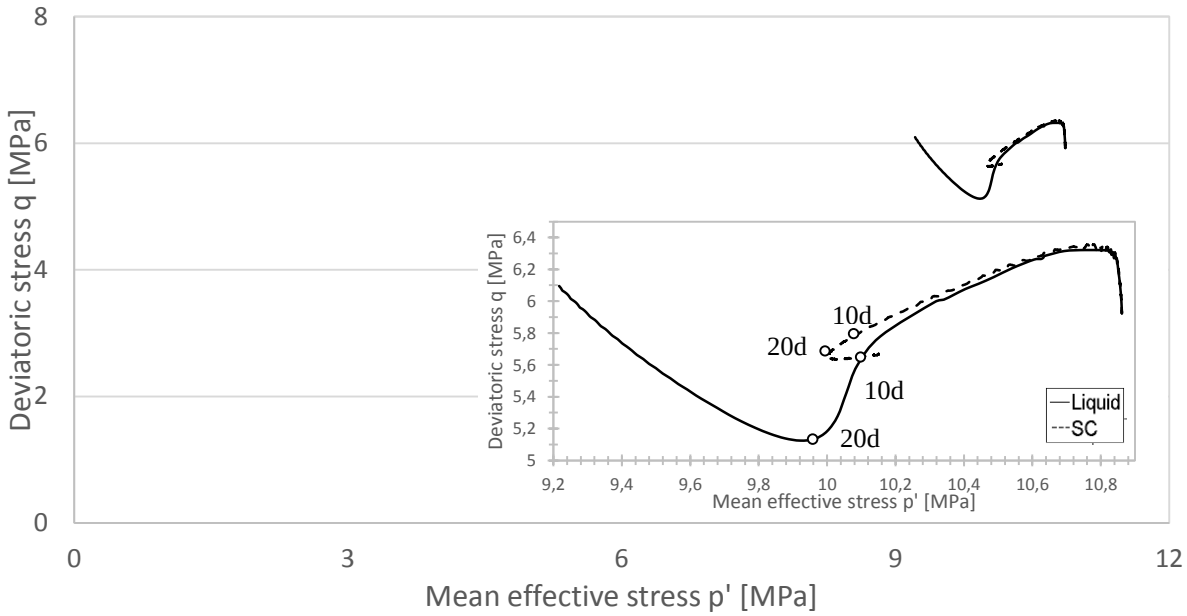

Figure 5.27 - Stress pass in a *q-p'* plane for an element 10 meters away from the injection well at the caprock for liquid and supercritical injections

In order to validate the explanation that the appearance of the effective stress reduction "peak", depends on the mechanical and thermal properties of the aquifer and caprock, a last simulation has been carried out. For this end, on the contrary to the simulations presented above, it has now been considered a higher stiffness and thermal expansion coefficient for the aquifer. Table 5.4, summarizes the material properties considered for each simulation.

The results obtained show the expected behaviour, i.e. the reduction "peak" verified at the caprock, is no longer found, being observed a continuous increase of the horizontal effective stress during the transition between the aquifer and caprock (Figure 5.28). This means, that properties such as Young modulus and thermal expansion coefficient, have a relevant role in the mechanical behaviour of the pair aquifer-caprock.

Table 5.4 – Material properties for the SC and Liquid simulations

Layer	SC		Liquid_1		Liquid_2	
	E [GPa]	α*10^{-5} [K^{-1}]	E [GPa]	α*10^{-5} [K^{-1}]	E [GPa]	α*10^{-5}[K^{-1}]
Caprock	5	-	5	1.5	1	1
Aquifer	2.5	-	2.5	1	2.5	1.5

Figure 5.28 - Vertical profile of the horizontal effective stress, 10 meters away the injection well, after 180 days of injection and for SC and two Liquid simulations

Finally and going back to Figure 5.22, after reaching the reduction peak, a much sharper increase in the horizontal effective stress is observed when compared to the vertical effective stress. The latter is due to the bending effect. This effect, can be related with the classic example of a beam loaded at mid-span. A beam in such loading conditions undergoes compression at the upper region and tensions at the lower ones. The latter resembles the interaction between the aquifer and the caprock, where the high decrease in vertical effective stress at the aquifer produces an increase in the horizontal effective stress at the caprock in order to support the overburden. Figure 5.29, shows the time windows in which each process is dominant in the horizontal effective stress evolution with liquid injection conditions, for three elements at the caprock. The "1st" element is the closest to the interface and the others are sequentially above. Fluid pressure, bending effect and thermal effects are represented in blue, black and red respectively. During the first few days fluid pressure is dominant due to the desaturation process, after which the bending effect begins to have more relevance due to the high decrease in vertical effective stress within the aquifer and at last, the temperature influence that reaches the caprock by conduction. With regard to the bending effect, as we head upwards the bending effect has more significance, due to its higher magnitude but also because the thermal effects are delayed allowing the bending effect to take place.

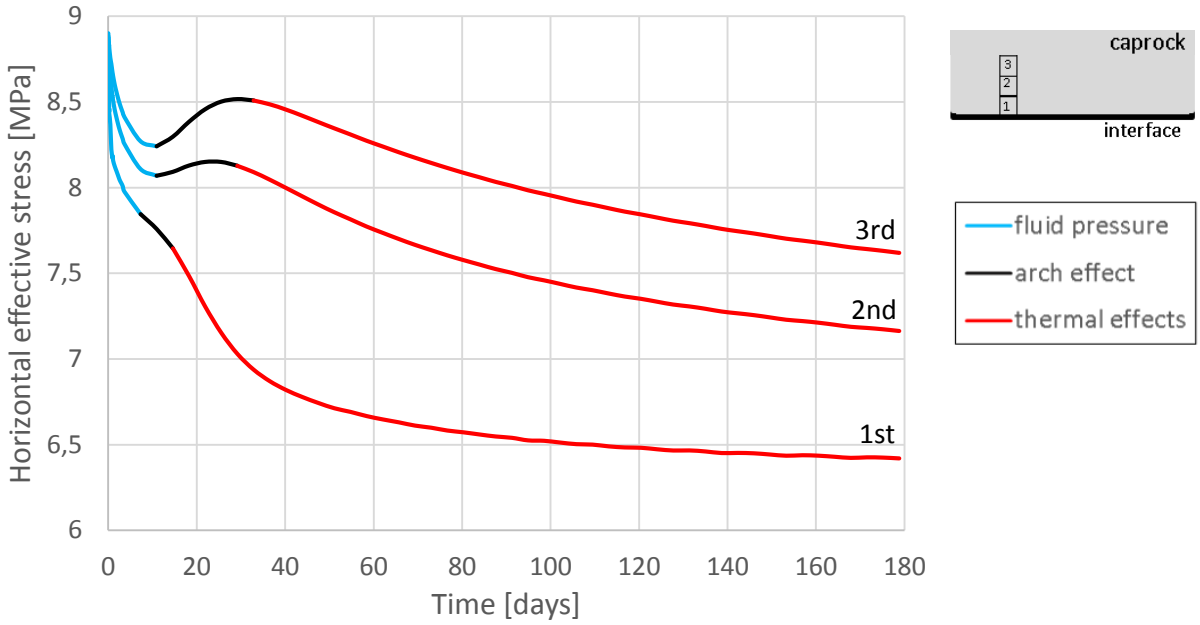

Figure 5.29 - Time window where fluid pressure, bending and thermal effects dominate for three elements at the caprock

6. CONCLUSIONS AND FUTURE DEVELOPMENTS

6.1. CONCLUSIONS

This study addresses the coupled effects related to CO_2 injection into deep aquifers, including hydro-mechanical coupling, thermo-hydraulic coupling and thermo-hydro-mechanical coupling. CO_2 injection into deep aquifers result in a desaturation process that induces an effective stress reduction. In addition, if the injected CO_2 is colder than the reservoir formation, a thermal contraction behaviour of the aquifer and caprock will occur, reducing even more the effective stress. Thus, being the main objective of this work, the study of the thermal effects, a comparison between liquid CO_2 injection (non-isothermal analysis) and supercritical CO_2 injection (isothermal analysis), was carried out in order to properly asses its influence on the mechanical behaviour.

Through the hydro-mechanical analysis, it has been verified that once CO_2 is injected into aquifers, the pores close to the injection well are filled with water, implying a very low relative permeability of the CO_2. This results in a very sharp increase in the fluid pressure during the first few days. This phenomenon is described as the desaturation process of the aquifer, during which the mechanical stability is less favourable. However, over time the pores close to the injection well will be filled with CO_2, increasing its relative permeability, thus decreasing fluid pressure and recovering better injection conditions.

Regarding the thermo-hydraulic analyses, it has been found that heat flow is governed by the convection term and by considering it, a greater amount of CO_2 is found with lower temperatures (i.e. higher densities), resulting in relatively lower fluid pressures. Nevertheless, the conduction term must not be neglected because it is the only phenomenon that allows the caprock to experience thermal effects. Furthermore, it has been observed that injecting liquid CO_2 implies higher densities and viscosities which influences the carbon dioxide plume evolution, resulting in a shorter distance covered by the CO_2 plume and a greater concentration close to the injection well. This implies higher containment periods and lower areas for future monitoring.

Comparing supercritical and liquid injection, a thermal contraction of the aquifer and caprock occurs close to the injection site when injecting liquid CO_2, being detected horizontal displacements towards the injection well, as well as a reduction in the vertical displacements, which is in agreement with stated by Goodarzi et al., 2010. These two injection scenarios imply slightly different mechanical behaviours by the geomaterial. By comparing the evolution of the vertical and horizontal effective stress, fluid pressure and temperature, it was observed that the difference in the mechanical behaviour is mainly due to thermal effects rather than fluid pressure. Furthermore, by analysing the stress path in a mean effective and deviatoric stress plane, it was verified that due to the permanent action of temperature, the

confinement pressure is not recovered such as in supercritical conditions, which implies less stable injection conditions, especially for the elements in the caprock.

Since the present study is based on Vilarrasa (2012), similar results were expected. Indeed the general results are in agreement, however a different conclusion is drawn regarding the horizontal effective stress evolution due to a slight different assessment of the thermal expansion coefficient of the caprock. Vilarrasa (2012) states that liquid injection results in a higher decrease in effective stress in the storage formation, inducing a stress redistribution tightening up the caprock and making it more stable, whereas the results presented here show that the mechanical behaviour of the aquifer-seal pair is strongly dependent on the mechanical and thermal properties of the geomaterial. In cases where the caprock is characterized by a higher stiffness and thermal expansion coefficient compared to the aquifer, a reduction of the horizontal effective stress is observed at the caprock, close to the interface. Whereas, in case properties are reversed, a continuous increase of the horizontal effective stress is verified during the transition of both layers, which is in agreement with stated by Vilarrasa (2012).

Moreover, it can be stated that injecting liquid CO_2 is more advantageous due to the higher density and viscosity which favours the containment period and the reduction of the monitoring area. Nevertheless, the thermal contraction behaviour should be carefully studied for high temperature gradients. It is advisable, that at a design stage, a detailed definition of the mechanical and thermal parameters, mainly Young modulus and thermal expansion coefficient of both layers is carried out, as well determining the thermal gradient found between aquifer-seal formations and injected fluid.

6.2. FUTURE DEVELOPMENTS

Since a THM analysis implies a considerable computational cost (see Appendix B), it was not feasible to carry out a reasonable amount of simulations. Therefore, a parametric study involving different temperature gradients, as well as, caprock and aquifer mechanical, thermal and hydraulic properties such as stiffness, intrinsic and relative permeabilities, water retention curve parameters and thermal expansion coefficients could be carried out in order to better assess their role in the overall behaviour.

This study considers a homogeneous aquifer and caprock but heterogeneities, in the caprock such as weak zones (fractures or faults), could be present. From this study it was observed in a *q-p'* plane that the stress paths of elements at the caprock and aquifer are reasonably far from a possible failure envelope, not raising major concerns. However, these weak zones can have a much closer failure envelopes. Therefore, modelling fractures in the geomaterial is an important subject to be implemented. Furthermore, carrying this study with an elasto-plastic constitutive model could be interesting to bring knowledge concerning porosity and permeability variation (e.g. Kozeny-Karman formulation) and its influence, during the injection stage.

A long-term analysis would be interesting in order to quantify other trapping mechanisms such as solubility and mineral carbonation. For this purpose, it is then necessary to implement a Thermo-Hydro-

Chemo-Mechanical analysis in order to simulate the chemical reactions between the minerals and the CO_2.

Finally, an interesting study, would be attempting to validate the model with *in situ* data.

REFERENCES

Abdulagatova Z, Abdulagatov IM, Emirov VN. Effect of temperature and pressure on the thermal conductivity of sandstone. International Journal of Rock Mechanics and Mining Sciences; 46(6):1055–71; 2009;

AGU (American Geophysical Union). AGU position statement on human impacts on climate change. EOS Trans AGU; 84:574; 2003;

Aya I, Kojima R, Yamane K, Shiozaki K, Brewer PG, Peltzer ET. In situ experiments of cold CO2 release in mid-depth. Energy; 29(9–10):1499–509; 2004;

Bachu S. CO2 storage in geological media: Role, means, status and barriers to deployment. Progress in Energy and Combustion Science; 34(2):254–73; 2008;

Bawendi M and Keith N. Thermodynamics and Kinetics. MIT OpenCourseWare, Lecture 4 – Enthalphy; 2008

Bear J. Dynamics of Fluids in Porous Media. Courier Dover Publications; 802 p; 2013;

Bock H. Experiment: Updated Review of the Rock mechanics Properties of the Opalinus Clay of the Mont Terri Project based on Laboratory and Field Testing; 2009;

Bradshaw J and Dance T. Mapping geological storage prospectivity of CO_2 for the world's sedimentary basins and regional source to sink matching. In: Rubin ES, Keith DW, Gilboy CF, editors. In: Proceedings of the 7th international conference on greenhouse gas control technologies, vol. I. London, UK: Elsevier, p. 583–91; 2005;

Brewer PG, Peltzer ET, Friederich G, Aya I, Yamane K. Experiments on the ocean sequestration of fossil fuel CO2: pH measurements and hydrate formation. Marine Chemistry; 72(2–4):83–93; 2000;

Charlier R. Approche unifiée de quelques problèmes non linéaires de mécanique des milieux continus par la méthode des éléments finis (grandes déformations des métaux et des sols, contact unilatéral de solides, conduction thermique et écoulements en milieu poreux); Thèse de doctorat, Faculté des Sciences Appliquées, Université de Liège; 1987;

Charlier R, Radu J-P, Collin F. Numerical modelling of coupled transient phenomena. Revue Française de Génie Civil; 5(6):719–41; 2001;

Chen B, Song Y, Nishio M, Someya S, Akai M. Modeling near-field dispersion from direct injection of carbon dioxide into the ocean. Journal of Geophysics; 110(C9):C09S15; 2005;

Chevalier G, Diamond LW, Leu W. Potential for deep geological sequestration of CO2 in Switzerland: a first appraisal. Swiss Journal of Geoscience; 103(3):427–55; 2010;

CO2CRC. (ONLINE). Available at http://www.co2crc.com.au/imagelibrary3/general.php. Accessed 2014;

Damen K, Faaij A, Turkenburg W. Health, Safety and Environmental Risks of Underground Co2 Storage – Overview of Mechanisms and Current Knowledge. Climatic Change; 74(1-3):289–318; 2006;

Eichenberger J. Rainfall thresholds for shallow landslides based on a numerical analysis. Programme doctoral Mécanique. Thèse École Polytechnique Fédérale de Lausanne EPFL, n 5880; 2013;

Eseme E, Littke R, Krooss BM. Factors controlling the thermo-mechanical deformation of oil shales: Implications for compaction of mudstones and exploitation. Marine and Petroleum Geology, 715–34, 2006;

Fenghour A, Wakeham WA, Vesovic V. The Viscosity of Carbon Dioxide. Journal of Physical and Chemical; 27(1):31–44; 1998;

Garcia E, Oka F, Kimoto S. Numerical analysis of a one-dimensional infiltration problem in unsaturated soil by a seepage–deformation coupled method. International Journal of Numerical Analytical Methods in Geomechanics; 35(5):544–68; 2011;

Gens A, Vaunat J, Garitte B, Wileveau Y. In situ behaviour of a stiff layered clay subject to thermal loading: observations and interpretation. Géotechnique; 57(2):207–28; 2007;

GiD. Personal pre- and postprocessor, Version 10. CIMNE International Center for Numerical Methods in Engineering, Barcelona, Spain, 2011;

Gilliam TM, Morgan IL. Shale: Measurement of thermal properties (ORNL/TM--10499. Oak Ridge National Lab., TN (USA); 135p-19; 1987;

Gor GY, Elliot TR, Prévost JH. Effects of thermal stresses on caprock integrity during CO2 storage. International Journal of Greenhouse Gas Control; 12:300–9; 2013;

Goodarzi S, Settari A, Zoback MD, Keith D. Thermal Aspects of Geomechanics and Induced Fracturing in CO2 Injection With Application to CO2 Sequestration in Ohio River Valley. Society of Petroleum Engineers; 2010

IPCC: Climate Change: the Scientific Basis Contribution of Working Group I to the Third Assessment Report of the Intergovernmental Panel on Climate Change. J.T. Houghton, Y. Ding, D.J. Griggs, M. Noguer, P.J. van der Linden, X. Dai, K. Maskell, and C.A. Johnson, (eds.). Cambridge University Press; 2001c;

IPCC (Intergovernmental Panel on Climate Change). In: Metz B, Davidson O, de Coninck HC, Loos M, Mayer LA, editors. Special report on carbon dioxide capture and storage. Cambridge University Press; 2005;

IPCC (Intergovernmental panel on climate change). Climate change: The physical science basis. Fourth assessment report, IPCC Secretariat; 2007;

IEA GHG: Overview of Long-term Framework for CO_2 Capture and Storage. Report Ph4/35. IEA Greenhouse Gas R&D Programme; 2004b;

IEA GHG: Overview of Monitoring Requirements for Geological Storage Projects. Report Ph4/29. IEA Greenhouse Gas R&D Programme; 2004c;

Itaoka K, Saito A, Akai M. Public acceptance of CO_2 capture and storage technology : a survey of public opinion to explore influential factors; 2005

Jobmann M and Polster M. The response of Opalinus clay due to heating: A combined analysis of in situ measurements, laboratory investigations and numerical calculations. Physics and Chemistry of the Earth, Parts A/B/C; 32(8–14):929–36; 2007;

Laloui L and Nuth M. On the use of the generalised effective stress in the constitutive modelling of unsaturated soils. Computers and Geotechnics; 36(1–2):20–3; 2009

Laloui L. Mechanics of unsaturated soils. USA: Wiley&Sons Inc./ London: ISTE Ltd; 2010;

Lewis R and Schrefler BA. The Finite Element Method in Static and Dynamic Deformation and Consolidation of Porous Media. USA: Wiley&Sons Inc./ New York; 1998;

Li C. Unpublished Report and personal communication. École Polytechnique Fédérale de Lausanne. Laboratory of Soil Mechanics; 2013;

He M, Sousa LR, Elsworth D, Jr EV. CO2 Storage in Carboniferous Formations and Abandoned Coal Mines. CRC Press; 220 p; 2011

Midttomme K, Roaldset E, Aagaard P. Thermal conductivity of selected claystones and mudstones from England, Clay Minerals; 33(1): 131-145;1998;

NIST Web Chemistry book. Available at: http://webbook.nist.gov/chemistry/fluid/. Accessed 2014;

Oldenburg CM. Screening and ranking framework for geologic CO2 storage site selection on the basis of health, safety, and environmental risk. Environmental Geology, Springer; 54(8):1687–94; 2008;

Olivella, S., Carrera, J., Gens, A. and Alonso E. E. Non-isothermal multiphase flow of brine and gas through saline media. *Transport In Porous Media* 15, 271–293; 1994;

Olivella, S., Gens, A., Carrera, J. and Alonso E. E. Numerical formulation for a simulator (CODE_BRIGHT) for the coupled analysis of saline media. *Engineering Computations* 13, 87–112; 1996;

Panday S and Corapcioglu MY. Reservoir transport equations by compositional approach. Transport in Porous Media; 4(4):369–93; 1989;

Peng DY and Robinson DB. A New Two-Constant Equation of State. Industrial Engineering Chemistry Fundamentals; 15(1):59–64; 1976;

Pruess K and García J. Multiphase flow dynamics during CO2 disposal into saline aquifers. Environmental Geology, Springer; 42(2-3):282–95; 2002;

Robertson EC and Peck DL. Thermal conductivity of vesicular basalt from Hawaii. Journal of Geophysical Research; 79(32):4875–88; 1974;

Rutqvist J and Tsang CF. A study of caprock hydromechanical changes associated with CO2-injection into a brine formation. Environmental Geology, Springer; 42(2-3):296–305; 2002;

Rutqvist J, Birkholzer JT, Tsang CF. Coupled reservoir–geomechanical analysis of the potential for tensile and shear failure associated with CO2 injection in multi layered reservoir–caprock systems. International Journal of Rock Mechanics and Mining Sciences; 45(2):132–43; 2008;

Schärli U and Rybach L. Determination of specific heat capacity on rock fragments. Journal Geothermics; 30(1):93–110; 2001;

Shackley S, McLachlan C, Gough C. The public perception of carbon dioxide capture and storage in the UK: results from focus groups and a survey. Climate Policy; 4(4):377–98; 2004;

Simone S., Vilarrasa V., Carrera J., Alcolea A., Meier P. Thermal coupling may control mechanical stability of geothermal reservoirs during cold water injection. Physic and Chemistry of the Earth. Elsevier; 64:117-126; 2013;

Somerton WH. Thermal Properties and Temperature-Related Behavior of Rock/Fluid Systems. Elsevier; 268 p; 1992;

Statoil. Available at: http://fotoweb.statoil.com/fotoweb/Default.fwx?search=(IPTC201%20contains%20(Sleipner)). Accessed 2014;

Van Genuchten MT. A Closed-form Equation for Predicting the Hydraulic Conductivity of Unsaturated Soils1. Soil Science Society of America Journal; 44(5):892; 1980;

Vilarrasa V. Thermo-Hydro-Mechanical Impacts of Carbon Dioxide (CO2) Injection in Deep Saline Aquifers. PhD. Thesis. Department of Geotechnical Engineering and Geosciences, Technical University of Catalonia; 2012;

Wileveau Y. Thermo-Hydro-Mechanical behaviour of host rock (HE-D) experiment: Progress report, Part1, Technical Report TR-03. Mont Terri Project; 2005;

Wu G, Wang Y, Swift G, Chen J. Laboratory Investigation of the Effects of Temperature on the Mechanical Properties of Sandstone. Geotechnical and Geological Engineering, Springer; 31(2):809–16; 2013;

Zhang Z. Numerical Simulation and Optimization of CO2 Sequestration in Saline Aquifers. Electronic Theses and Dissertations. Paper 1097; 2013.

APPENDIX A

Solid density

$$\frac{1}{\rho_s}\frac{d^s\rho_s}{dt} = -\frac{1}{V_s}\frac{d^sV_s}{dt} \tag{8.1}$$

$$(=)\frac{1}{\rho_s}\frac{d^s\rho_s}{dt} = -\frac{1}{K_s}\frac{\partial p_s}{\partial t} - \beta_s\frac{\partial T}{\partial t} - \frac{1}{3(n-1)K_s}\frac{\partial(tr\boldsymbol{\sigma}')}{\partial t} \tag{8.2}$$

$$(=)\frac{1}{\rho_s}\frac{d^s\rho_s}{dt} = \frac{1}{(1-n)}\left[(b-n)\frac{1}{K_s}\frac{\partial p_s}{\partial t} - \beta_s(b-n)\frac{\partial T}{\partial t} - (1-b)div\boldsymbol{v_s}\right] \tag{8.3}$$

Mass balance conservation equation for the solid species

$$\frac{\partial}{\partial t}\big((1-n)\rho_s\big) + div\left[(1-n)\rho_s\left(\frac{\partial \boldsymbol{u}}{\partial t}\right)\right] = 0 \tag{8.4}$$

$$(=)\frac{\partial(1-n)}{\partial t}\rho_s + (1-n)\frac{\partial\rho_s}{\partial t} + \boldsymbol{grad}(\rho_s)(1-n)\boldsymbol{v_s} + \rho_s div((1-n)\boldsymbol{v_s}) = 0 \tag{8.5}$$

$$(=) -\frac{\partial n}{\partial t}\rho_s + (1-n)\frac{\partial\rho_s}{\partial t} - (1-n)\boldsymbol{grad}(\rho_s)\boldsymbol{v_s} + \rho_s div\big((1-n)\boldsymbol{v_s}\big) = 0 \tag{8.6}$$

$$(=)\frac{\partial n}{\partial t} = (1-n)\frac{1}{\rho_s}\frac{d^s\rho_s}{dt} + div[(1-n)\boldsymbol{v_s}] \tag{8.7}$$

$$(=)\frac{\partial n}{\partial t} = (1-n)\left(\frac{\partial\rho_s}{\partial p_s}\frac{\partial p_s}{\partial t} + \frac{\partial\rho_s}{\partial T}\frac{\partial T}{\partial t}\right) + div\big((1-n)\boldsymbol{v_s}\big) \tag{8.8}$$

$$(=)\frac{\partial n}{\partial t} = (1-n)\left(\frac{1}{K_s}\frac{\partial p_s}{\partial t} - \beta_s\frac{\partial T}{\partial t}\right) + div\big((1-n)\boldsymbol{v_s}\big) \tag{8.9}$$

$$(=)\frac{\partial n}{\partial t} = (b-n)\left\{\frac{1}{K_s}\frac{d}{dt}[S_w p_w + (1-S_w)p_c] + div(\boldsymbol{v_s}) - \beta_s\frac{\partial T}{\partial t}\right\} \tag{8.10}$$

Mass balance conservation equation for the water species

$$\frac{d^w(nS_w\rho_w)}{dt} + \rho_w nS_w div(\boldsymbol{v_w}) = 0 \tag{8.11}$$

$$(=)\frac{\partial}{\partial t}(nS_w\rho_w) + \boldsymbol{grad}(\rho_w nS_w)\boldsymbol{v_{ws}} + \rho_w nS_w div(\boldsymbol{v_w}) = 0 \tag{8.12}$$

$$(=)S_w\rho_w\frac{\partial n}{\partial t} + n\rho_w\frac{\partial S_w}{\partial t} + nS_w\frac{\partial\rho_w}{\partial t} + \boldsymbol{grad}(\rho_w nS_w)\boldsymbol{v_{ws}} + \rho_w nS_w div(\boldsymbol{v_w}) = 0 \tag{8.13}$$

$$(=)(b-n)S_w\rho_w\left\{\left[\frac{1}{K_s}\frac{d}{dt}(S_w p_w + (1-S_w)p_c\right] - \beta_s\frac{\partial T}{\partial t} + div(\boldsymbol{v_s})\right\} \tag{8.14}$$

$$+n\rho_w \frac{\partial S_w}{\partial t} + nS_w \frac{\partial \rho_w}{\partial t} + \boldsymbol{grad}(\rho_w n S_w)\boldsymbol{v_{ws}} + \rho_w n S_w div(\boldsymbol{v_w}) = 0$$

$$(=)(b-n)S_w\rho_w \left[\frac{1}{K_s}\left(\frac{\partial S_w}{\partial t}p_w + \frac{\partial p_w}{\partial t}S_w + \frac{\partial p_c}{\partial t} - \frac{\partial S_w}{\partial t}p_c - \frac{\partial p_c}{\partial t}S_w\right) - \beta_s \frac{\partial T}{\partial t} + div(\boldsymbol{v_s})\right]$$
$$+n\rho_w \frac{\partial S_w}{\partial t} + nS_w \frac{\partial \rho_w}{\partial t} + \boldsymbol{grad}(\rho_w n S_w)\boldsymbol{v_{ws}} + \rho_w n S_w div(\boldsymbol{v_w}) = 0 \quad (8.15)$$

$$(=)(b-n)S_w\rho_w \left[\frac{1}{K_s}\left(-\frac{\partial S_w}{\partial t}s + \frac{\partial p_w}{\partial t}S_w - \frac{\partial p_c}{\partial t}S_w + \frac{\partial p_c}{\partial t}\right) - \beta_s \frac{\partial T}{\partial t} + div(\boldsymbol{v_s})\right]$$
$$+n\rho_w \frac{\partial S_w}{\partial s}\frac{\partial p_c}{\partial t} - n\rho_w \frac{\partial S_w}{\partial s}\frac{\partial p_w}{\partial t} + n\rho_w \frac{\partial S_w}{\partial T}\frac{\partial T}{\partial t} + nS_w\left(\frac{\partial \rho_w}{\partial p_w}\frac{\partial p_w}{\partial t} + \frac{\partial \rho_w}{\partial T}\frac{\partial T}{\partial t}\right) \quad (8.16)$$
$$+\boldsymbol{grad}(\rho_w n S_w)\boldsymbol{v_{ws}} + \rho_w n S_w div(\boldsymbol{v_w}) = 0$$

$$(=)(b-n)S_w\rho_w \left\{\begin{array}{c}\frac{1}{K_s}\left[-s\frac{\partial S_w}{\partial s}\left(\frac{\partial p_c}{\partial t} - \frac{\partial p_w}{\partial t}\right) + \frac{\partial p_w}{\partial t}S_w - \frac{\partial p_c}{\partial t}S_w + \frac{\partial p_c}{\partial t}\right] \\ -\beta_s \frac{\partial T}{\partial t} + div(\boldsymbol{v_s})\end{array}\right\}$$
$$+n\rho_w \frac{\partial S_w}{\partial s}\frac{\partial p_c}{\partial t} - n\rho_w \frac{\partial S_w}{\partial s}\frac{\partial p_w}{\partial t} + n\rho_w \frac{\partial S_w}{\partial T}\frac{\partial T}{\partial t} + nS_w\left(\frac{\partial \rho_w}{\partial p_w}\frac{\partial p_w}{\partial t} - \beta_w \frac{\partial T}{\partial t}\right) \quad (8.17)$$
$$+\boldsymbol{grad}(\rho_w n S_w)\boldsymbol{v_{ws}} + \rho_w n S_w div(\boldsymbol{v_w}) = 0$$

$$(=)(b-n)S_w\rho_w \left\{\frac{1}{K_s}\left[\left(S_w + \frac{\partial S_w}{\partial s}s\right)\frac{\partial p_w}{\partial t} + \left(1 - S_w - \frac{\partial S_w}{\partial s}s\right)\frac{\partial p_c}{\partial t}\right] - \beta_s \frac{\partial T}{\partial t} + div(\boldsymbol{v_s})\right\}$$
$$+n\rho_w \frac{\partial S_w}{\partial s}\frac{\partial p_c}{\partial t} - n\rho_w \frac{\partial S_w}{\partial s}\frac{\partial p_w}{\partial t} + n\rho_w \frac{\partial S_w}{\partial T}\frac{\partial T}{\partial t} + nS_w\left(\frac{\partial \rho_w}{\partial p_w}\frac{\partial p_w}{\partial t} - \beta_w \frac{\partial T}{\partial t}\right) \quad (8.18)$$
$$+\boldsymbol{grad}(\rho_w n S_w)\boldsymbol{v_{ws}} + \rho_w n S_w div(\boldsymbol{v_w}) = 0$$

$$(=)(b-n)S_w\rho_w \left\{\frac{1}{K_s}\left[\left(S_w + \frac{\partial S_w}{\partial s}s\right)\frac{\partial p_w}{\partial t} + \left(1 - S_w - \frac{\partial S_w}{\partial s}s\right)\frac{\partial p_c}{\partial t}\right] - \beta_s \frac{\partial T}{\partial t}\right\}$$
$$+n\rho_w \frac{\partial S_w}{\partial s}\frac{\partial p_c}{\partial t} - n\rho_w \frac{\partial S_w}{\partial s}\frac{\partial p_w}{\partial t} + n\rho_w \frac{\partial S_w}{\partial T}\frac{\partial T}{\partial t} + nS_w\left(\frac{\partial \rho_w}{\partial p_w}\frac{\partial p_w}{\partial t} - \beta_w \frac{\partial T}{\partial t}\right) \quad (8.19)$$
$$+\boldsymbol{grad}(\rho_w n S_w)\boldsymbol{v_{ws}} + \rho_w n S_w div(\boldsymbol{v_w}) + (b-n)S_w\rho_w div(\boldsymbol{v_s}) = 0$$

$$(=)(b-n)S_w\rho_w \left\{\frac{1}{K_s}\left[\left(S_w + \frac{\partial S_w}{\partial s}s\right)\frac{\partial p_w}{\partial t} + \left(1 - S_w - \frac{\partial S_w}{\partial s}s\right)\frac{\partial p_c}{\partial t}\right] - \beta_s \frac{\partial T}{\partial t}\right\}$$
$$+n\rho_w \frac{\partial S_w}{\partial s}\frac{\partial p_c}{\partial t} - n\rho_w \frac{\partial S_w}{\partial s}\frac{\partial p_w}{\partial t} + n\rho_w \frac{\partial S_w}{\partial T}\frac{\partial T}{\partial t} + nS_w\left(\frac{\partial \rho_w}{\partial p_w}\frac{\partial p_w}{\partial t} - \beta_w \frac{\partial T}{\partial t}\right) \quad (8.20)$$
$$+div(S_w n\rho_w \boldsymbol{v_{ws}}) - S_w n\rho_w div(\boldsymbol{v_{ws}}) + S_w n\rho_w div(\boldsymbol{v_{ws}} + \boldsymbol{v_s}) + (b-n)S_w\rho_w div(\boldsymbol{v_s}) = 0$$

$$(=)(b-n)S_w\rho_w \left\{\frac{1}{K_s}\left[\left(S_w + \frac{\partial S_w}{\partial s}s\right)\frac{\partial p_w}{\partial t} + \left(1 - S_w - \frac{\partial S_w}{\partial s}s\right)\frac{\partial p_c}{\partial t}\right] - \beta_s \frac{\partial T}{\partial t}\right\}$$
$$+n\rho_w \frac{\partial S_w}{\partial s}\frac{\partial p_c}{\partial t} - n\rho_w \frac{\partial S_w}{\partial s}\frac{\partial p_w}{\partial t} + n\rho_w \frac{\partial S_w}{\partial T}\frac{\partial T}{\partial t} + nS_w\left(\frac{\partial \rho_w}{\partial p_w}\frac{\partial p_w}{\partial t} + \frac{\partial \rho_w}{\partial T}\frac{\partial T}{\partial t}\right) \quad (8.21)$$

$$+div\left[\rho_w \frac{k_{rw}\boldsymbol{k}_{int}}{\mu_w}(-\boldsymbol{grad}(p_w)+\rho_w \boldsymbol{g})\right]+S_w\rho_w div(\boldsymbol{v_s})(n+b-n)=0$$

$$\left[n\rho_w \frac{\partial S_w}{\partial s}+\frac{(b-n)}{K_s}S_w\,\rho_w\left(1-S_w-\frac{\partial S_w}{\partial s}s\right)\right]\frac{\partial p_c}{\partial t}$$
$$\left[-n\rho_w \frac{\partial S_w}{\partial s}+S_w\,n\frac{\partial \rho_w}{\partial p_w}+\frac{(b-n)}{K_s}S_w\,\rho_w\left(S_w+\frac{\partial S_w}{\partial s}s\right)\right]\frac{\partial p_w}{\partial t}$$
$$-\left[nS_w\,\rho_w\,\beta_w+(\mathrm{b-n})S_w\,\rho_w\,\beta_s+n\rho_w\frac{\partial S_w}{\partial T}\right]\frac{\partial \mathrm{T}}{\partial t}+b\,\rho_w\,S_w\,div(\boldsymbol{v_s}) \quad (8.22)$$
$$+\boldsymbol{div}\left(\rho_w\frac{k_{rw}\boldsymbol{k}_{int}}{\mu_w}(-\boldsymbol{grad}(p_w)+\rho_w\,\boldsymbol{g})\right)=0$$

Mass balance conservation equation for dry CO_2

$$\frac{d^c(n(1-S_w)\rho_c)}{dt}+\rho_c n(1-S_w)div(\boldsymbol{v_c})=f_{CO_2-w} \quad (8.23)$$

$$(=)\frac{\partial}{\partial t}(n(1-S_w)\rho_c)+\boldsymbol{grad}(n(1-S_w)\rho_c)\boldsymbol{v_{cs}}+n(1-S_w)\rho_c div(\boldsymbol{v_c})=f_{CO_2-w} \quad (8.24)$$

$$(=)(1-S_w)\rho_c\frac{\partial n}{\partial t}+n\rho_c\frac{\partial(1-S_w)}{\partial t}+n(1-S_w)\frac{\partial \rho_c}{\partial t}+\boldsymbol{grad}(\rho_c n(1-S_w))\boldsymbol{v_{cs}}$$
$$+\rho_c n(1-S_w)div(\boldsymbol{v_c})=f_{CO_2-w} \quad (8.25)$$

$$(=)(b-n)(1-S_w)\rho_c\left\{\left[\frac{1}{K_s}\frac{d}{dt}(S_w p_w+(1-S_w)p_c\right]-\beta_s\frac{\partial T}{\partial t}+div(\boldsymbol{v_s})\right\}$$
$$+n\rho_c\frac{\partial(1-S_w)}{\partial s}\frac{\partial p_c}{\partial t}-n\rho_c\frac{\partial(1-S_w)}{\partial s}\frac{\partial p_w}{\partial t}+n\rho_c\frac{\partial(1-S_w)}{\partial T}\frac{\partial T}{\partial t}$$
$$+(1-S_w)n\frac{\partial \rho_c}{\partial p_c}\frac{\partial p_c}{\partial t}+(1-S_w)n\frac{\partial \rho_c}{\partial T}\frac{\partial T}{\partial t} \quad (8.26)$$
$$+\boldsymbol{grad}(\rho_c n(1-S_w))\boldsymbol{v_{cs}}+\rho_c n(1-S_w)div(\boldsymbol{v_c})=f_{CO_2-w}$$

$$(=)(b-n)(1-S_w)\rho_c\left\{\frac{1}{K_s}\left[\left(S_w+\frac{\partial S_w}{\partial s}s\right)\frac{\partial p_w}{\partial t}+\left(1-S_w-\frac{\partial S_w}{\partial s}s\right)\frac{\partial p_c}{\partial t}\right]-\beta_s\frac{\partial T}{\partial t}\right\}$$
$$+n\rho_c\frac{\partial(1-S_w)}{\partial s}\frac{\partial p_c}{\partial t}-n\rho_c\frac{\partial(1-S_w)}{\partial s}\frac{\partial p_w}{\partial t}+n\rho_c\frac{\partial(1-S_w)}{\partial T}\frac{\partial T}{\partial t}$$
$$+(1-S_w)n\frac{\partial \rho_c}{\partial p_c}\frac{\partial p_c}{\partial t}+(1-S_w)n\frac{\partial \rho_c}{\partial T}\frac{\partial T}{\partial t} \quad (8.27)$$
$$+div\left[\rho_c\frac{k_{rc}\boldsymbol{k}_{int}}{\mu_c}(-\boldsymbol{grad}(p_c)+\rho_c\boldsymbol{g})\right]+(1-S_w)\rho_c div(\boldsymbol{v_s})b=f_{CO_2-w}$$

$$\left[-n\rho_c \frac{\partial S_w}{\partial s} + (1-S_w)n\,\rho_c \frac{\partial \rho_c}{\partial p_c} + \frac{(b-n)}{K_s}(1-S_w)\,\rho_c \left(1 - S_w - \frac{\partial S_w}{\partial s}s\right)\right]\frac{\partial p_c}{\partial t}$$
$$+\left[n\rho_c \frac{\partial S_w}{\partial s} + \frac{(b-n)}{K_s}(1-S_w)\,\rho_c \left(S_w + \frac{\partial S_w}{\partial s}s\right)\right]\frac{\partial p_w}{\partial t}$$
$$+\left[-(b-n)(1-S_w)\,\rho_c \beta_s + (1-S_w)n\,\rho_c \frac{\partial \rho_c}{\partial T} + n\rho_c \frac{\partial(1-S_w)}{\partial T}\right]\frac{\partial T}{\partial t} \quad (8.28)$$
$$+b\,\rho_c (1-S_w)\,div(\boldsymbol{v_s})$$
$$+div\left(\rho_c \frac{k_{rc}\boldsymbol{k}_{int}}{\mu_c}(-\boldsymbol{grad}(p_c) + \rho_c \boldsymbol{g})\right) = f_{co2-w}$$

Mass balance conservation equation for dissolved CO_2

$$\frac{d^{dc}(nS_w\rho_{dc})}{dt} + \rho_{dc}nS_w div(\boldsymbol{v_w}) + div(\boldsymbol{i_{dc}}) = f_{w-CO_2} \quad (8.29)$$

$$(=)S_w\rho_{dc}\frac{\partial n}{\partial t} + n\rho_{dc}\frac{\partial S_w}{\partial t} + nS_w\frac{\partial \rho_{dc}}{\partial t} + \boldsymbol{grad}(\rho_{dc}nS_w)\boldsymbol{v_{ws}} + \rho_{dc}nS_w div(\boldsymbol{v_w})$$
$$+div(\boldsymbol{i_{dc}}) = f_{w-CO_2} \quad (8.30)$$

$$(=)(b-n)S_w\rho_{dc}\left\{\frac{1}{K_s}\left[\left(S_w + \frac{\partial S_w}{\partial s}s\right)\frac{\partial p_w}{\partial t} + \left(1 - S_w - \frac{\partial S_w}{\partial s}s\right)\frac{\partial p_c}{\partial t}\right] - \beta_s\frac{\partial T}{\partial t}\right\}$$
$$+n\rho_{dc}\frac{\partial S_w}{\partial s}\frac{\partial p_c}{\partial t} - n\rho_{dc}\frac{\partial S_w}{\partial s}\frac{\partial p_w}{\partial t} + n\rho_{dc}\frac{\partial S_w}{\partial T}\frac{\partial T}{\partial t} + S_w n\left(\frac{\partial \rho_{dc}}{\partial p_c}\frac{\partial p_c}{\partial t} + \frac{\partial \rho_c}{\partial T}\frac{\partial T}{\partial t}\right) \quad (8.31)$$
$$+\boldsymbol{grad}(\rho_{dc}nS_w)\boldsymbol{v_{ws}} + \rho_{dc}nS_w div(\boldsymbol{v_w}) + (b-n)S_w\rho_{dc}div(\boldsymbol{v_s}) + div(\boldsymbol{i_{dc}}) = f_{w-CO_2}$$

$$(=)(b-n)S_w\rho_{dc}\left\{\frac{1}{K_s}\left[\left(S_w + \frac{\partial S_w}{\partial s}s\right)\frac{\partial p_w}{\partial t} + \left(1 - S_w - \frac{\partial S_w}{\partial s}s\right)\frac{\partial p_c}{\partial t}\right] - \beta_s\frac{\partial T}{\partial t}\right\}$$
$$+n\rho_{dc}\frac{\partial S_w}{\partial s}\frac{\partial p_c}{\partial t} - n\rho_{dc}\frac{\partial S_w}{\partial s}\frac{\partial p_w}{\partial t} + n\rho_{dc}\frac{\partial S_w}{\partial T}\frac{\partial T}{\partial t} + S_w n\left(\frac{\partial \rho_{dc}}{\partial p_c}\frac{\partial p_c}{\partial t} + \frac{\partial \rho_c}{\partial T}\frac{\partial T}{\partial t}\right) \quad (8.32)$$
$$+div(\rho_{dc}nS_w\boldsymbol{v_{ws}}) - \rho_{dc}nS_w div(\boldsymbol{v_{ws}}) + \rho_{dc}nS_w div(\boldsymbol{v_{ws}} + \boldsymbol{v_s})$$
$$+(b-n)S_w\rho_{dc}div(\boldsymbol{v_s}) + div(\boldsymbol{i_{dc}}) = f_{w-co2}$$

$$(=)(b-n)S_w\rho_{dc}\left\{\frac{1}{K_s}\left[\left(S_w + \frac{\partial S_w}{\partial s}s\right)\frac{\partial p_w}{\partial t} + \left(1 - S_w - \frac{\partial S_w}{\partial s}s\right)\frac{\partial p_c}{\partial t}\right] - \beta_s\frac{\partial T}{\partial t}\right\}$$
$$+n\rho_{dc}\frac{\partial S_w}{\partial s}\frac{\partial p_c}{\partial t} - n\rho_{dc}\frac{\partial S_w}{\partial s}\frac{\partial p_w}{\partial t} + n\rho_{dc}\frac{\partial S_w}{\partial T}\frac{\partial T}{\partial t} + S_w n\left(\frac{\partial \rho_{dc}}{\partial p_c}\frac{\partial p_c}{\partial t} + \frac{\partial \rho_c}{\partial T}\frac{\partial T}{\partial t}\right)$$
$$+div\left[\rho_{dc}\frac{k_{rw}\boldsymbol{k}_{int}}{\mu_w}(-\boldsymbol{grad}(p_w) + \rho_w\boldsymbol{g})\right] + b\rho_{dc}nS_w div(\boldsymbol{v_s}) \quad (8.33)$$
$$+div\left[nS_w\tau D_c\rho_w\boldsymbol{grad}\left(\frac{\rho_w}{\rho_{dc}}\right)\right] = f_{w-co2}$$

$$\left[n\rho_{dc}\,\frac{\partial S_w}{\partial s}+\ n\,S_w\,\frac{\partial \rho_{dc}}{\partial p_c}+\ \frac{(b-n)}{K_s}\ \ S_w\,\rho_{dc}\ \left(1-S_w\ -\frac{\partial S_w}{\partial s}s\right)\right]\frac{\partial p_c}{\partial t}$$

$$\left[-n\rho_{dc}\,\frac{\partial S_w}{\partial s}+\frac{(b-n)}{K_s}\ \ S_w\,\rho_{dc}\,(S_w\ +\ \frac{\partial S_w}{\partial s}s)\right]\frac{\partial p_w}{\partial t}$$

$$\left[-(b-n)\ \ S_w\,\rho_{dc}\,\beta_s\ \ +nS_w\,\frac{\partial \rho_{dc}}{\partial T}\right]\frac{\partial T}{\partial t}$$

$$+b\,\rho_{dc}\,S_w\ \ div(\boldsymbol{v_s})$$

$$+div\ \left[\rho_{dc}\,\frac{k_{rw}\boldsymbol{k}_{int}}{\mu_w}\ \ (-\boldsymbol{grad}(p_w)+\rho_w\,\boldsymbol{g})\right]$$

$$-div\ \left[n\ \ S_w\,\tau\ \ D_c\,\rho_w\,\boldsymbol{grad}\ \left(\frac{\rho_{dc}}{\rho_w}\right)\right]=f_{w-co2} \tag{8.34}$$

Energy Conservation Equation

$$\frac{\partial H}{\partial t}+div\left(-\lambda_{medium}\boldsymbol{grad}(T)\right)+div(\boldsymbol{q})=0 \tag{8.35}$$

$$(=)\left[nS_w\rho_w c_{p,w}+n(1-S_w)\rho_c c_{p,c}+(1-n)\rho_s c_{p,s}\right]\frac{\partial T}{\partial t}+div\left(-\lambda_{medium}\boldsymbol{grad}(T)\right)+div(\boldsymbol{q})=0 \tag{8.36}$$

$$(=)\left[nS_w\rho_w c_{p,w}+n(1-S_w)\rho_c c_{p,c}+(1-n)\rho_s c_{p,s}\right]\frac{\partial T}{\partial t}$$
$$+div\left[-\lambda_{medium}\boldsymbol{grad}(T)+\left(n\rho_w c_{p,w}\boldsymbol{q_w}+n\rho_c c_{p,c}\boldsymbol{q_c}+n\rho_s c_{p,s}\boldsymbol{q_s}\right)\right]=0 \tag{8.37}$$

$$(=)\left[nS_w\rho_w c_{p,w}+n(1-S_w)\rho_c c_{p,c}+(1-n)\rho_s c_{p,s}\right]\frac{\partial T}{\partial t}$$
$$-div[(n\lambda_w+n\lambda_c+(1-n)\lambda_s)\boldsymbol{grad}(T)]$$
$$+\left[n\rho_w c_{p,w}\boldsymbol{q_w}+n\rho_c c_{p,c}\boldsymbol{q_c}\right]grad(T)=0 \tag{8.38}$$

APPENDIX B

The simulations were carried with a computer with the following characteristics:

- CPU: Intel® Core™ i7-3517U CPU @ 1.90GHz 2.40GHz;
- RAM: 8GB (7,89 GB usable).

The following Table presents the average time for each simulation

Type of Simulation	Time
Hydraulic	30 min
Thermo-Hydraulic	1 hour
Hydro-Mechanical	2,5 weeks
Thermo-Hydro-Mechanical	3,5 weeks